National Library of Canada

Acquisitions and Bibliographic Services Branch

395 Wellington Street
Ottawa, Ontario
K1A 0N4

Bibliothèque nationale du Canada

Direction des acquisitions et des services bibliographiques

395, rue Wellington
Ottawa (Ontario)
K1A 0N4

Your file Votre référence

Our file Notre référence

NOTICE

The quality of this microform is heavily dependent upon the quality of the original thesis submitted for microfilming. Every effort has been made to ensure the highest quality of reproduction possible.

If pages are missing, contact the university which granted the degree.

Some pages may have indistinct print especially if the original pages were typed with a poor typewriter ribbon or if the university sent us an inferior photocopy.

Reproduction in full or in part of this microform is governed by the Canadian Copyright Act, R.S.C. 1970, c. C-30, and subsequent amendments.

AVIS

La qualité de cette microforme dépend grandement de la qualité de la thèse soumise au microfilmage. Nous avons tout fait pour assurer une qualité supérieure de reproduction.

S'il manque des pages, veuillez communiquer avec l'université qui a conféré le grade.

La qualité d'impression de certaines pages peut laisser à désirer, surtout si les pages originales ont été dactylographiées à l'aide d'un ruban usé ou si l'université nous a fait parvenir une photocopie de qualité inférieure.

La reproduction, même partielle, de cette microforme est soumise à la Loi canadienne sur le droit d'auteur, SRC 1970, c. C-30, et ses amendements subséquents.

Canada

Optical Beat Interference Countermeasures in Subcarrier Multiplexed Wavelength Division Multiple Access Networks

By
MOHAMMAD M. BANAT, B.Sc., M.Sc.

A dissertation submitted to the
School of Graduate Studies and Research,
University of Ottawa
in partial fulfillment of the requirements
for the degree of
Doctor of Philosophy (Electrical Engineering)

Ottawa-Carleton Institute for Electrical Engineering

Department of Electrical Engineering
Faculty of Engineering
University of Ottawa
January 1995

© 1995, Mohammad M. Banat

National Library of Canada
Acquisitions and Bibliographic Services Branch
395 Wellington Street
Ottawa, Ontario
K1A 0N4

Bibliothèque nationale du Canada
Direction des acquisitions et des services bibliographiques
395, rue Wellington
Ottawa (Ontario)
K1A 0N4

Your file Votre référence

Our file Notre référence

THE AUTHOR HAS GRANTED AN IRREVOCABLE NON-EXCLUSIVE LICENCE ALLOWING THE NATIONAL LIBRARY OF CANADA TO REPRODUCE, LOAN, DISTRIBUTE OR SELL COPIES OF HIS/HER THESIS BY ANY MEANS AND IN ANY FORM OR FORMAT, MAKING THIS THESIS AVAILABLE TO INTERESTED PERSONS.

L'AUTEUR A ACCORDE UNE LICENCE IRREVOCABLE ET NON EXCLUSIVE PERMETTANT A LA BIBLIOTHEQUE NATIONALE DU CANADA DE REPRODUIRE, PRETER, DISTRIBUER OU VENDRE DES COPIES DE SA THESE DE QUELQUE MANIERE ET SOUS QUELQUE FORME QUE CE SOIT POUR METTRE DES EXEMPLAIRES DE CETTE THESE A LA DISPOSITION DES PERSONNE INTERESSEES.

THE AUTHOR RETAINS OWNERSHIP OF THE COPYRIGHT IN HIS/HER THESIS. NEITHER THE THESIS NOR SUBSTANTIAL EXTRACTS FROM IT MAY BE PRINTED OR OTHERWISE REPRODUCED WITHOUT HIS/HER PERMISSION.

L'AUTEUR CONSERVE LA PROPRIETE DU DROIT D'AUTEUR QUI PROTEGE SA THESE. NI LA THESE NI DES EXTRAITS SUBSTANTIELS DE CELLE-CI NE DOIVENT ETRE IMPRIMES OU AUTREMENT REPRODUITS SANS SON AUTORISATION.

ISBN 0-612-04864-0

Canada

UNIVERSITÉ D'OTTAWA
UNIVERSITY OF OTTAWA

I hereby declare that I am the sole author of this thesis.

I authorize the University of Ottawa to lend this thesis to other institutions or individuals for the purpose of scholarly research.

Mohammad M. Banat

I further authorize the University of Ottawa to reproduce this thesis by photocopy, or by other means, in total, or in part, at the request of other institutions or individuals for the purpose of scholarly research.

Mohammad M. Banat

Abstract

Several countermeasures to optical beat interference (OBI) in subcarrier multiplexed wavelength division multiple access (SCM/WDMA) networks are presented. The solutions studied in this thesis can be classified in two broad categories: one for which the objective is to expand the OBI spectrum by as much as possible, and one which can theoretically provide complete elimination of OBI. Using the first category of solutions, expanding the OBI spectrum results in less OBI power at the input of the electronic detection circuitry. Using the second category, OBI is reduced substantially by averaging out (using multimode fiber), or by addition and subtraction operations (balanced detection).

Increasing the laser intensity modulation index, polarization scrambling, and optical carrier frequency hopping constitute the main solutions in the first category. Balanced detection, and passing the optical fields through pieces of multimode fiber or through a depolarizer are two proposed solutions that theoretically offer OBI elimination.

For most of the solutions above, analytical expressions for well-known system performance measures are presented. Performance measures studied include average bit error rate, average carrier-to-interference ratio, and outage probability. Computer simulations and numerical analyses are used whenever appropriate to support or replace the analytical results. The multimode fiber method is verified experimentally, as well.

In deriving the signal-to-OBI ratio for the large modulation index solution, a large signal model is used for the first time to describe the laser behavior under direct intensity modulation. Such a model is needed because small-signal models do not provide accurate representation of the modulated laser spectrum at the modulation indices of interest here.

While each method discussed in this thesis offers a certain degree of OBI reduction, it is observed that optical frequency hopping (OFH) provides the most significant reduction. OFH is expected to be a very practical scheme in the near future; because the availability of tunable lasers is increasing, and their price is dropping.

Even further reduction in OBI power spectral density is expected to be achievable by optical spread spectrum, where the use of coherent ultrashort laser pulses can virtually eliminate OBI, and result in an extremely high network throughput. Such schemes are anticipated to become feasible countermeasures of OBI when all-optical processing becomes well-established.

Acknowledgements

I wish to express my sincere gratitude to my academic supervisor Professor Mohsen Kavehrad for his excellent scientific guidance and continuous moral support during the course of the program.

A very special word of thanks is due to my parents, brothers, and sisters in Jordan. Even though very far away, they provided me with the greatest possible support and encouragement.

The advice and constructive comments of my Ph.D. examining committee - Dr. R. I. MacDonald, Dr. W. Steenaart, Dr. J. -Y. Chouinard, and Dr. M. El-Tanany are very highly appreciated.

I am grateful to the Jordan University of Science and Technology and the Canadian International Development Agency for providing me with a joint scholarship to complete my studies at the University of Ottawa.

I would like to thank fellow members of the Lightwave Communications Research Laboratory at the University of Ottawa for the fruitful discussions and help. Special gratitude is due to Dr. Q. Jiang and Dr. R. Hui for their help with the experiment.

This research was partially supported by the Telecommunications Research Institute of Ontario, Photonics Networks and Systems Thrust. This support is highly appreciated.

Contents

List of Tables

List of Figures

Abbreviations

ASK	Amplitude Shift Keying.
AWGN	Additive White Gaussian Noise.
BER	Bit Error Rate.
BPF	Bandpass Filter.
CDMA	Code Division Multiple Access.
CIR	Carrier-to-Interference Ratio.
DBR	Distributed Bragg Reflector.
DD	Direct Detection.
DS	Direct Sequence.
FDMA	Frequency Division Multiple Access.
FH	Frequency Hopping.
FSK	Frequency Shift Keying.
FWM	Four Wave Mixing.
IF	Intermediate Frequency.
IMP	Intermodulation Products.
OBI	Optical Beat Interference.
OFH	Optical Frequency Hopping.
PD	Photodetector, Photodetection.

PN	Pseudonoise, Pseudorandom.
PSD	Power Spectral Density.
PSK	Phase Shift Keying.
RF	Radio Frequency.
Rx	Receiver.
SBS	Stimulated Brilouin Scattering.
SCM	Subcarrier Multiplexing.
SCM-CD	Subcarrier Multiplexing with Coherent Detection.
SCM-DD	Subcarrier Multiplexing with Direct Detection.
SCM-MOC	Subcarrier Multiplexing with Multiple Optical Carriers.
SCM-SOC	Subcarrier Multiplexing with a Single Optical Carrier.
SRS	Stimulated Raman Scattering.
TDMA	Time Division Multiple Access.
Tx	Transmitter.
WDMA	Wavelength Division Multiple Access.

List of Symbols

$\{a_n\}$	A set of coefficients used in the derivation of the characteristic function of the decision variable in a two-subcarrier/channel network.
$\{b_k\}$	A random variable of values ±1, representing the two possible phases in a polarization-scrambled SCM/WDMA network.
d	Height of the $LiNbO_3$ crystal in an electro-optic phase modulator.
$e(t)$	Sum of all electric field amplitudes coming into a photodetector.
$e_i(t)$	i -th user electric field amplitude.
$e_{i,n}^{(x)}(z)$	n -th mode component of the i -th user field spatial variation in the x polarization direction.
$e_{i,n}^{(y)}(z)$	n -th mode component of the i -th user field spatial variation in the y polarization direction.
$\vec{e}_{lo}$	Local oscillator electric field vector.
$\vec{e}_s$	Received signal electric field vector.
f_k	Microwave subcarrier frequency corresponding to user number k .
$g(t)$	A unit pulse function used in representing the transmitted signal in a polarization-scrambled network.
l	Length of the $LiNbO_3$ crystal in an electro-optic phase modulator.

m	Intensity modulation index.
$\overline{n}$	Effective refractive index.
n_{sp}	Spontaneous emission coefficient.
n_x	Refractive index of $LiNbO_3$ in the x direction.
n_z	Refractive index of $LiNbO_3$ in the z direction.
r_{ij}	The element in row i and column j of the elecrtooptic tensor of $LiNbO_3$.
$\hat{u}_{lo}$	Unit vector in the direction of the local oscillator field.
$\hat{u}_s$	Unit vector in the direction of the signal field.
$\hat{u}_x$	Unit vector in the x direction.
$\hat{u}_y$	Unit vector in the y direction.
$w(t)$	A single-frequency signal.
$x_i(t)$	Modulated subcarrier signal for user number i.
$\langle x \rangle$	Ensemble average of x.
$A^2(n)$	The n-th term coefficient in the infinite sum expression of $S_{e_i}(f)$.
B	Bandwidth of the electronic bandpass filter in the receiver.
C_{tot}	Total network throughput.
$C_{Z_c}(j2\pi\lambda)$	Characteristic function of the OBI component of the decision variable in a polarization-scrambled network.
$E_+(t)$	Sum of the input and the local oscillator field amplitudes in a

balanced detection receiver.

$E_{-}(t)$	Difference between the input and the local oscillator field amplitudes in a balanced detection receiver.
F_i	i -th user optical frequency.
F_{il}	$F_i - F_l$.
F_{lo}	Local oscillator optical frequency.
F_x	Optical frequency separation in a two-subcarrier/optical channel SCM/WDMA network.
F_L	optical frequency of channel number L.
$G_k(F_x, m_2)$	The k -th term in the sum expression of the OBI component of the decision variable in a two-subcarrier/channel polarization-scrambled network.
$G_{k+}(F_x)$	$G_k(F_x, m_2)$ for positive m_2 (positive data bit for the second user).
$G_{k-}(F_x)$	$G_k(F_x, m_2)$ for negative m_2 (negative data bit for the second user).
$H_{\text{det}}(f)$	Photodetector frequency response.
$H_k(f)$	Frequency response of the electric bandpass filter in the k -th user receiver.
I	Photodetector output current
$I_i(t)$	i -th user signal term in the photodetector output current.

$I_c(t)$	Cross-terms in the photodetector output current.
$I_{c_{il}}(t)$	Cross-terms in the photodetector output current due to beating of fields number i and l.
$I_s(t)$	Signal term in the photodetector output current.
$I_{sf}(t)$	Filter signal term in the photodetector output current.
$J_\nu(x)$	Bessel function of the first kind of order ν.
K	Ratio of bit duration to PN chip duration in a polarization-scrambled network.
K_{tot}	Total Spontaneous emission enhancement factor.
L	Number of modes in a multimode fiber.
$\mathbf{LP}\{\ \}$	Operator to take the lowpass component of the argument.
M	Number of subcarriers in an optical channel.
M_R	Maximum number of subcarriers/channel permissible in an OFH SCM/WDMA network with lasers tunable over a range R.
N	Number of optical channels in an SCM/WDMA network.
P	Output Power per laser facet.
$P(e)$	Probability of error.
P_{lo}	Local oscillator power.
P_{obi}	OBI power.
$P_{obi.R}$	OBI power in an OFH SCM/WDMA network with lasers tunable over a range R.

P_s	Signal power.
$P_{F_x}(e)$	Probability of error given a certain value of F_x.
$P_{F_x}(F)$	Probability density function of optical frequency separations.
$Q_{il}(k,n,r)$	The (n,r)-th term of OBI power at the output of the k-th user BPF due to the beating of fields number i and number l. This term is used in the large-signal model of modulated lasers. Its coefficient is $A^2(n)A^2(r)$.
$Q_{n,k}(F_x,m_2)$	A function used in the evaluation of $G_k(F_x,m_2)$.
R	Fluctuation range of the laser operating frequency.
R_p	Photodetector responsivity.
R_b	PSK modulation bit rate.
S_0	Unmodulated field intensity.
$S_{e_i}(f)$	Power spectral density of the i-th user field.
$S_i(t)$	i-th user electric field intensity.
$S_{il}(t)$	$S_i(t)-S_l(t)$.
$S_{lo}(t)$	Local oscillator field intensity.
$S_{obi,R}$	OBI power spectral density in an OFH SCM/WDMA network with lasers tunable over a range R.
$S_I(f)$	Power spectral density of photodetected current.
$S_{I;M}(f)$	Power spectral density of photodetected current in an M-

	subcarrier/channel SCM/WDMA network.
$S_{I_c}(f)$	OBI power spectral density.
$S_{I_s}(f)$	Power spectral density of the signal component of the photodetected current.
$S_{I_i}(f)$	Power spectral density of the i -th user photodetected current.
$S_w(f)$	Power spectral density of $w(t)$
T_b	Bit duration.
V_π	Voltage needed to induce a phase shift of π radians in an electro-optic phase modulator.
Z	Decision variable in the receiver.
Z_c	Cross-term component of the decision variable in the receiver.
Z_s	Signal component in the decision variable in the receiver.
α	Laser linewidth enhancement factor.
α_m	Mirror loss in a semiconductor laser.
β_n	Coefficient of the n -th term in the series expansion of the chirp component of the modulated laser phase.
$\delta(f)$	Dirac delta function.
γ	Signal-to-noise ratio.
$\varphi_i(t)$	i -th user field phase.
$\varphi_{lo}(t)$	Local oscillator phase.
$\varphi_{mi}(t)$	Chirp component of the modulated laser phase.

$\dot{\varphi}_{mi}(t)$	Time derivative of the chirp component of the modulated laser phase.
$\dot{\varphi}_{mi,1}(t)$	First component of the time derivative of the chirp component of the modulated laser phase.
$\dot{\varphi}_{mi,2}(t)$	Second component of the time derivative of the chirp component of the modulated laser phase.
$\dot{\varphi}_{mi,3}(t)$	Third component of the time derivative of the chirp component of the modulated laser phase.
$\varphi_{ni}(t)$	Phase noise component of the modulated laser phase.
$\varphi_{nil}(t)$	$\varphi_{ni}(t)-\varphi_{nl}(t)$.
φ_p	Phase shift due to polarization scrambling.
$\varphi_{pi}(t)$	Polarization fluctuation component of the laser phase.
$\varphi_{pi,k}$	Phase shift of the i-th user field due to polarization scrambling in the k-th PN chip duration.
$\varphi_{pil,k}$	$\varphi_{pi,k}-\varphi_{pl,k}$.
κ	Nonlinear power gain coefficient.
κ_s	Nonlinear photon number gain coefficient.
λ	Wavelength.
$\{\nu_n\}$	Set of frequencies used in the approximation of the OBI characteristic function.
θ	Phase quantity.

σ_{obi}^2	OBI variance at higher polarization scrambling rates.
τ_0	PN chip duration.
τ_{ph}	Photon lifetime.
ω_{lo}	Local oscillator radian frequency.
ω_s	Signal radian frequency.
$\xi(F_x)$	Indicator function used in the outage probability calculation.
ψ	Phase quantity.
Δf	Laser full width at half maximum (FWHM) linewidth.
$\Phi(f)$	Laser phase noise spectrum.
$\Phi^{(2)}(f)$	$\Phi(f)*\Phi(f)$.
$\Theta_{il}(f,n,r)$	$\Phi^{(2)}(f-nf_i+rf_l)+\Phi^{(2)}(f+nf_i-rf_l)$.

Chapter One

1. Introduction

1.1 Motivation

Ever since communication theory concepts started to be applied to practical information transmission systems, there has been a steady growth in the demand for higher system capacities. To a great extent, this is due to the ever increasing need of human beings for exchanging information in a wide variety of formats. As the theory advanced over the years, new technologies emerged to serve one of two purposes: provide more efficient use of existing transmission techniques and media, or facilitate the utilization of new transmission techniques and media. The most recent outcome of this progress is optical fiber communications.

Data transmission over optical fibers is capable of supporting very high bit rates; due to the huge bandwidth of the fiber itself. A single-mode optical fiber can potentially have a low-loss bandwidth as high as 30 THz in the wavelength ranges around $\lambda = 1.3\,\mu m$ and $\lambda = 1.55\,\mu m$. This vast bandwidth offers integration of a variety of high-capacity information signals, like voice, video, and computer data that can be transmitted

simultaneously over the same fiber. Abundance of fiber bandwidth makes it particularly useful for future wideband applications like video-on-demand.

In addition to large bandwidth, optical fibers have other interesting features that make them a very attractive medium for information transmission. Among these features are [1]: low loss, small size and bending radius, light weight, and immunity to radiative interference. Low loss is useful for data transmission over long distances. A good example of a long-distance system is an intercontinental undersea communication link. Losses on the order of 0.2 dB/km are easily achievable with today's fibers. Size and weight considerations are of special importance in situations when space is at a premium, such as in aircraft and ships.

In spite of the availability of fiber bandwidth, many system- and network-related factors can limit the exploitation of this bandwidth for data transmission. Fiber attenuation and nonlinearities and laser phase noise and frequency instability are a few of these factors. While there is room for improvement on the fabrication front, physical limits do exist. As a result of this fact, it seems inevitable that extensive research needs to be conducted to get the most out of the current state of the art of the fiber, laser, and other component technologies.

Simple cost-effective network and system designs that can make use of the fiber bandwidth while taking into account the limitations associated with it, are necessary. Many signal modulation formats and network architectures have been suggested to maximize the amount of data transmitted over the fiber's bandwidth. Most of these modulation formats and network architectures have roots in other well-established communication systems. While achieving the important goal of high capacity, a network must also have a

reasonable level of performance. This is significant in ensuring the reliability of information transmission over the network. As in all communication systems, optical communication performance is usually measured in terms of error rates, signal-to-noise ratios, and outage probabilities.

In this thesis, we study one of the simplest optical fiber networking systems. This system uses subcarrier multiplexing (SCM) along with wavelength division multiple access (WDMA). As it is often the case, the price of the simplicity of this system is a fundamental performance problem. Mixing (beating) of the multichannel signals in such a network results in the so-called optical beat interference (OBI). Optical beating arises in SCM/WDMA networks as a result of the nonlinear (square-law) nature of the light detection process. The presence of OBI in an SCM/WDMA network has the potential of degrading the network capacity and performance to unacceptable levels.

The most important fact about OBI is that it is a problem caused by nonlinearity, not just a problem in the photodetection stage, and not definitely just in the SCM/WDMA networks. This implies that OBI can be generated by any nonlinear phenomenon in any multichannel optical transmission environment. It also implies that the same family of solutions can be useful (to varying extents, somehow) in reducing OBI in all of these environments.

However, since there are many sources of nonlinearity in an optical network, and in order to present a reasonably good picture of OBI and its countermeasures, we limit our attention to the photodetector nonlinearity. This is not meant to underestimate the role of other network components (fibers, lasers, amplifiers, ..., etc.) in producing OBI-like effects.

With the above in mind, we investigate OBI in SCM/WDMA networks, and study several ideas to reduce the effects of this problem on the network performance and capacity. We also point to ideas that may not be quite feasible with today's components, but are very likely to be in the near future.

If there should be a last word in this section, one would say that optical communication still has a long way to go before it matures, and this is why so much is anticipated to be achievable with a steady progress in this field.

1.2 Optical Fiber Communications

Like other methods of signal transmission, optical fiber communications employs a number of transmitter and receiver designs. Among the many possibilities are analog versus digital modulation, and coherent versus noncoherent reception. The trend in modern communications systems is towards the use of digital modulation techniques like phase shift keying (PSK), frequency shift keying (FSK), and amplitude shift keying (ASK) [2]. One main reason for this trend is the possibility of digital multiplexing [2], which allows more information to be sent over the same medium. Another important reason is the possibility of incorporating error checking and correction coding, which enhances the information transmission reliability [2]. Coherent reception offers a better error rate performance compared to noncoherent reception. This is because the former utilizes the signal phase information in the detection process, while the latter ignores it.

The definition of coherent reception in optical communications is different from its definition in other communications systems. In optical communications, the coherence is both temporal and spatial. The received signal must be spatially coherent to a locally

generated reference signal [3]. In other words, both the received and locally generated signals must have the same polarization. If this condition is not satisfied, severe performance degradation may result. In non-optical communications systems, however, the coherence is only temporal. Optical coherent detection is shown schematically in Figure 1.1.

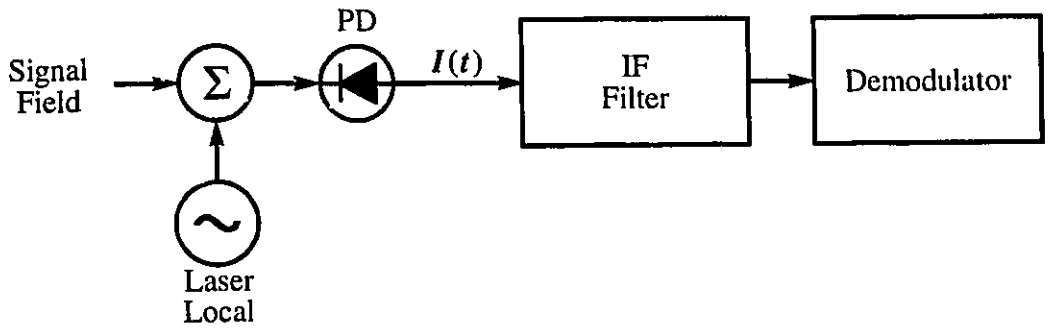

Figure 1.1: Optical coherent detection receiver

There is a significant performance advantage for coherent optical reception over the so-called direct detection (DD), which is a noncoherent scheme [3]. In direct detection, the received optical field is applied to a photodetector (PD). The PD generates a current that is proportional to the power (optical intensity) of the incoming field. In coherent detection, as shown in Figure 1.1, the incoming field is first added to a locally generated field which has the same polarization. The sum of these two fields is applied to a photodetector, which converts it into a current proportional to the sum field power. In general, this results in the so-called heterodyne detection. However, in the special case when both the frequency and the phase of the local laser are locked to those of the received field, the process is called homodyne detection. There is a 3 dB performance

advantage for homodyne detection over heterodyne detection [3]. However, the former is much more difficult for realization [3]. The performance advantage of coherent detection over direct detection is due to two factors: the gain resulting from the use of a high-power local laser signal, and the use of sophisticated modulation schemes that are superior to intensity modulation [3]. Such modulation schemes include PSK and FSK, among others. Another advantage of coherent detection is that it allows for increased frequency selectivity [3]. This feature is important for multiwavelength transmission. In spite of these advantages, coherent reception is a rather complicated scheme; because it requires elaborate received and reference field polarization alignment, and sophisticated circuitry for the stabilization of the received optical field carrier frequency. It also requires a high-power local laser to generate the reference field. Restrictions on source and local laser spectral characteristics such as linewidth and FM response also exist. With this discussion in mind, the need for simple optical communication systems that achieve a good error rate performance is apparent.

To see the importance of polarization matching between the received and the local laser fields in a coherent optical receiver, assume these fields to be linearly polarized and given by [4]:

$$\vec{e}_s = \hat{u}_s \sqrt{P_s} e^{j\omega_s t + \theta} \tag{1.1}$$

and

$$\vec{e}_{lo} = \hat{u}_{lo} \sqrt{P_{lo}} e^{j\omega_{lo} t} \tag{1.2}$$

where P_s and P_{lo} are the received and local laser powers, respectively, ω_s and ω_{lo} are their respective frequencies, θ is the relative phase between them, and $\hat{u}_s$ and $\hat{u}_{lo}$ are unit

vectors in the directions of the field polarizations. The two polarization unit vectors are assumed to have an angle of ψ between them. This relation may be expressed as:

$$\hat{u}_s \cdot \hat{u}_{lo} = \cos\psi \tag{1.3}$$

Detection of the combined field by a photodetector of responsivity R_p produces:

$$\begin{aligned} I &= R_p\left|\vec{e}_s + \vec{e}_{lo}\right|^2 \\ &= R_p\left[P_s + P_{lo} + 2\sqrt{P_s P_{lo}}\cos\psi\cos\left[(\omega_{lo} - \omega_s)t - \theta\right]\right] \end{aligned} \tag{1.4}$$

Note that in eq. (1.4), the only term needed for information extraction is the last one, which depends vitally on the polarization angle difference. It is easy to visualize the severe degradation that can result from this term in the case of any polarization misalignment. For instance, when $\psi = \pi/2$, that term is zero, and the signal cannot be detected.

In a multiuser environment (e.g., a communications network), the issue of system error rate performance cannot be separated from the issue of network throughput (total bit rate transmitted over the network). In other words, the optimum optical network has as high a throughput as possible, and as low a bit error rate as possible. Other important features of networks like the transmission delay and blocking probability are beyond the scope of this thesis. In the next two sections, we look at optical networking and optical multiplexing schemes associated with optical networks.

1.3 Optical Networking

The demand for exchanging large amounts of data in various forms among many users makes networking an indispensable element of today's telecommunications. With the availability of a wide transmission bandwidth, the use of point-to-point links would

represent a waste of resources. Optical networking aims at taking maximum advantage of the fiber bandwidth to provide new services to the end user, as well as to provide the existing services in a more efficient and in a higher-quality manner.

To coordinate network access and services, some switching mechanism has to be employed. This can serve the following purposes [5]:

1. using data processing equipment to efficiently share the total network resources.
2. reducing the number of connections needed to link all the users on the network.
3. allowing various combinations of users to communicate at different times.

Essentially, two kinds of switching exist [5]: circuit switching and message switching. The latter is alternatively referred to as the store-and-forward technique [6]. In circuit switching, widely used in telephony, a communication link is established between two network users as long as it takes them to complete their call [5], [6]. In message switching, a call is entirely received and stored before it is forwarded to the destination user [5]. Packet switching is a variation of message switching in which messages transmitted over the network are segmented into limited-size blocks known as packets [6]. For data communications, packet switching is more convenient than circuit and message switching for several reasons [5], [6] among which are:

1. Data communications usually takes the form of exchanging messages among computers (electronic mail, file transfer, ..., etc.).
2. Small size of packets makes packet switching require less storage.
3. Likelihood of blocking a small packet at a node on the network is much less than that of a whole message.

4. Less average end-to-end transmission delay.
5. Dynamic and fair allocation of the bandwidth.
6. More efficient error correction; because of the smaller size of packets.

1.4 Optical Multiple Access Methods

Multiple access provides the ability of simultaneous transmission of a multitude of signals that occupy the same spectral range over the same communications medium with a minimal or no interference among these signals. Several multiple access methods have been studied for both optical and non-optical systems. The main multiple access schemes are:

1. Time Division Multiple Access (TDMA)
2. Code Division Multiple Access (CDMA)
3. Frequency Division Multiple Access (FDMA)

While these multiple access schemes are common to all kinds of communications systems, there are some other schemes unique to optical communications. Among these are:

1. Wavelength Division Multiple Access (WDMA)
2. Space Division Multiple Access
3. Polarization Multiplexing
4. Subcarrier Multiplexing (SCM)

In the following subsections, the main optical multiple access methods will be briefly covered. The objective of this discussion is to emphasize and justify the strong trend towards the wide use of WDMA as the ultimate optical multiple access method.

1.4.1 Time Division Multiple Access

In optical time division multiple access (TDMA), transmission time is divided into slots, each assigned to one of the signals to be multiplexed [7]. In each time slot a sample of the assigned signal is transmitted. A block diagram illustrating this process appears in Figure 1.2 [7]. The optical transmitter and receiver in each user branch are shown in Figure 1.3 and Figure 1.4, respectively. The sampler in Figure 1.3 converts the incoming data into lower duty cycle pulses which are placed in their proper time slots by the multiplexer.

In a TDMA network, all user signals have the same bit rate R_b. If such a network has M users, the clock source must have a rate of MR_b. As the demand for more users and higher bit rates continues, TDMA becomes less and less practical, because of the physical limitations on electronic switching times. Using optical processing is suggested in [8] to reduce the bit rate limitation in TDMA.

Another difficulty with TDMA is the required synchronization among the network users. Each transmitter has to send a sample only in its own time slot. The assignment of time slots can be fixed or varying. In both cases, the required synchronization circuitry can be very sophisticated, especially at high bit rates.

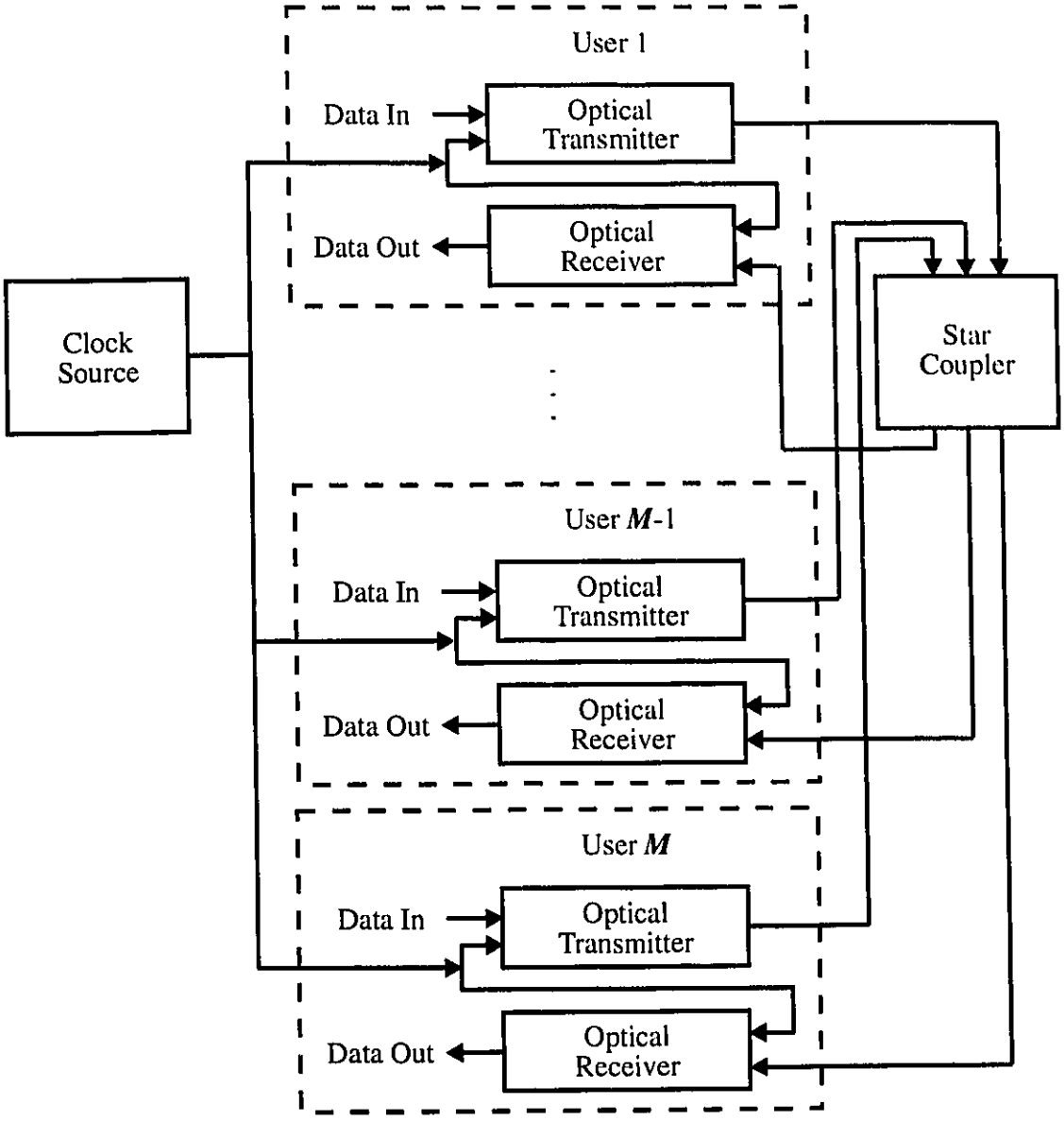

Figure 1.2: TDMA or CDMA network block diagram

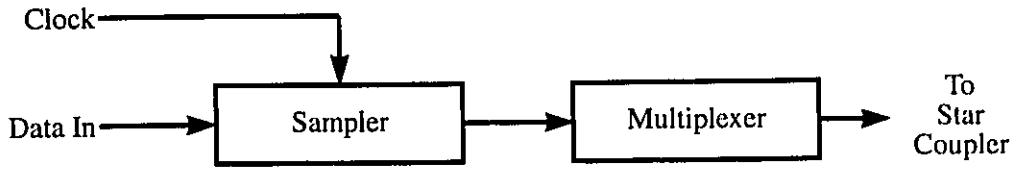

Figure 1.3: TDMA transmitter

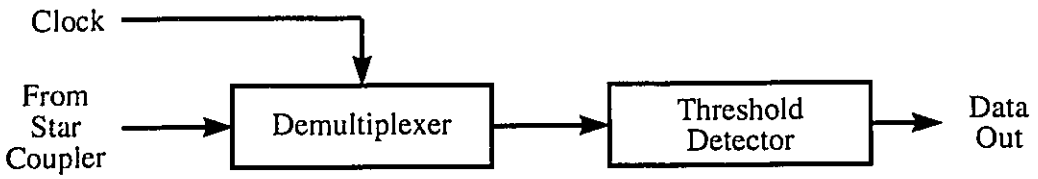

Figure 1.4: TDMA receiver

1.4.2 Code Division Multiple Access

In a CDMA network, each user is assigned a unique code sequence which is used in preparing that user's data for transmission [9]. This can be done in several ways, the two most used of which are direct sequence (DS) and frequency hopping (FH). The block diagram of a network based on CDMA is shown in Figure 1.2 [7]. The transmitter and receiver in each user branch are shown in Figure 1.5 and Figure 1.6, respectively.

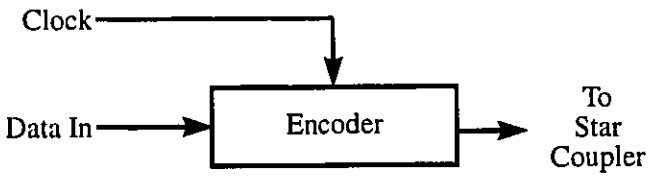

Figure 1.5: CDMA Transmitter

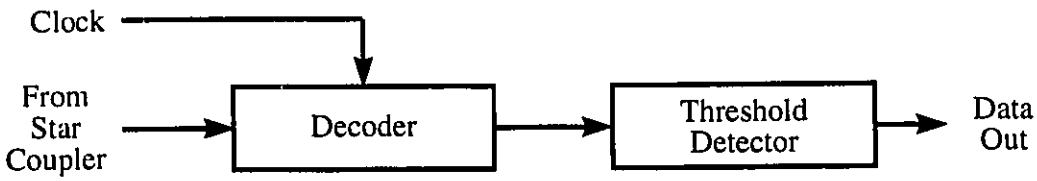

Figure 1 6: CDMA Receiver

If direct sequence is used, the data to be transmitted is modulo-2 added to the code sequence. The resulting pattern is then used in the subsequent transmission stages instead of the original data. If frequency hopping is used, the carrier frequency during the data bit to be transmitted is shifted by an amount that depends on the code sequence.

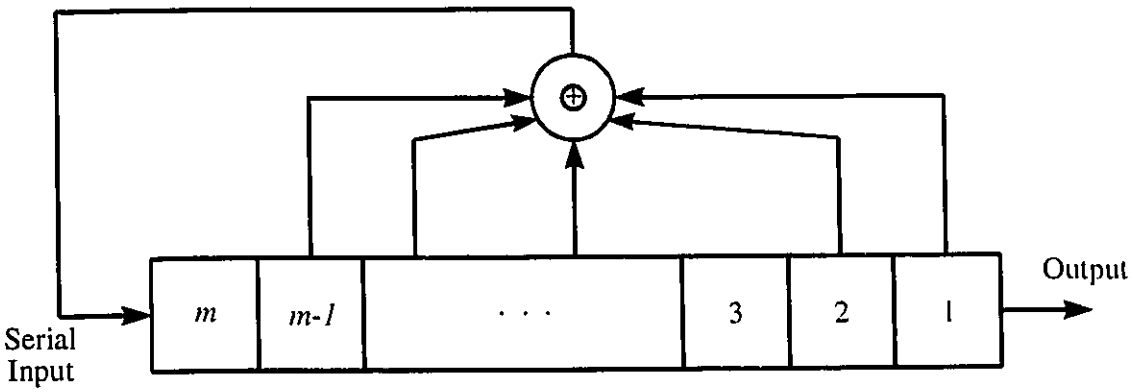

Figure 1.7: Maximal-length code sequence generator

Code sequences used in CDMA are usually pseudorandom (PN). Well-known maximal-length PN sequences are the simplest choice [9]. A maximal-length code sequence generator is shown in Figure 1.7 [10]. Other kinds of code sequences include Gold and Kasami sequences [10]. In all these cases, the code sequence has to have the following properties:

1. Its rate has to be much higher than the bit rate of the user data to be transmitted. This has to be the case in order to reduce interference among users. The ratio of the code sequence rate to the information rate provides a measure of interference suppression. This ratio is often referred to as the processing gain.

2. It has to be unique, no two users on one network can have the same code sequence. This is because the code sequence is considered an address for the destination receiver.
3. It has to have a high autocorrelation and low cross-correlation with other sequences used in the same network. This is needed to minimize interference among users at a given code sequence rate.
4. A transmitter has to use the same code sequence used in the receiver to which the information is being sent. At the receiver, any signal that does not have the right code sequence will look like interference. Thus, the code sequences at the transmitter and at the intended receiver have to be time synchronized.

Maximal-length sequences have good correlation properties. Figure 1.8 shows these correlation properties. The solid curve with a peak around zero lag represents the autocorrelation function of a PN sequence of period 31 which is generated by a five-stage shift register. The period and the peak autocorrelation of a maximal-length sequence generated by an n-stage shift register are both equal to $2^n - 1$. A peak autocorrelation value of 31 can be seen in Figure 1.8. The dotted curve represents the correlation of the same sequence above with a shifted version of itself. The dashed curve represents the cross-correlation of two different sequences generated by the same five-stage shift register using two different feedback tap connections.

Maximal-length sequences are easy to generate (using shift registers). However, the number of maximal-length sequences possible to produce with a certain number of shift register stages is small [11]. Gold and Kasami sequences, which are derived from maximal-length sequences [10], can offer a lot more unique sequences with good correlation properties.

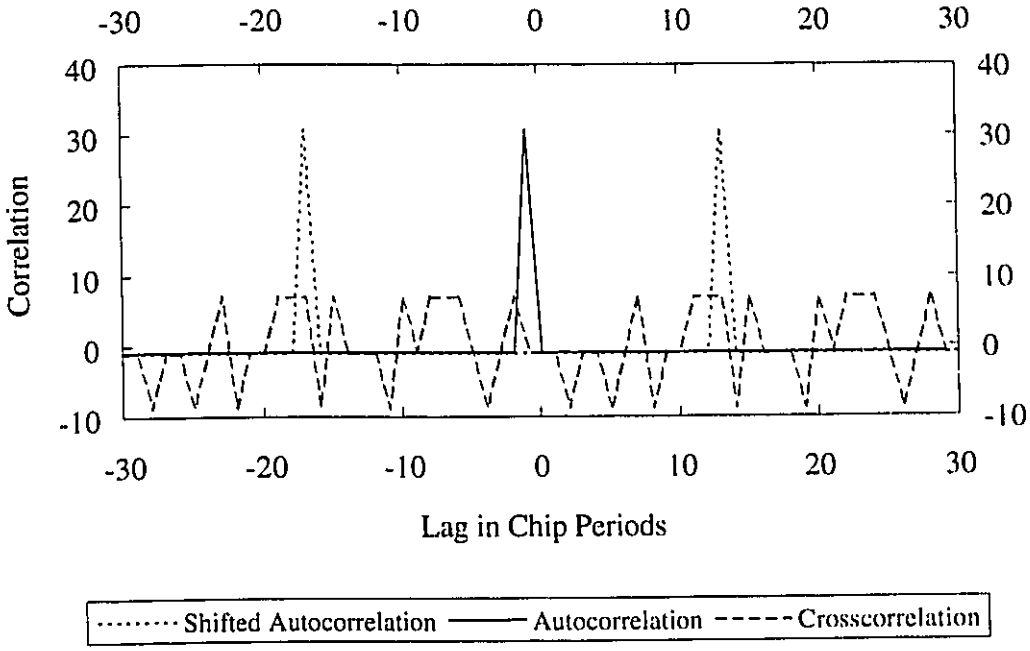

Figure 1.8: Autocorrelation and cross-correlation of PN sequences

Optical frequency hopping has not been widely used so far; because of the many difficulties associated with a laser tuning speed and range, laser frequency stabilization, and laser frequency chirp and transients. Laser tuning time is currently on the order of 1 ns, and its tuning range is around 1000 GHz [12]. Some work on optical frequency hopping has been reported [13], however. In the coming paragraphs, wherever CDMA is mentioned, direct sequence is implied.

It should be emphasized that code sequences in optical CDMA are usually of the one-zero type. The reason behind this is the need to correlate the received signal with the receiver's code sequence. Correlation at the receiver has so far been done using fiber delay lines which act as power combiners and can have only positive or zero coefficients [11]. CDMA systems with one-zero code sequences and power combining fiber delay line

correlators are referred to as incoherent CDMA systems. The so-called optical orthogonal codes [14]-[16] were developed to work with such systems. Other work on incoherent CDMA has also been reported [17]-[22].

Coherent all-optical CDMA using electro-optic phase modulators was reported in [23]. The advantage of coherent CDMA over its incoherent counterpart can be illustrated as follows [24]: Bipolar code sequences used in coherent CDMA have drastically better correlation properties than unipolar sequences used in incoherent CDMA. This results in a much less interference among the users in a coherent CDMA network. In addition to that, the number of bipolar code sequences that can be generated with a given code generator complexity is a lot higher than the corresponding number of unipolar sequences. This allows many more users to be accommodated on the network. Coherent CDMA using ladder networks has been reported in [25], [26].

The same argument made for TDMA requirements regarding clock rate and synchronization holds true for CDMA. The two schemes are limited by the physical switching properties of electronic devices.

1.4.3 Frequency and Wavelength Division Multiple Access

FDMA and WDMA share the same multiplexing principle. A general block diagram of a WDMA or FDMA network is shown in Figure 1.9. Both schemes divide the optical spectrum into channels each assigned to one user in the network.

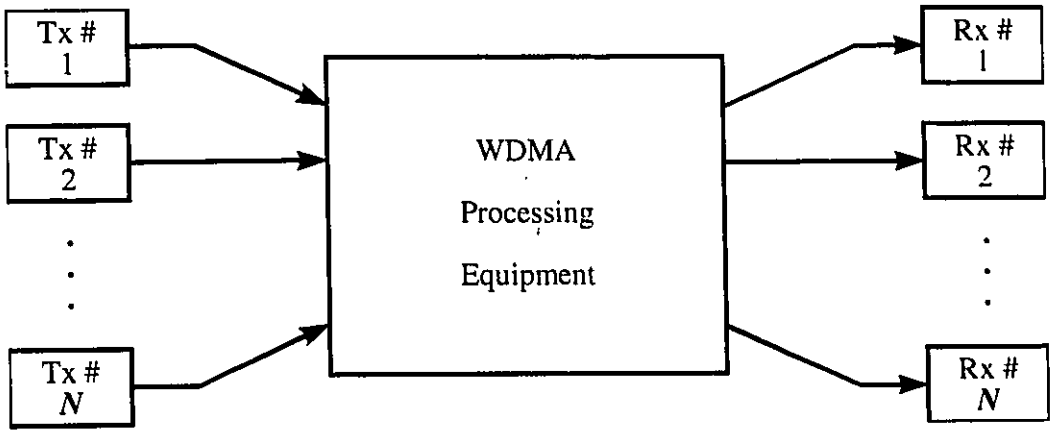

Figure 1.9: General WDMA network block diagram

The distinction between FDMA and WDMA depends on the spacing between adjacent channels [27], [28]. The channel spacing in FDMA is about 0.1 nm [27] which is on the order of the signal bandwidth [28]. A channel spacing on the order of 1 nm results in dense WDMA [27], [28]. Higher channel spacings result in conventional WDMA [27], [28] which was originally introduced to upgrade the capacity of existing point-to-point systems [28].

While a large channel spacing leads to an inefficient use of the fiber bandwidth, a small channel spacing (FDMA, for instance) can lead to limitations on the signal power and transmission distance. Such limitations may arise from nonlinear interactions between the signal and fiber [29]. The small core size and the low loss of a single-mode fiber result in signals with high intensities and long interaction lengths [30]. These nonlinearities can result in crosstalk among channels, which is one of the sources of optical beat interference, namely, the main problem addressed in this thesis. The three most important kinds of nonlinear signal-fiber interactions are four wave mixing (FWM), stimulated Brillouin scattering (SBS), and stimulated Raman scattering (SRS). For a channel separation of

about 10 GHz and a fiber length of about 100 km, SBS is the limiting nonlinear effect in the fiber. As the number of channels increases further and further, FWM and SRS become dominant [30].

Another important source of limitation to FDMA is laser phase noise [31]. For externally-modulated lasers, the permissible FDMA channel spacing increases with the sum of the laser linewidth and the signal bit rate. In the case of a directly-modulated laser, additional factors, like frequency chirp, affect FDMA minimum channel spacing [32]. Although using multilevel signaling increases the spectral efficiency of radio systems [10], however, it was shown in [33] that multilevel signaling does not affect the spectral efficiency of optical FDMA systems.

WDMA network architecture can generally have one of the two forms: wavelength routing and broadcast-and-select [28]. In wavelength routing WDMA networks, the signal path through the network depends on the source user and the transmission wavelength [28]. For instance, If the block diagram in Figure 1.9 is to represent a four-user wavelength routing WDMA network, then a possible interconnection scheme that uses only four wavelengths (rather than sixteen) may look like the one given in Table 1.1 [28]. The information in Table 1.1 can be interpreted as in the following examples: user number 1 sends to user number 3 on wavelength λ_3, while user number 4 sends to user number 1 on wavelength λ_4.

	Rx # 1	Rx # 2	Rx # 3	Rx # 4
Tx # 1	λ_1	λ_2	λ_3	λ_4
Tx # 2	λ_2	λ_1	λ_4	λ_3
Tx # 3	λ_3	λ_4	λ_1	λ_2
Tx # 4	λ_4	λ_3	λ_2	λ_1

Table 1.1: A 4×4 wavelength routing WDMA network interconnection scheme

Broadcast-and-select WDMA can also be represented by Figure 1.9, where transmitters, receivers, or both can be tunable [28]. A signal sent to one receiver on the network is broadcast to all the receivers, but only the one operating at the right wavelength can detect it.

Both wavelength routing and broadcast-and-select WDMA networks belong to the so-called single-hop class of multiple access networks. The signal is sent directly to the receiver without stopping at intermediate nodes. The need for tunable transmitters (lasers) and tunable receivers (filters) in single-hop networks motivated the search for a different approach which uses a less sophisticated technology. Multihop networks evolved as a result of this trend [34]. In a multihop network, the signal is received by intermediate nodes before it is finally routed to the destination node. The need for tunable transmitters and/or receivers is alleviated in this class of networks.

Using the multihop approach, the logical connectivity graph of an N -user WDMA network consists of k columns each with p^k nodes, where each node has p transmitters and p receivers [34]. This configuration is called a (p,k) ShuffleNet [35]. An 8-user

multihop WDMA network can be arranged using the so-called perfect shuffle connectivity as in Figure 1.10, where each node has two transmitters and two receivers.

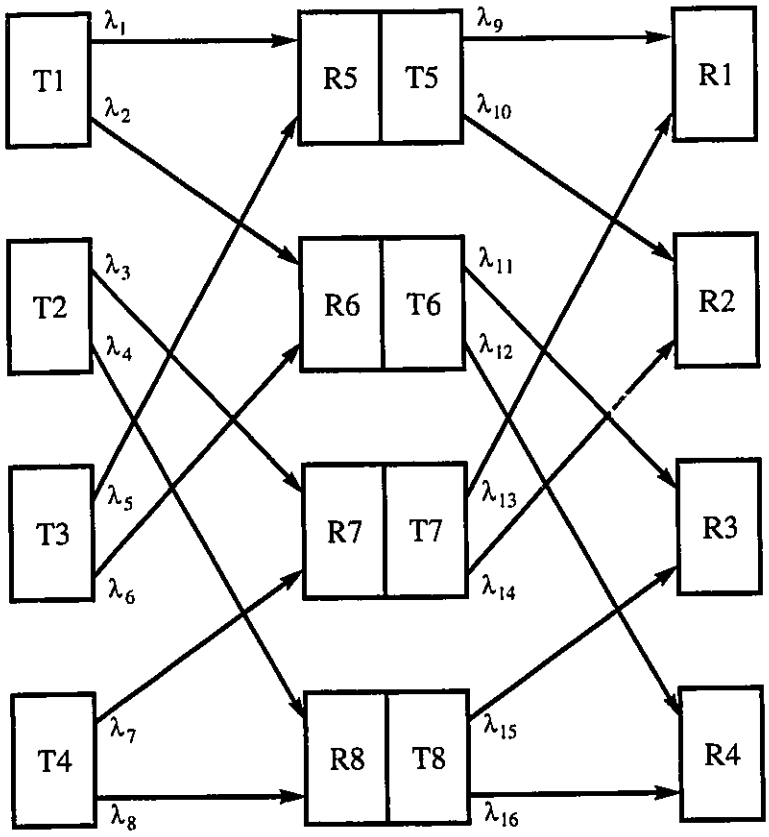

Figure 1.10: Perfect shuffle connectivity graph for an 8-user multihop WDMA network

While a (p,k) ShuffleNet appears to need kp^{k+1} wavelengths [34] in the conventional topology of Figure 1.10, It was shown in [35] that only p wavelengths are actually needed if WDM cross-connects [35] are used. The proposed topology in [35] overcomes two other significant limitations of the familiar star topology. These limitations are the star coupler $1/N$ power splitting loss, and the need for filtering at the receiver inputs. The design of an integrated-optic WDM cross-connect is detailed in [36].

In light of the above discussion, WDMA appears to be the ultimate multiple access choice for tapping the huge bandwidth offered by the fiber. While both TDMA and CDMA critically depend on the rate of clock signals to achieve higher capacities, WDMA depends on segmenting the fiber bandwidth into as many channels as desired, and on reuse methods of wavelength. One of the simplest wavelength reuse strategies is shown in Table 1.1. Currently, electronic switching speed is almost at its physical limits. Clock rates higher than a few Gb/s are very difficult to achieve. Photonic switching is still in a very early stage of development, and it has physical limits, too.

1.4.4 SCM/WDMA

In subcarrier multiplexing (SCM), the transmitted signal is generated in two stages. First, several microwave subcarriers are modulated by user data. Second, the resulting microwave signals modulate the optical carrier [37]. Some of the advantages of SCM are:

1. It can take advantage of the well-established microwave radio modulation and demodulation techniques and devices [37].
2. Subcarrier channels are independent, hence, there is no need for synchronization among them using, for instance, a high-speed master clock source [37].
3. Individual subcarrier channels can have different formats of analog or digital modulation.
4. SCM does not need very sharp optical filters at the receiving side.

All microwave subcarriers can modulate one optical carrier [38], or each one of them can modulate a separate optical carrier [39]. SCM with a single optical carrier (SCM-SOC) is illustrated in Figure 1.11, while SCM with multiple optical carriers (SCM-

MOC) is illustrated in Figure 1.12. Optical carriers in an SCM-MOC configuration have the same average center frequency.

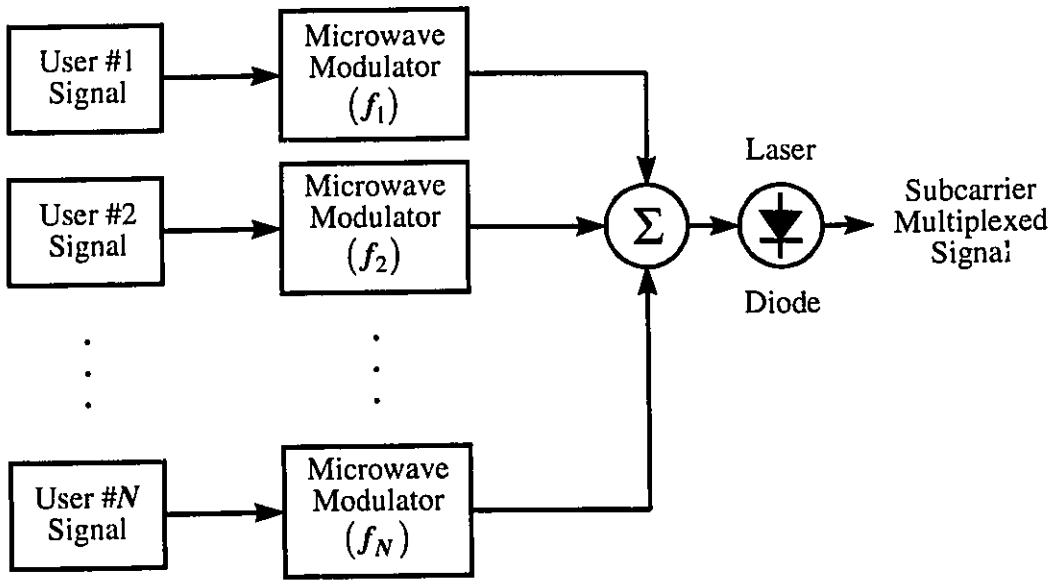

Figure 1.11: Subcarrier multiplexing with a single optical carrier (SCM-SOC)

Both single-optical-carrier and multiple-optical-carrier SCM can be used in conjunction with coherent detection [40]-[43], or direct detection [38], [39], [44]-[50]. While coherent detection of SCM signals (SCM-CD) offers a better performance than direct detection SCM (SCM-DD), the latter has several features that make it simpler, less expensive, and hence, more attractive. Among these features are:

1. SCM-DD systems avoid the sophistications in coherent detection such as laser frequency stabilization.
2. In SCM-DD, there is no need for polarization alignment between the incoming signal field and a local field. Such polarization alignment would normally require the use of a polarization maintaining fiber or a polarization controller.

3. Laser linewidth and frequency modulation response are not factors in direct detection systems [37], so less expensive lasers could be used.

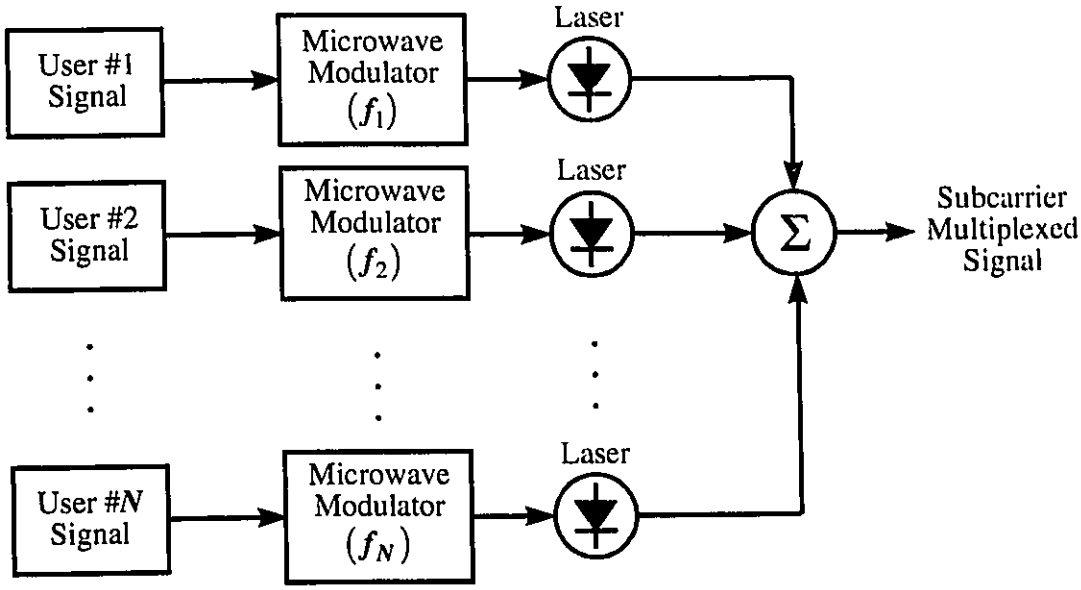

Figure 1.12: Subcarrier multiplexing with multiple optical carriers (SCM-MOC)

A multiple access scheme that benefits from the advantages of both WDMA and SCM is a hybrid of both, as among other places was suggested in [47]. This scheme is called subcarrier multiplexing wavelength division multiple access (SCM/WDMA). Two levels of multiplexing are employed: subcarrier multiplexing (SCM), and wavelength division multiple access (WDMA). In the WDMA step, the optical bandwidth is divided into a number of nonoverlapping channels. The result is an ordinary WDMA network. Hence, any of the network architectures discussed in the previous subsections can be applied to it. Channel spacing can be adjusted for optimized performance and throughput; depending on the network architecture, and devices and components used.

If SCM with a single optical carrier is used (Figure 1.11), then each user signal modulates a separate RF subcarrier which has a unique frequency. The modulated subcarriers are then summed and used to modulate a laser operating at one of the optical wavelengths chosen in the WDMA step. If SCM with multiple optical carriers is to be used (Figure 1.12), then each of the modulated subcarriers modulates a separate laser. However, in SCM-MOC, several lasers can operate at the same wavelength. The same number of channels can be achieved with both schemes. Laser modulation can be coherent or noncoherent, and it can be direct or external. The hierarchy of multiplexing levels in SCM/WDMA is shown in Figure 1.13.

The subject of this thesis is SCM/WDMA with multiple optical carriers. However, a brief comparison with the single-optical-carrier approach is in order. In the latter, the number of subcarriers per optical channel cannot be increased indefinitely. Intermodulation products (IMP) interference poses a serious limit on the number and frequency distribution of subcarriers modulating a laser [45]. Using SCM with multiple optical carriers, IMP interference is not present, however, another problem called optical beat interference (OBI) can be a source of significant limitations on the performance and throughput of SCM/WDMA networks with multiple optical carriers. The OBI problem is investigated in this thesis. Several solutions to eliminate or reduce OBI are presented throughout the forthcoming chapters.

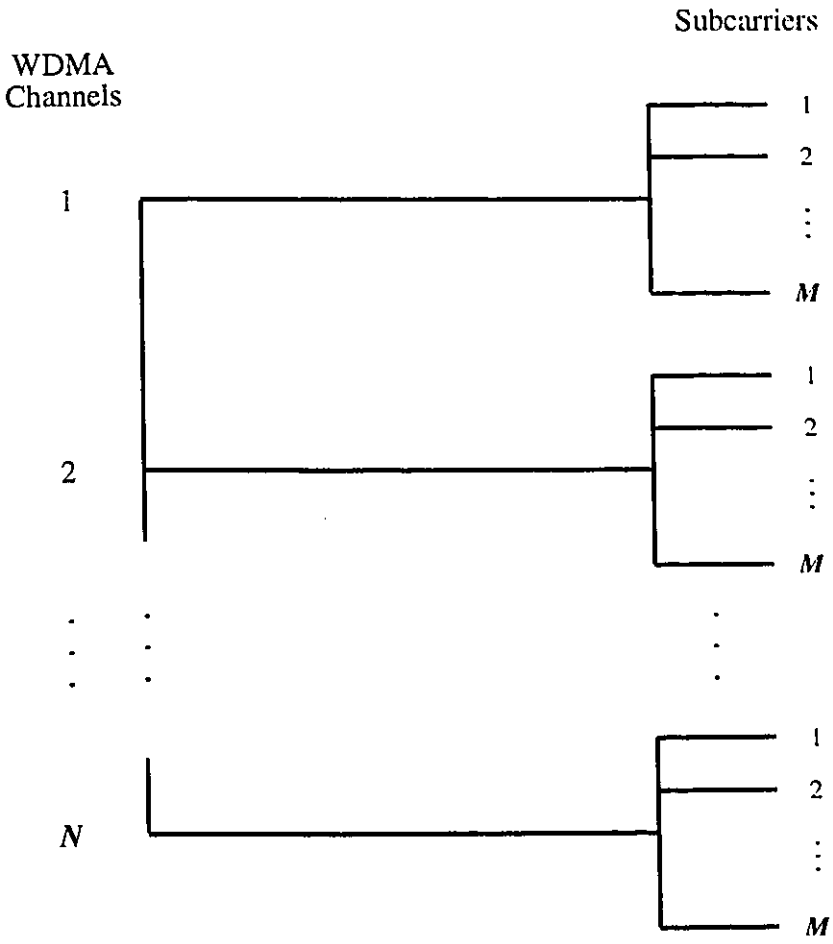

Figure 1.13: Hierarchy of SCM/WDMA multiplexing schemes

The greatest advantage of SCM/WDMA is its natural growth capability, i.e., new users can be accommodated by the network without modifying the existing architecture. This can be done by simply adding new optical channels (Figure 1.13). More users can, as well, be added to any optical channel by introducing more subcarriers. This capability is not available as easily to other multiple access methods, where adding more users may require basic changes to the network architecture. In summary, SCM/WDMA offers a cost-effective means to make best use of the optical bandwidth.

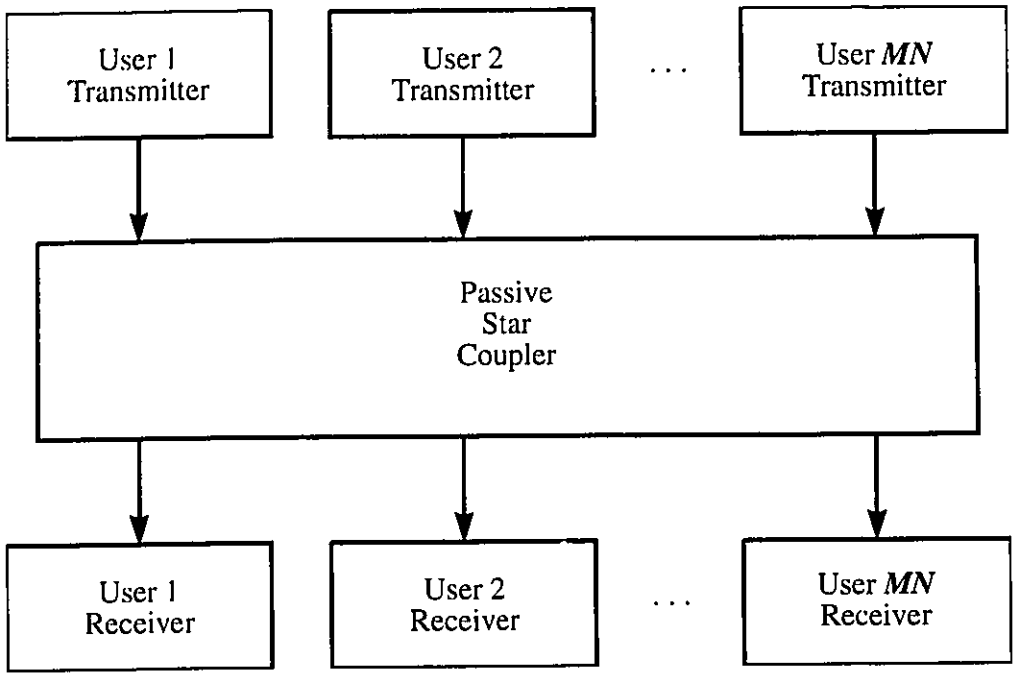

Figure 1.14: SCM/WDMA general block diagram

A block diagram that illustrates an SCM/WDMA system is shown in Figure 1.14. As shown, a key component of the system is a passive star coupler. Although N wavelengths are used, the system supports communications links for MN users, as opposed to only N links in the case of conventional WDMA or FDMA. To send to user number k on optical channel number L, the sending party has to use optical carrier frequency F_L modulated by a subcarrier at f_k.

1.5 Contributions

The following is a list of contributions in this thesis:

1. Presenting SCM/WDMA with direct detection as a simple, cost-effective networking system for data transmission over optical fibers.

2. Studying the optical beat interference problem in SCM/WDMA networks and highlighting its effects on network capacity and performance.
3. Evaluating several novel solutions to OBI. Solutions can be classified in two broad categories:
   a) OBI removal. Solutions in this category include techniques that are ideally capable of canceling out OBI. This category of solutions includes:
      i) Balanced detection
      i i) Using a piece of multimode fiber
   b) OBI reduction. Solutions in this category tend to spread the OBI spectrum such that only a fraction of its power can interfere with signal terms in subsequent detection stages. This category of solutions includes:
      i) Increasing laser intensity modulation index
      i i) Polarization scrambling
      i i i) Optical frequency hopping
4. Development of a large-signal model to calculate the spectrum of a directly intensity modulated laser. This model is based on rate equations.
5. Experimental verification of the effect of mode scrambling on the OBI.

1.6 Thesis Outline

The sources of OBI are first identified in section 2.1. OBI is mathematically modeled in section 2.2. The effect of OBI on SCM/WDMA network performance is presented in section 2.3, before proceeding to discuss the proposed solutions in the subsequent parts of the thesis. The suggested solutions to the OBI problem can be divided

in two groups: those which require laser frequency locking, and those which do not. Because laser frequency stabilization is difficult at the present state of the art, the first group of solutions tends to be more complicated than the second one. Hence, one solution that belongs to that group will be summarized in section 2.4, while separate chapters are devoted to each of the second group solutions. Balanced detection is considered as a possible solution to OBI using frequency-locked lasers.

In Chapter 3, we elaborate on the effect of large laser modulation index on the system performance. A large-signal model is used for the first time to compute the modulated laser field spectrum. The result is used to derive the interference spectrum from which expressions and plots for the output carrier-to-interference ratio (CIR) are obtained. The effects of laser linewidth on OBI are also discussed in Chapter 3. In Chapter 4, polarization scrambling is used to reduce OBI. Analytical and simulation results that demonstrate this method are presented. Use of multimode fiber to eliminate OBI is described in Chapter 5. Mathematical and experimental results are discussed. In Chapter 6, optical frequency hopping is considered as another solution to the OBI problem. Simulation results which illustrate the strength of this technique are presented. Finally, Chapter 7 presents main conclusions of this thesis and suggestions for further research. In future work, use of optical spread spectrum is expected to drastically reduce OBI and achieve extremely high network throughputs. Several spread spectrum ideas are listed in section 7.2. Most of these methods make use of ultrashort laser pulse technology and ultrafast optical logic circuits.

Chapter Two

2. The Optical Beat Interference Problem

2.1 Sources of OBI

The problem addressed in this thesis is called optical beat noise or optical beat interference (OBI). If the optical signal passes through a nonlinearity, mixing among optical carriers occurs, resulting in undesired cross-terms. Sources of such a nonlinearity are almost countless. Examples include nonlinear phenomena in the fiber [30], optical amplifier crosstalk and intermodulation [51], and square-law detection by the photodetector (PD) [44]. The focus of this thesis is on SCM-MOC/WDMA networks. In this kind of network, cross-terms, and hence, OBI produced by mixing of subcarriers can occur as well. Mixing of subcarriers results when the SCM/WDMA signal is directly detected at the photodetector. To see that, consider the function of the PD in one of the user receivers shown below in Figure 2.1. A total of M optical fields is present at the photodetector input. Because of the square envelope detection law, we would expect at the photodetector output M terms representing the field intensities, plus $M(M-1)$ cross-terms. If the spectral content of any one of these cross-terms falls within the passband of the bandpass filter in the intended user channel, it will cause interference. As

will be shown, the power spectral density of the cross-terms is comparable to that of the desired signal, hence, optical beat interference can represent a serious limitation on the transmission capacity.

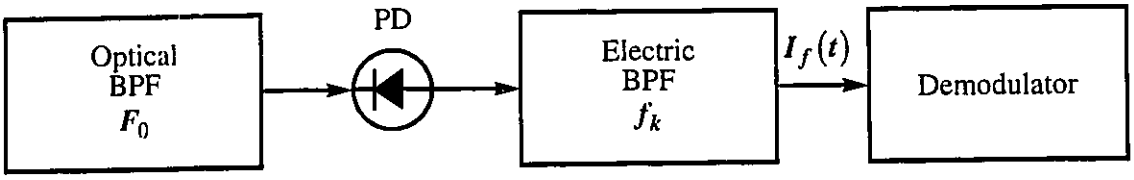

Figure 2.1: Reference user receiver

Since OBI is the result of the presence of cross-terms at the input of electronic detection circuitry, and since all sorts of nonlinearities tend to produce cross-terms; the emphasis of this thesis will be on OBI caused by direct photodetection. All other kinds of OBI produce the same type of effects on network performance and throughput, and all of them can be eliminated or reduced using the same techniques.

OBI has been defined and briefly studied in a few references [44], [46], [48]-[50]. Limited previous attempts have been made to reduce OBI. In [48] and [50], some work is reported on the effect of laser intensity modulation index on SCM system OBI performance. Changing the laser direct intensity modulation index was employed. It was found that larger modulation indices result in lower OBI. However, there are certain limits beyond which the modulation index cannot be increased. Laser nonlinearity is an important factor in this respect. Besides, it is physically impossible to get an intensity modulation index larger than unity.

In this thesis, we present several new solutions to the OBI problem. Most of these solutions are based on the idea of broadening the OBI spectrum, so that less interference power will appear at the intended user bandpass filter at the front end of the electronic processing circuitry.

2.2 Mathematical Definition of OBI

As suggested by Figure 1.13 , M optical fields in a given optical channel have the same average center frequency. However, the simultaneous optical frequencies are generally different and can be randomly varying with time. The amplitude of each of these fields can be represented by:

$$e_i(t) = \left[S_i(t)\right]^{1/2} \cos\left[2\pi F_i t + \varphi_i(t)\right] \tag{2.1}$$

where the intensity modulation by an RF subcarrier is represented by:

$$S_i(t) = S_0\left\{1 + m \cdot x_i(t)\right\} \tag{2.2}$$

where $x_i(t)$ can have any form of digital or analog modulation, and where m represents the intensity modulation index. The additional phase $\varphi_i(t)$ of the electric field in eq. (2.1) can have a chirp component $\varphi_{mi}(t)$ in the case of direct laser modulation, a phase noise component $\varphi_{ni}(t)$ modeled by a Wiener-Levy process, and possibly a random component $\varphi_{pi}(t)$ due to polarization fluctuation. Hence, the total phase can be written as:

$$\varphi_i(t) = \varphi_{mi}(t) + \varphi_{ni}(t) + \varphi_{pi}(t) \tag{2.3}$$

The front end of the reference receiver (corresponding to user number k), as shown in Figure 2.1, is an optical filter centered on the optical carrier frequency of the

intended user WDMA channel. As a result, out of a possible total of MN optical fields coming into the optical filter, only M continue their way to the photodetector. The center frequency of the optical filter in the reference receiver will be denoted by F_0. All M users in the same optical channel will have similar optical filters.

The total field amplitude $e(t)$ at the input of the photodetector is the sum of M field amplitudes each of which can be written as in eq. (2.1). Hence,

$$e(t) = \sum_{i=1}^{M} e_i(t) \tag{2.4}$$

The photodetector converts this field into an electric signal proportional to the field intensity. Since the same constant of proportionality applies to all terms in the PD output current, it will be set to unity without loss of generality. This yields the (normalized) photodetector output as:

$$\begin{aligned} I(t) &= \mathbf{LP}\left\{\left|e(t)\right|^2\right\} \\ &= \mathbf{LP}\left\{\sum_{i=1}^{M}\sum_{l=1}^{M} e_i(t)e_l(t)\right\} \end{aligned} \tag{2.5}$$

where the $\mathbf{LP}\{\}$ operator denotes taking the low-pass part of the argument. The right hand side of eq. (2.5) can be broken into a signal component $I_s(t)$ and a cross-term component $I_c(t)$ as follows:

$$\begin{aligned} I(t) &= \mathbf{LP}\left\{\sum_{i=1}^{M} e_i^2(t) + 2\sum_{i=1}^{M-1}\sum_{l=i+1}^{M} e_i(t)e_l(t)\right\} \\ &= I_s(t) + I_c(t) \end{aligned} \tag{2.6}$$

Note that, $I_c(t)$ constitutes an interference term that is generally nonzero. If any of the spectral components of $I_c(t)$ falls within the bandwidth of one of the M users' BPFs, it will cause OBI. To see that, let's look at one of the terms in $I_c(t)$:

$$\begin{aligned} I_{c_{il}}(t) &= \mathbf{LP}\{2e_i(t)e_l(t)\} \\ &= [S_i(t)S_l(t)]^{1/2}\cos[2\pi(F_i - F_l)t + \varphi_i(t) - \varphi_l(t)] \end{aligned} \tag{2.7}$$

Note that, in eq. (2.7) the term corresponding to the sum of the optical frequencies $F_i + F_l$ has been filtered out by the $\mathbf{LP}\{\ \}$ operator. It can be seen from eq. (2.7) that there are two sources of OBI; beating of the subcarrier frequencies, and beating of the optical frequencies. The two sources have the potential of combining to produce spectral components that can overlap any of the subcarrier bands. The objective of the solutions to be presented in this thesis is to either totally eliminate the OBI term or to broaden its spectrum as much as possible. Among the solutions presented, those with laser frequency locking can theoretically eliminate OBI, while those without laser frequency locking tend to broaden the OBI spectrum such that only a small fraction of its power can pass the electronic BPF shown in Figure 2.1 above.

2.3 Effects of OBI on the Operation of SCM/WDMA Networks

In this section, we use simulation to calculate the average bit-error-rate (BER), the average carrier-to-interference ratio (CIR) at the PD output, and the network outage probability [52]. We assume a two-subcarrier per optical channel situation. Laser field amplitudes are given by eq. (2.1). As for the field phase we make a few assumptions.

Because of its minor effect [53], phase noise $\varphi_{ni}(t)$ will be neglected. $\varphi_{mi}(t)$ is also neglected because we assume external modulation of the lasers. As a worst case assumption, the two fields will be assumed to have the same polarization phase, hence, $\varphi_{pi}(t)$ will be set to zero. These assumptions help to demonstrate how serious the OBI problem can be.

In either of the two optical channels, the total field amplitude $e(t)$ at the input of the photodetector is the sum of the two field amplitudes, each of which can be written as in eq. (2.1). Hence,

$$e(t) = e_1(t) + e_2(t) \tag{2.8}$$

Substituting eq. (2.8) into eq. (2.5) yields the photodetector normalized output current as:

$$\begin{aligned} I(t) &= \mathbf{LP}\left\{\left|e(t)\right|^2\right\} \\ &= \mathbf{LP}\left\{\left|e_1(t)\right|^2 + \left|e_2(t)\right|^2 + 2e_1(t)e_2(t)\right\} \end{aligned} \tag{2.9}$$

The signal and cross-term currents are:

$$I_s(t) = \mathbf{LP}\left\{\left|e_1(t)\right|^2 + \left|e_2(t)\right|^2\right\} \tag{2.10}$$

and

$$I_c(t) = \mathbf{LP}\left\{2e_1(t)e_2(t)\right\} \tag{2.11}$$

In the following three subsections we use MATLAB to numerically calculate important system performance measures. Subcarrier center frequencies are assumed to have the values $f_1 = 4\,\text{GHz}$ and $f_2 = 5\,\text{GHz}$. Each laser is externally modulated by an independent PSK signal at a modulation index value of $\sqrt{0.5}$. The electronic BPF bandwidth B is equal to twice the PSK signal bit rate. Laser frequencies were assumed to

fluctuate according to a uniformly distributed random variable in a range R equal to 50 GHz.

2.3.1 Average CIR

The two subcarriers are assumed to be PSK modulated at the same rate R_b. The bit duration is defined as:

$$T_b = \frac{1}{R_b} \tag{2.12}$$

Thus, the subcarrier signals can be written as:

$$x_i(t) = \pm\cos(2\pi f_i t) \tag{2.13}$$

Since power ratios are being evaluated; S_0, which is common to signal and OBI terms, can be set to unity without loss of generality. Substituting eq. (2.13) in eq. (2.2) yields the laser intensities,

$$S_i(t) = 1 \pm m\cos(2\pi f_i t) \tag{2.14}$$

which can be substituted in eq. (2.1) and eq. (2.11) to produce the OBI current in the form:

$$I_c(t) = \sqrt{\left[1 \pm m\cos(2\pi f_1 t)\right]}\sqrt{\left[1 \pm m\cos(2\pi f_2 t)\right]}\cos(2\pi F_x t) \tag{2.15}$$

where

$$F_x = |f_1 - f_2| \tag{2.16}$$

To calculate the average CIR, we need the signal and OBI power spectral densities. It can be deduced from eq. (2.10) that the i-th user's signal current is:

$$I_i(t) = \pm\frac{m}{2}\cos(2\pi f_i t) \tag{2.17}$$

Hence, the signal current power spectral density for either user is:

$$S_{I_i}(f) = \frac{m^2 T_b}{16}\left[\mathbf{sinc}^2\{\pi(f - f_i)T_b\} + \mathbf{sinc}^2\{\pi(f + f_i)T_b\}\right] \tag{2.18}$$

The signal power is thus,

$$P_s = \frac{m^2}{8} \tag{2.19}$$

To find the OBI power we need to approximate eq. (2.15) into a more mathematically tractable form. OBI PSD cannot be found directly from eq. (2.15). Using the square root expansion:

$$\sqrt{1+x} \approx 1 + \frac{x}{2} \tag{2.20}$$

we can express eq. (2.15) in the form:

$$\begin{aligned} I_c(t) &\approx \left[1 \pm \frac{m}{2}\cos(2\pi f_1 t)\right]\left[1 \pm \frac{m}{2}\cos(2\pi f_2 t)\right]\cos(2\pi F_x t) \\ &= \left[1 \pm \frac{m}{2}\cos(2\pi f_1 t) \pm \frac{m}{2}\cos(2\pi f_2 t) \pm \frac{m^2}{4}\cos(2\pi f_1 t)\cos(2\pi f_2 t)\right]\cos(2\pi F_x t) \end{aligned} \tag{2.21}$$

This can be expanded in the form:

$$\begin{aligned} I_c(t) \approx\ & \cos(2\pi F_x t) \\ & \pm\frac{m}{4}\left[\cos 2\pi(F_x - f_1)t + \cos 2\pi(F_x + f_1)t\right] \\ & \pm\frac{m}{4}\left[\cos 2\pi(F_x - f_2)t + \cos 2\pi(F_x + f_2)t\right] \\ & \pm\frac{m^2}{16}\left[\cos 2\pi(F_x - f_1 - f_2)t + \cos 2\pi(F_x + f_1 + f_2)t\right] \\ & \pm\frac{m^2}{16}\left[\cos 2\pi(F_x + f_1 - f_2)t + \cos 2\pi(F_x - f_1 + f_2)t\right] \end{aligned} \tag{2.22}$$

Note that, the PSD of a sinusoid of the form:

$$w(t) = a\cos(2\pi f_s t) \tag{2.23}$$

is given by:

$$S_w(f) = \frac{a^2}{4}\left[\delta(f - f_s) + \delta(f + f_s)\right] \tag{2.24}$$

This makes the coefficients of the OBI PSD terms corresponding to the last two terms in eq. (2.22) negligible compared to those of the other terms. Thus, the last two terms in eq. (2.22) can be ignored, and the OBI PSD can be approximated by:

$$\begin{aligned} S_{I_c}(f) \approx \frac{1}{4}\left[\delta(f - F_x) + \delta(f + F_x)\right] + \frac{m^2 T_b}{64} \\ \times \Big[\mathbf{sinc}^2\left\{\pi(f - f_1 - F_x)T_b\right\} + \mathbf{sinc}^2\left\{\pi(f + f_1 + F_x)T_b\right\} \\ + \ \mathbf{sinc}^2\left\{\pi(f - f_1 + F_x)T_b\right\} + \mathbf{sinc}^2\left\{\pi(f + f_1 - F_x)T_b\right\} \\ + \ \mathbf{sinc}^2\left\{\pi(f - f_2 - F_x)T_b\right\} + \mathbf{sinc}^2\left\{\pi(f + f_2 + F_x)T_b\right\} \\ + \ \mathbf{sinc}^2\left\{\pi(f - f_2 + F_x)T_b\right\} + \mathbf{sinc}^2\left\{\pi(f + f_2 - F_x)T_b\right\}\Big] \end{aligned} \tag{2.25}$$

It should be emphasized that including more terms in the square root approximation in eq. (2.20) results in a lot more terms with negligible coefficients in eq. (2.25). To find the OBI power, eq. (2.25) is integrated over the bandwidth of the BPF in the first user receiver:

$$P_{obi} = 2\int_{f_1 - B/2}^{f_1 + B/2} S_{I_c}(f)\,df \tag{2.26}$$

Note from eq. (2.25) that, the OBI power in eq. (2.26) is a function of F_x. The integration in eq. (2.26) was performed using MATLAB for different values of F_x. The CIR was then calculated from:

$$CIR = \frac{P_s}{P_{obi}} \tag{2.27}$$

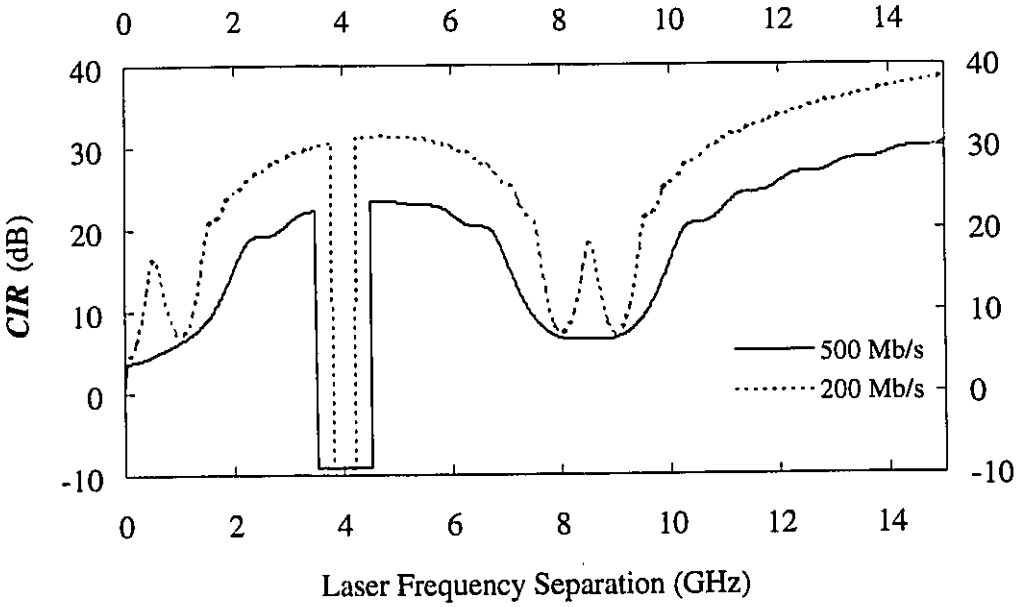

Figure 2.2: *CIR* in a two-subcarrier/channel SCM/WDMA network as a function of optical carrier frequency separation $F_x = |F_1 - F_2|$

The result is shown in Figure 2.2 in the form of CIR as a function of F_x for subcarrier PSK modulation rates of 500 Mb/s and 200 Mb/s. There is a sharp drop in the CIR when the carrier separation satisfies:

$$|F_x - f_1| < \frac{B}{2} \tag{2.28}$$

The above result demonstrates the severity of performance degradation due to OBI when the optical carriers get too close to one another.

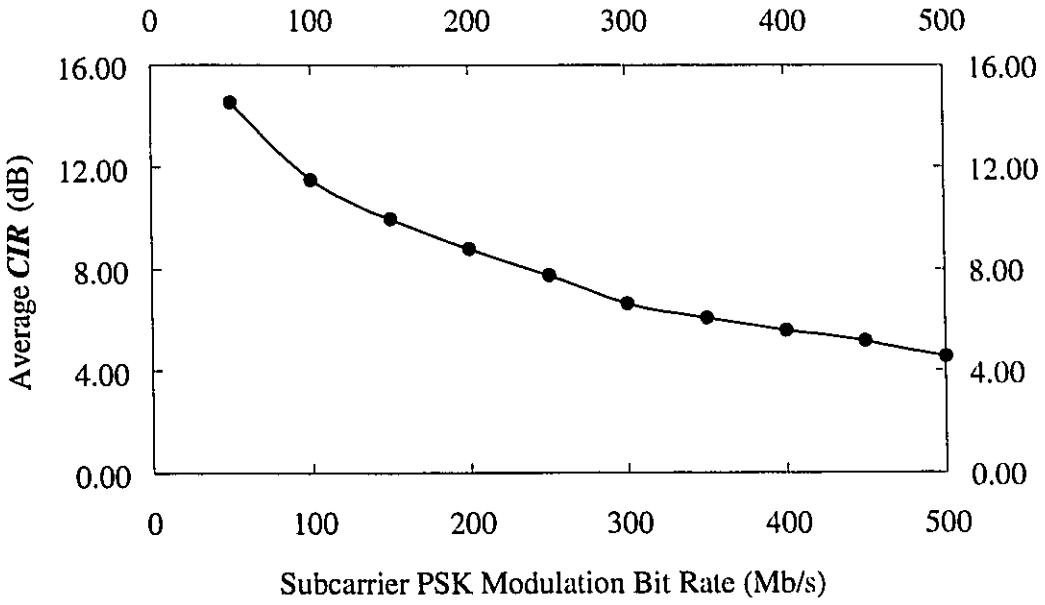

Figure 2.3: *CIR* in a two-subcarrier/channel SCM/WDMA network averaged over optical carrier frequency separation

Figure 2.3 shows the CIR averaged over all possible optical carrier separations. Optical frequencies were varied according to uniformly distributed random variables covering 50 GHz ranges. OBI was computed for each trial. The average of all OBI values was used in eq. (2.27) to calculate the average CIR. The same results would be obtained if the data used in Figure 2.2 were averaged using the pdf for F_x given by:

$$P_{F_x}(F) = \frac{2}{R^2}(R - F) \tag{2.29}$$

In Figure 2.3, the CIR is plotted versus the subcarrier bit rate to test the achievable network capacity under OBI. As this figure shows, the CIR becomes very poor at subcarrier bit rates higher than about 150 Mb/s.

2.3.2 Average Probability of Error

To evaluate the average bit error probability $P(e)$, we find the signal and the OBI contributions to the final decision variable in the electronic detection stage. In doing this, we assume that the demodulator in Figure 2.1 is as shown in Figure 2.4.

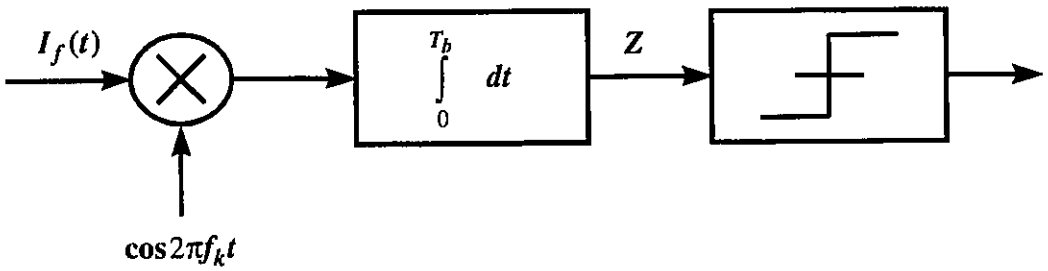

Figure 2.4: A typical user electronic PSK correlation demodulator

It is mathematically very difficult to prove that this is the optimum demodulator. However, it will be seen in chapter 4 that the correlator (integrator) output becomes Gaussian-distributed as field polarizations become uniformly distributed and quickly varying with time, in which case this demodulator is the optimum one indeed.

Noting that, the BPF in Figure 2.1 can be absorbed in the correlator receiver in Figure 2.4. Note also that, only the term corresponding to the difference of the optical frequencies appears at the output of the PD (see eq. (2.11) above). Performing the operations shown in the demodulator structure in Figure 2.4, the decision variable in the first user's receiver can be shown to be:

$$Z = \frac{m_1 T_b}{4} + \int_0^{T_b} \sqrt{(1+m_1 \cos 2\pi f_1 t)(1+m_2 \cos 2\pi f_2 t)}\, \cos 2\pi f_1 t \, \cos 2\pi F_x t \, dt \quad (2.30)$$

The decision variable Z was computed numerically as m_2, F_1, and F_2 were varied, in their respective ranges, according to independent uniformly distributed random number generators.

Figure 2.5 shows the simulation result for the system average probability of error $P(e)$. As can be seen from the figure, the probability of error is very high even at bit rates as low as 50 Mb/s. Furthermore, $P(e)$ keeps increasing at higher bit rates.

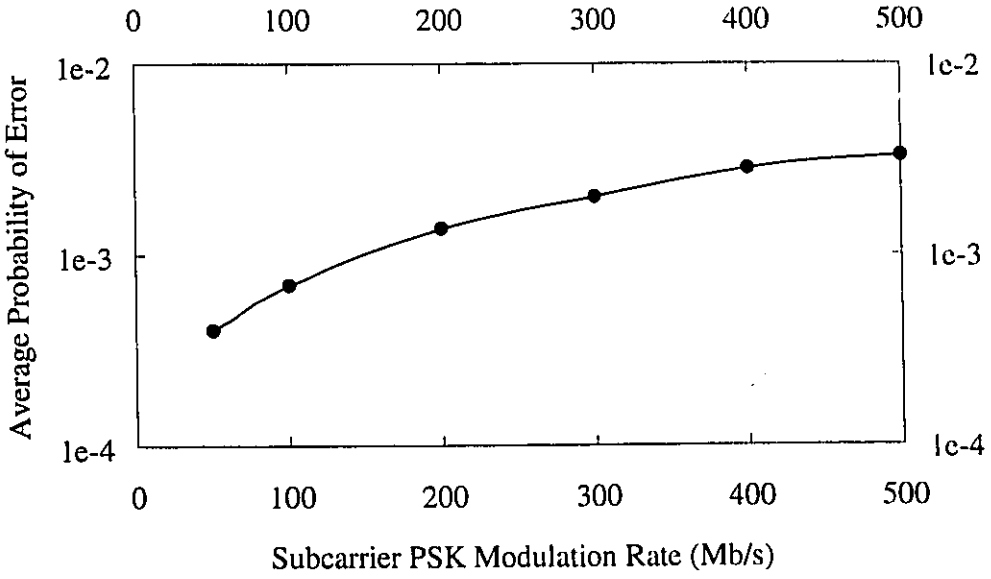

Figure 2.5: Average probability of error in a two-subcarrier/channel SCM/WDMA network due to OBI

It can be seen from the $P(e)$ chart and the discussions above that the network performance under OBI is not acceptable. In section 4.5, we demonstrate how polarization randomness can bring significant improvements to the network performance

and throughput. Polarization scrambling will be shown to support network throughputs as high as 150 Gb/s.

2.3.3 Outage Probability

Outage probability computation starts with finding the probability of bit error as a function of the difference in optical frequencies, F_x. The probability of error at a given F_x was calculated by first evaluating the decision variable in eq. (2.30) for all possible values of m_1 and m_2. The decision variable is then compared with m_1. If the two quantities have the same sign, no error is recorded. If the two quantities have different signs, an error is recorded. Finally, the probability of error is obtained by dividing the number of errors by the number of symbol combinations.

After the probability of error is obtained as function of F_x, an indicator function $\xi(F_x)$ was generated in the form:

$$\xi(F_x) = \begin{cases} 1 & P_{F_x}(e) > 10^{-9} \\ 0 & \text{Otherwise} \end{cases} \tag{2.31}$$

where $P_{F_x}(e)$ is the probability of error given a certain value of F_x. The indicator function was finally averaged over all values of F_x using the pdf given in eq. (2.29). The resulting outage probability is shown in Figure 2.6.

As can be seen from the average CIR, average error rate, and outage probability graphs, the SCM/WDMA network performance level is not acceptable in the presence of OBI. The objective of the solutions to be presented in this thesis, starting the following section, is to provide means to limit performance degradation due to OBI.

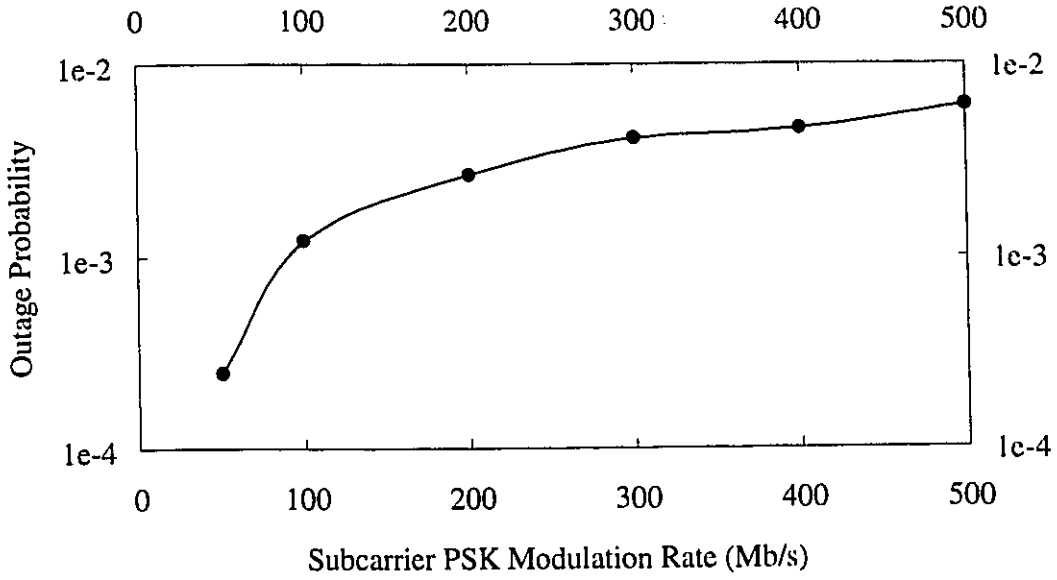

Figure 2.6: Outage probability in a two-subcarrier/channel SCM/WDMA network

2.4 OBI Elimination Using Balanced Detection

In this section, we look at a receiver configuration that offers a total solution to the OBI problem, although it requires laser frequency locking. It is a little difficult to achieve laser frequency locking with the present technology, however, a lot of progress on that front is expected to be made in the coming few years.

Assuming known, stable optical carriers, we can devise SCM/WDMA systems that can have no OBI at all, without the need to widely space the optical carrier frequencies. Balanced direct detection at the receiver front end will be briefly introduced in the forthcoming discussion as a complete solution to OBI.

Instead of using one photodetector to detect the total input field, a configuration like the one shown in Figure 2.7 below can be used. In this structure, the total input field and a reference local laser field are combined by a 3 dB directional coupler. The first output of the directional coupler $E_+(t)$ is proportional to the sum of the two field amplitudes, while the other output $E_-(t)$ is proportional to their difference. The resulting two fields are then detected by two identical PD's to produce $I_1(t)$ and $I_2(t)$, respectively. The difference between the detectors' outputs $I(t)$ is finally processed by electronic detection circuitry to recover the transmitted signal. As will be shown shortly, $I(t)$ is OBI-free.

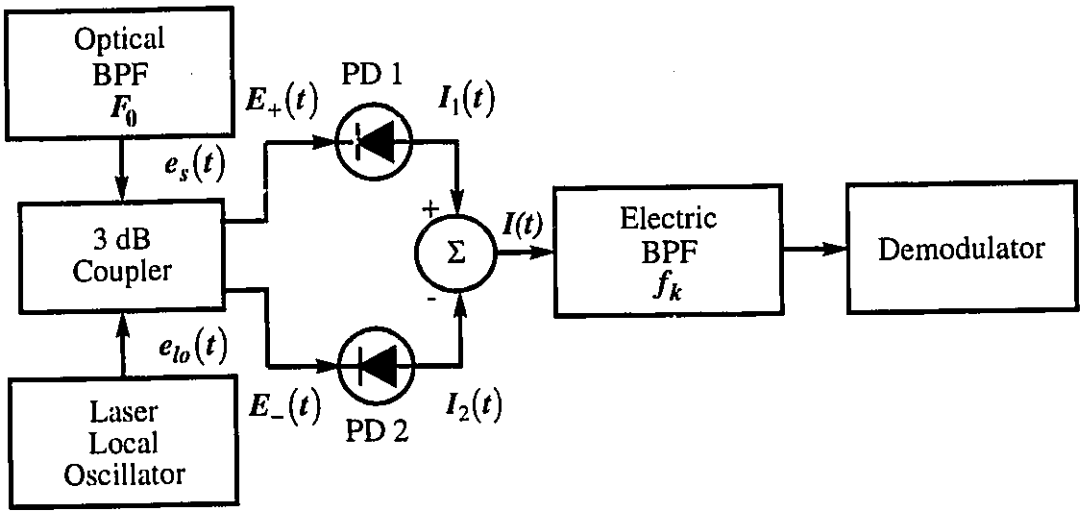

Figure 2.7: Balanced detection reference user receiver

The same structure was used by Kazovsky [54] in a multichannel coherent optical communication system. The brief analysis in this subsection follows that of Kazovsky [54]. To clarify the notation, eq. (2.4) will be written in the form:

$$e_s(t) = \sum_{i=1}^{M} e_i(t) \tag{2.32}$$

The directional coupler outputs are:

$$E_+(t) = \frac{1}{\sqrt{2}}\left[e_s(t) + e_{lo}(t)\right] \tag{2.33}$$

and

$$E_-(t) = \frac{1}{\sqrt{2}}\left[e_s(t) - e_{lo}(t)\right] \tag{2.34}$$

The two detectors' outputs are:

$$\begin{aligned} I_1(t) &= \mathbf{LP}\left\{\left|E_+(t)\right|^2\right\} \\ &= \frac{1}{2}\mathbf{LP}\left\{\left|e_s(t)\right|^2\right\} + \frac{1}{2}\mathbf{LP}\left\{\left|e_{lo}(t)\right|^2\right\} + \mathbf{LP}\left\{e_s(t)e_{lo}(t)\right\} \end{aligned} \tag{2.35}$$

and

$$\begin{aligned} I_2(t) &= \mathbf{LP}\left\{\left|E_-(t)\right|^2\right\} \\ &= \frac{1}{2}\mathbf{LP}\left\{\left|e_s(t)\right|^2\right\} + \frac{1}{2}\mathbf{LP}\left\{\left|e_{lo}(t)\right|^2\right\} - \mathbf{LP}\left\{e_s(t)e_{lo}(t)\right\} \end{aligned} \tag{2.36}$$

Note that, the terms $|e_s(t)|^2$ and $|e_{lo}(t)|^2$ are repeated with the same sign in both $I_1(t)$ and $I_2(t)$. Note also that, $|e_s(t)|^2$ contains all the OBI terms. The last term in both $I_1(t)$ and $I_2(t)$ represents the mixing of the individual user fields with the local laser field, similar to the case of heterodyne detection. This last term contains all the information about the subcarriers without having the cross-terms. As a result, both $|e_s(t)|^2$ and $|e_{lo}(t)|^2$ have not to be present in $I(t)$. Subtracting $I_2(t)$ from $I_1(t)$ achieves this goal, while keeping the needed heterodyne terms. The resulting current is:

$$I(t) = I_1(t) - I_2(t) \\ = 2\,\mathrm{LP}\{e_s(t)e_{lo}(t)\} \tag{2.37}$$

Assuming the local laser field has an intensity $S_{lo}(t)$, a frequency F_{lo}, and a phase $\varphi_{lo}(t)$, the amplitude of this field can be written as:

$$e_{lo}(t) = E_{lo}(t)\cos\left[2\pi F_{lo}t + \varphi_{lo}(t)\right] \tag{2.38}$$

Hence,

$$I(t) = \sum_{i=1}^{M}\left[S_i(t)S_{lo}(t)\right]^{1/2}\cos\left[2\pi\left(F_i - F_{lo}\right)t + \varphi_i(t) - \varphi_{lo}(t)\right] \tag{2.39}$$

Our focus is on the frequency difference $F_i - F_{lo}$ rather than intensity or phase noises associated with this kind of detection. Intensity and phase noise problems in optical heterodyne detection have been extensively studied in the literature. If both F_i and F_{lo} are known, the center frequency of the reference user BPF can be adjusted so as to receive its corresponding signal. Needless to say, for successful reception, the subcarriers within one optical channel have to have nonoverlapping spectra in any SCM/WDMA system.

As seen in the discussion above, balanced detection has the potential of completely eliminating OBI. It does, however, need elaborate laser frequency stabilization, but as the optical technology keeps progressing at an accelerating rate, this is expected to become more feasible in the near future.

Chapter Three

3. Laser Modulation Index and OBI

In this chapter, we introduce for the first time to the best of our knowledge, a large-signal model to evaluate the directly-modulated laser field spectrum [53]. Small-signal models are widely used in the literature. In [55], for example, a small-signal model is used to find the power spectrum of directly modulated semiconductor laser fields. The same model was used in [50] to analyze the effect of increasing the intensity modulation on OBI performance of SCM systems. For the small-signal model to be useful, the modulation index should be less than 0.3, which contradicts the objective of increasing the modulation index to reduce OBI. This is why we introduce the large-signal model in this chapter.

3.1 Large-Signal Laser Field Spectrum

Lasers are assumed to be directly modulated as shown in Figure 3.1. Because of frequency chirp, directly modulated laser fields have broader spectral widths than externally modulated laser fields. Since the primary motivation for this chapter is to widen the OBI spectrum, it makes more sense to assume direct laser modulation. For simplicity, lasers will be assumed to be modulated by purely sinusoidal RF subcarriers. Using

modulated subcarriers results in slightly broader spectral widths of the laser fields, however, it makes the analysis a lot more involved.

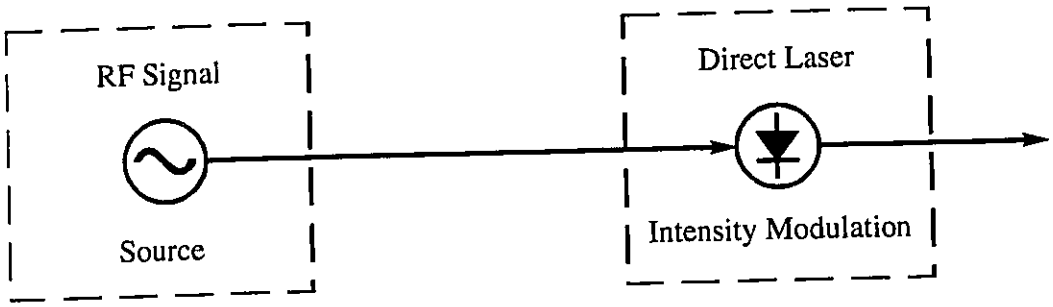

Figure 3.1: Laser direct intensity modulation by subcarriers

Users' laser field spectra are needed for the calculation of the total electric field spectrum at the input of the photodetector. The input field spectrum is used to derive expressions for the PD output current spectrum, which is used in calculating the CIR at the input of the electronic processing circuitry.

Spectral shapes for these laser fields are assumed to be identical. However, details of laser field spectra may differ from user to user, depending on the optical center frequency and the RF subcarrier frequency and modulation. The i-th user electric field amplitude and intensity were represented by eq. (2.1) and eq. (2.2). All laser fields are assumed to have the same polarization, a worst case assumption in the analysis of OBI [47], [50], [53], [56]. Hence, spatial dependence of the fields is dropped in the derivations to follow. As a result, the polarization component of the field phase will be dropped.

3.1.1 The Modulated Field Phase

Using the assumptions just outlined above, field phases in eq. (2.3) will be rewritten in the form:

$$\varphi_i(t) = \varphi_{mi}(t) + \varphi_{ni}(t) \tag{3.1}$$

According to rate equations, laser light phase (frequency) modulation is related to intensity modulation by [57]:

$$\begin{aligned}\dot{\varphi}_{mi}(t) &= \frac{\alpha}{2}\left[\frac{\mathrm{d}}{\mathrm{dt}}\{\ln S_i(t)\} + \frac{\kappa_s}{\tau_{ph}} S_i(t) - \frac{K_{tot} n_{sp}}{\tau_{ph}} \frac{1}{S_i(t)}\right] \\ &= \dot{\varphi}_{mi,1}(t) + \dot{\varphi}_{mi,2}(t) + \dot{\varphi}_{mi,3}(t)\end{aligned} \tag{3.2}$$

where $\dot{\varphi}_{mi}(t)$ represents the instantaneous laser frequency shift - due to chirp - from the operating frequency. The various constants in eq. (3.2) are defined in Table 3.1.

Assuming the modulating signal $x(t)$ in eq. (2.2) is an unmodulated sinusoid in the form:

$$x(t) = \cos(2\pi f_i t) \tag{3.3}$$

we can substitute it in eq. (3.2) and obtain:

$$\begin{aligned}\dot{\varphi}_{mi,1}(t) = &\frac{\alpha}{2}\frac{\mathrm{d}}{\mathrm{dt}}\{\ln S_i(t)\} \\ &-\frac{\alpha}{2}\frac{m\omega_i \sin(\omega_i t)}{1 + m\cos(\omega_i t)}\end{aligned} \tag{3.4}$$

This is an odd periodic function which can be expanded in a Fourier series in the form:

$$\dot{\varphi}_{mi,1}(t) = \sum_{n=1}^{\infty} b_n \sin(n\omega_i t) \tag{3.5}$$

where

$$b_n = (-1)^n \alpha\omega_i \left[\frac{1-\sqrt{1-m^2}}{m} \right]^n \tag{3.6}$$

Parameter	Symbol	Value	Source, page
Subcarrier frequency	f_i	5.0 GHz	
Operating wavelength	λ	1.55 μm	
Linewidth enhancement factor	α	5.0	[58], 227
Output Power per laser facet	P	3.0 mW	[57], 121
Effective refractive index	$\bar{n}$	3.5	[57], 27
Nonlinear power gain coefficient	κ	4.4/W	[57], 121
Mirror loss	α_m	4500/m	[58], 227
Total Spontaneous emission enhancement factor	K_{tot}	1.0	[57], 44
Spontaneous emission coefficient	n_{sp}	1.7	[57], 15
Photon lifetime	τ_{ph}	1.0 ps	[57], 121
Nonlinear photon number gain coefficient	κ_s	1.008×10^7	
Unmodulated (average) photon number	S_0	1.2×10^5	

Table 3.1: Typical laser parameter values

Similarly,

$$\begin{aligned} \dot{\varphi}_{mi,2}(t) &= \frac{\alpha}{2} \frac{\kappa_s}{\tau_{ph}} S_i(t) \\ &= \frac{\alpha\kappa_s S_0}{2\tau_{ph}} + \frac{\alpha\kappa_s S_0}{2\tau_{ph}} m \cos(\omega_i t) \end{aligned} \tag{3.7}$$

The first term in eq. (3.7) is a constant frequency term that will be absorbed in F_i. Finally,

$$\begin{aligned}\dot{\varphi}_{mi,3}(t) &= -\frac{\alpha}{2}\frac{K_{tot}n_{sp}}{\tau_{ph}}\frac{1}{S_i(t)} \\ &= -\frac{\alpha}{2}\frac{K_{tot}n_{sp}}{\tau_{ph}S_0}\frac{1}{1+m\cos(\omega_i t)}\end{aligned} \tag{3.8}$$

This is an even periodic function which can be expanded in a Fourier series in the form:

$$\dot{\varphi}_{mi,3}(t) = \sum_{n=0}^{\infty} a_n \cos(n\omega_i t) \tag{3.9}$$

where

$$a_n = (-1)^{n+1}\frac{\alpha K_{tot}n_{sp}}{\tau_{ph}S_0\sqrt{1-m^2}}\left[\frac{1-\sqrt{1-m^2}}{m}\right]^n \tag{3.10}$$

The first term in eq. (3.9) is a constant frequency term that will be absorbed in F_i. Adding terms in eqs. (3.5), (3.7) and (3.9) produces the total laser frequency chirp as:

$$\dot{\varphi}_{mi}(t) = \sum_{n=1}^{\infty}\left[A_n\cos(n\omega_i t) + B_n\sin(n\omega_i t)\right] \tag{3.11}$$

where

$$B_n = b_n \tag{3.12}$$

$$A_n = \begin{cases} \dfrac{\alpha\kappa_s S_0 m}{2\tau_{ph}} + \dfrac{\alpha K_{tot}n_{sp}}{\tau_{ph}S_0\sqrt{1-m^2}}\left[\dfrac{1-\sqrt{1-m^2}}{m}\right], & n=1 \\ (-1)^{n+1}\dfrac{\alpha K_{tot}n_{sp}}{\tau_{ph}S_0\sqrt{1-m^2}}\left[\dfrac{1-\sqrt{1-m^2}}{m}\right]^n, & n>1 \end{cases} \tag{3.13}$$

Recalling the Integral relationship between phase and frequency, we could write the total laser phase modulation due to chirp as:

$$\varphi_{mi}(t) = \sum_{n=1}^{\infty}\left[C_n \cos(n\omega_i t) + D_n \sin(n\omega_i t)\right] \tag{3.14}$$

where

$$C_n = -\frac{B_n}{n\omega_i} \tag{3.15}$$

$$D_n = \frac{A_n}{n\omega_i} \tag{3.16}$$

Alternatively, $\varphi_{mi}(t)$ can be expressed as:

$$\varphi_{mi}(t) = \sum_{n=1}^{\infty}\beta_n \cos(n\omega_i t + \psi_n) \tag{3.17}$$

where

$$\beta_n = (-1)^{n+1}\left[C_n^2 + D_n^2\right]^{1/2} \tag{3.18}$$

$$\psi_n = \tan^{-1}\left(\frac{D_n}{C_n}\right) \tag{3.19}$$

The infinite sum in eq. (3.17) cannot be easily used in the calculation of the power spectrum of the laser field. To find the number of significant terms in eq. (3.17), one needs to look at typical values of various system parameters affecting the series. Values for such parameters are listed in Table 3.1. The value of κ_s is found from [58]:

$$\kappa_s = \frac{\kappa}{2}\left(h\frac{c}{\lambda}\right)\frac{c}{\bar{n}}\alpha_m \tag{3.20}$$

where c is the speed of light in free space, h is Plank's constant, and the other parameters are as in Table 3.1. S_0 is found from [57]:

$$\kappa_s S_0 = \kappa P \tag{3.21}$$

From the data in Table 3.1 and the relations for the coefficients in eqs. (3.14) and (3.17), values for the first few of these coefficients are computed as in Table 3.2. In these calculations, the modulation index is assumed to be 0.9, a value that is in the range required by the suggested solution to the OBI problem. This value for the modulation index is possible because each laser is modulated by a single subcarrier. It should be kept in mind that fewer terms are needed at smaller modulation indices. So, the approximation is reasonable for the entire range of values of m.

n	C_n	D_n	β_n	ψ_n
1	4.074	1.219	4.252	0.29
2	-1.277	-1.32×10^{-3}	-1.277	0
3	0.534	5.517×10^{-4}	0.534	0
4	-0.251	-2.594×10^{-4}	-0.251	0
5	0.126	1.301×10^{-4}	0.126	0

Table 3.2: First few coefficient values in eq. (3.17)

Based on the data in Table 3.2, D_n and ψ_n will be neglected and only the first three terms of β_n will be kept. Thus,

$$\varphi_{mi}(t) = \sum_{n=1}^{3} \beta_n \cos(n\omega_i t) \tag{3.22}$$

where

$$\beta_n = \frac{(-1)^{n+1}}{n}\alpha\left[\frac{1-\sqrt{1-m^2}}{m}\right]^n \tag{3.23}$$

For very small $m \le 0.3$, β_1 is the only significant coefficient, and in that case using the same square root approximation in eq. (2.20):

$$\sqrt{1-m^2} \approx 1-\frac{m^2}{2} \tag{3.24}$$

we find that the frequency modulation index is:

$$\beta_1 \approx \frac{\alpha m}{2} \tag{3.25}$$

The last result in eq. (3.25) is the one widely used in the literature to represent the frequency modulation index [50]. As shown above, it is a good enough approximation only if $m \le 0.3$ while otherwise, eq. (3.23) should be used instead.

3.1.2 The Modulated Field Spectrum

Having computed all phase components, we can substitute eq. (3.1) into eq. (2.1) to obtain the field amplitude in the form:

$$e_i(t) = \left[S_i(t)\right]^{1/2}\cos\left[2\pi F_i t + \varphi_{ni}(t) + \varphi_{mi}(t)\right] \tag{3.26}$$

The equivalent complex representation of eq. (3.26) is:

$$\begin{aligned}\tilde{e}_i(t) &= \left[S_i(t)\right]^{1/2} e^{j\varphi_{mi}(t)} e^{j\varphi_{ni}(t)} e^{j2\pi F_i t} \\ &= e_{il}(t)\tilde{e}_{mi}(t)\tilde{e}_{ni}(t)e^{j2\pi F_i t} \\ &= E_i(t)e^{j2\pi F_i t}\end{aligned} \tag{3.27}$$

The corresponding power spectral densities (PSD's) are known to be related by:

$$S_{e_i}(f) = \frac{1}{4}\left[S_{\tilde{e}_i}(f) + S_{\tilde{e}_i}(-f)\right] \tag{3.28}$$

$$S_{\tilde{e}_i}(f) = S_{E_i}(f - F_i) \tag{3.29}$$

$$S_{E_i}(f) = S_{e_{iI}}(f) * S_{\tilde{e}_{mi}}(f) * S_{\tilde{e}_{ni}}(f) \tag{3.30}$$

Because $f_i << F_i$, the term $S_{e_{iI}}(f)$ that represents the PSD contribution of $\left[S_i(t)\right]^{1/2}$ will be assumed equal to a constant S_0. The phase noise spectrum can be shown to be given by [57]:

$$S_{\tilde{e}_{ni}}(f) = \frac{2\tau_c}{1 + (2\pi f \tau_c)^2} \tag{3.31}$$

where the laser coherence time τ_c is related to its full width at half maximum (FWHM) linewidth Δf by (both values are assumed to be the same for all user lasers) [57]:

$$\tau_c = \frac{1}{\pi \Delta f} \tag{3.32}$$

Next we calculate the chirp contribution to the PSD, $S_{\tilde{e}_{mi}}(f)$. From eq. (3.27):

$$\begin{aligned} \tilde{e}_{mi}(t) &= e^{j\varphi_{mi}(t)} \\ &= \exp\left[j \sum_{n=1}^{3} \beta_n \cos(n\omega_i t) \right] \end{aligned} \tag{3.33}$$

which can be expanded in the following series:

$$\tilde{e}_{mi}(t) = \sum_{k_1=-\infty}^{\infty} \sum_{k_2=-\infty}^{\infty} \sum_{k_3=-\infty}^{\infty} J_{k_1}(\beta_1) J_{k_2}(\beta_2) J_{k_3}(\beta_3) \exp\left[j \sum_{l=1}^{3} k_l \left(l\omega_i + \frac{\pi}{2} \right) \right] \tag{3.34}$$

where $J_r(x)$ is a Bessel function of the first kind of order r. Alternatively, a change of summation indices produces:

$$\tilde{e}_{mi}(t) = \sum_{n=-\infty}^{\infty} \sum_{k_2=-\infty}^{\infty} \sum_{k_3=-\infty}^{\infty} J_{n-2k_2-3k_3}(\beta_1) J_{k_2}(\beta_2) J_{k_3}(\beta_3) \times \exp\left[j\left\{ n\omega_i t + (n - k_2 - 2k_3)\frac{\pi}{2} \right\} \right] \tag{3.35}$$

Note that, eq. (3.35) shows the coefficients of the individual harmonics of f_i. Note, furthermore, that the phases of the different terms involving f_i are not the same. Hence, the effects of these terms in the power spectrum add noncoherently. As a result, the chirp spectrum can be written in the form:

$$S_{\tilde{e}_{mi}}(f) = \sum_{n=-\infty}^{\infty} \left[\sum_{k_2=-\infty}^{\infty} \sum_{k_3=-\infty}^{\infty} J^2_{n-2k_2-3k_3}(\beta_1) J^2_{k_2}(\beta_2) J^2_{k_3}(\beta_3) \right] \delta(f - nf_i) \tag{3.36}$$

As mentioned earlier, $S_{e_{il}}(f)$ will be assumed constant. From eqs. (3.31) and (3.32) we get:

$$S_{\tilde{e}_{ni}}(f) = \frac{2}{\pi\Delta f \left(1 + \frac{2f}{\Delta f}\right)^2} = \Phi(f) \tag{3.37}$$

Hence, the spectral density of the complex field becomes:

$$S_{\tilde{e}_i}(f) = S_0 \sum_{n=-\infty}^{\infty} A^2(n) \Phi(f - F_i - nf_i) \tag{3.38}$$

where

$$A^2(n) = \sum_{k_2=-\infty}^{\infty} \sum_{k_3=-\infty}^{\infty} J^2_{n-2k_2-3k_3}(\beta_1) J^2_{k_2}(\beta_2) J^2_{k_3}(\beta_3) \tag{3.39}$$

The spectrum of the real field is thus

$$S_{e_i}(f) = \frac{S_0}{4} \sum_{n=-\infty}^{\infty} A^2(n)\left[\Phi(f - F_i - nf_i) + \Phi(f + F_i + nf_i)\right] \qquad (3.40)$$

3.2 Photodetector Output CIR

The front end of the receiver is, as was shown in Figure 2.1, an optical filter centered on the optical carrier frequency of the intended user channel. As was indicated earlier, out of a possible total of MN optical fields incoming to the optical filter, only M continue their way to the photodetector. The center frequency of the optical filter in the intended user receiver will be denoted by F_0. All M users in the same optical channel will have identical optical filters. The total field amplitude at the input of the photodetector $e(t)$ is the sum of M field amplitudes each of which can be written as in eq. (2.1). The sum field amplitude is given by eq. (2.4). The photodetector converts this field into an electric signal proportional to the field intensity. Since we are performing signal-to-interference ratio calculations, the constant of proportionality will be set to unity. The photodetector output is given by eqs. (2.5) and (2.6).

The power spectral density of a two-term sum of the form in eq. (2.6) is given in [59] as:

$$S_{I;2} = |H_{\text{det}}(f)|^2 \left[S_{I_1}(f) + S_{I_2}(f) + 4S_{e_1}(f) * S_{e_2}(f) + 2\langle \bar{I}_1(t)\bar{I}_2(t)\rangle \delta(f)\right] \qquad (3.41)$$

where $H_{\text{det}}(f)$ is the photodetector frequency response. The operator $\langle x \rangle$ denotes statistical averaging, and the overbar denotes time averaging. The first two terms in eq. (3.41) represent the two signals' power spectral densities. The third term is a beat between

the two field spectra. The last term is a dc term that is filtered-out in subsequent stages, hence, it will be dropped from here on.

Similar to eq. (3.41), one can obtain a formula for the power spectral density of an M-term field sum that produces a current given by eq. (2.6). Generalizing eq. (3.41), the spectral density of the current signal given by eq. (2.6) is [47]:

$$\begin{aligned} S_I(f) &= S_{I;M}(f) \\ &= |H_{\text{det}}(f)|^2 \left[\sum_{i=1}^{M} S_{I_i}(f) + 4 \sum_{i=1}^{M-1} \sum_{l=i+1}^{M} S_{e_i}(f) * S_{e_l}(f) \right] \\ &= S_{I_s}(f) + S_{I_c}(f) \end{aligned} \tag{3.42}$$

Obviously, the first and the second terms in eq. (3.42) correspond to the first and the second terms in eq. (2.6), respectively. Note that, the effect of the low-pass operator in the time domain is equivalent to multiplication by $|H_{\text{det}}(f)|^2$ in the frequency domain. For the sake of simplicity, $|H_{\text{det}}(f)|^2$ will be set to unity in the subcarrier frequencies range and to zero, otherwise.

To calculate the ratio of the power in the intended subcarrier signal to beat noise interference power, we need to evaluate both powers at the output of the bandpass filter. Assuming user number k is the intended one, and that this user is transmitting at subcarrier frequency f_k, the bandpass filter must have its frequency response flat around f_k. In fact, the bandpass filter frequency response is assumed to be:

$$|H_k(f)| = \begin{cases} 1; & f_k - B/2 < f < f_k + B/2 \\ 0; & \text{otherwise} \end{cases} \tag{3.43}$$

To determine the signal power, we need to evaluate $I_s(t)$ in eq. (2.6) by using eqs. (2.1), (2.2), and (2.4) as follows

$$
\begin{aligned}
I_s(t) &= \mathrm{LP}\left\{\sum_{i=1}^{M} e_i^2(t)\right\} \\
&= \mathrm{LP}\left\{\sum_{i=1}^{M} S_i(t)\cos^2\left(2\pi F_i t + \varphi_i(t)\right)\right\} \\
&= \frac{S_0}{2}\sum_{i=1}^{M}\left[1 + m\cos\left(2\pi f_i t\right)\right]
\end{aligned}
\tag{3.44}
$$

At the output of the bandpass filter, only the intended user signal intensity $I_{sf}(t)$ appears. From eq. (3.43) and eq. (3.44), the filtered signal current is:

$$
I_{sf}(t) = \frac{S_0}{2} m\cos\left(2\pi f_k t\right) \tag{3.45}
$$

The filtered signal power spectral density is thus:

$$
S_{I_{sf}}(f) = \frac{S_0^2 m^2}{16}\left[\delta\left(f - f_k\right) + \delta\left(f + f_k\right)\right] \tag{3.46}
$$

The total power in the signal subcarrier is obtained by integrating eq. (3.46) over the passband of the bandpass filter. This produces:

$$
P_s = \frac{S_0^2 m^2}{8} \tag{3.47}
$$

In the following two subsections, we find the beat noise power based on two different assumptions. In subsection 3.2.1, the lasers are assumed to have zero linewidth. In subsection 3.2.2, the effect of nonzero linewidth is considered.

3.2.1 Lasers with a Zero Linewidth

Assuming that all the lasers have a zero linewidth is a worst case assumption as far as OBI is concerned. This is because a zero laser linewidth implies that all the power in an interference term centered on f_k will pass through the electric bandpass filter in the

receiver. In such a case, the phase noise contribution to the field spectrum in eq. (3.40) is assumed to be:

$$\Phi(f) = \delta(f) \tag{3.48}$$

Hence, repeating for $I_c(t)$ the procedure performed above on $I_s(t)$, one obtains from eq. (2.6):

$$I_c(t) = \mathbf{LP}\left\{2\sum_{i=1}^{M-1}\sum_{l=i+1}^{M} e_i(t)e_l(t)\right\} \tag{3.49}$$

Then, the beat noise power spectral density is:

$$\begin{aligned} S_{I_c}(f) &= \mathbf{LP}\left\{4\sum_{i=1}^{M-1}\sum_{l=i+1}^{M} S_{e_i}(f) * S_{e_l}(f)\right\} \\ &= \frac{S_0^2}{4}\sum_{i=1}^{M-1}\sum_{l=i+1}^{M}\sum_{n=-\infty}^{\infty}\sum_{r=-\infty}^{\infty} A^2(n)A^2(r) \\ &\quad \times\left\{\delta\left(f - nf_i + rf_l\right) + \delta\left(f + nf_i - rf_l\right)\right\} \end{aligned} \tag{3.50}$$

Note that, this is the beat noise PSD at the input (rather than at the output) of the bandpass filter. The total beat noise interference power at the filter output is:

$$P_{obi} = 2\int_{f_k - B/2}^{f_k + B/2} S_{I_c}(f)df \tag{3.51}$$

To calculate the last integral, one has to find out which frequency components in eq. (3.50) are actually in the passband of $H_k(f)$. To do so, we'll let the subcarrier frequencies be multiples of the filter bandwidth B away from a frequency offset f_0, i.e.,

$$f_i = f_0 + iB \tag{3.52}$$

A typical frequency component in eq. (3.50) is:

$$nf_i - rf_l = (n - r)f_0 + (ni - rl)B \tag{3.53}$$

For this component to interfere with the intended user signal, the following condition on n and r must be satisfied:

$$\begin{aligned}(n-r)f_0 + (ni - rl)B &= f_k \\ &= f_0 + kB\end{aligned} \tag{3.54}$$

which can be transformed into:

$$(n-r-1)f_0 + (ni - rl - k)B = 0 \tag{3.55}$$

Thus, we can write the interference power in eq. (3.51) in the form:

$$P_{obi} = \frac{S_0^2}{2}\sum_{i=1}^{M-1}\sum_{l=i+1}^{M}\left[\sum_{n=-\infty}^{\infty}\sum_{r=-\infty}^{\infty}A^2(n)A^2(r)\right]_{n,r \text{ satisfy eq. (3.55)}} \tag{3.56}$$

Finally, the carrier-to-interference ratio obtained by dividing eq. (3.47) by eq. (3.56) is:

$$\begin{aligned}CIR &= \frac{P_s}{P_{obi}} \\ &= \frac{m^2}{4\sum_{i=1}^{M-1}\sum_{l=i+1}^{M}\left[\sum_{n=-\infty}^{\infty}\sum_{r=-\infty}^{\infty}A^2(n)A^2(r)\right]_{n,r \text{ satisfy eq. (3.55)}}}\end{aligned} \tag{3.57}$$

3.2.2 Lasers with Nonzero Linewidth

An actual laser never has a zero linewidth. This can be explained on the basis of the rate equations which suggest that laser linewidth is always larger than zero. Spontaneous emission is the main factor behind this behavior. In this subsection, the phase noise contribution in eq. (3.40) will be substituted for from eq. (3.37). Assumptions regarding the number of subcarriers per optical channel, the subcarrier frequencies, and the filter bandwidths are still as before. Following the same procedure as in the previous subsection, the beat noise power spectral density can be written in the form:

$$S_{I_c}(f) = \mathrm{LP}\left\{4\sum_{i=1}^{M-1}\sum_{l=i+1}^{M} S_{e_i}(f) * S_{e_l}(f)\right\}$$
$$= \frac{S_0^2}{4}\sum_{i=1}^{M-1}\sum_{l=i+1}^{M}\left[\sum_{n=-\infty}^{\infty}\sum_{r=-\infty}^{\infty} A^2(n)A^2(r)\Theta_{il}(f,n,r)\right] \quad (3.58)$$

where

$$\Theta_{il}(f,n,r) = \Phi^{(2)}(f - nf_i + rf_l) + \Phi^{(2)}(f + nf_i - rf_l) \quad (3.59)$$

and

$$\Phi^{(2)}(f) = \Phi(f) * \Phi(f)$$
$$= \frac{1}{\pi\Delta f}\frac{1}{1+\left(\frac{f}{\Delta f}\right)^2} \quad (3.60)$$

The beat noise power at the output of the k-th user bandpass filter can be calculated again using eq. (3.51). Substituting eq. (3.50) and eq. (3.60) into eq. (3.51) and performing the integration yields:

$$P_{obi} = \frac{S_0^2}{2}\sum_{i=1}^{M-1}\sum_{l=i+1}^{M}\left[\sum_{n=-\infty}^{\infty}\sum_{r=-\infty}^{\infty} A^2(n)A^2(r)Q_{il}(k,n,r)\right] \quad (3.61)$$

where

$$Q_{il}(k,n,r) = \frac{1}{\pi}\left[\tan^{-1}\left\{\frac{B}{\Delta f}\left(k+\frac{1}{2}-ni+rl\right)\right\} - \tan^{-1}\left\{\frac{B}{\Delta f}\left(k-\frac{1}{2}-ni+rl\right)\right\}\right] \quad (3.62)$$

Dividing eq. (3.47) by eq. (3.61) provides the signal-to-interference ratio in the k-th user channel as:

$$CIR = \frac{P_s}{P_{obi}}$$

$$= \frac{m^2}{4\sum_{i=1}^{M-1}\sum_{l=i+1}^{M}\left[\sum_{n=-\infty}^{\infty}\sum_{r=-\infty}^{\infty}A^2(n)A^2(r)Q_{il}(k,n,r)\right]} \tag{3.63}$$

3.3 Simulation Results

The carrier-to-interference ratios in eq. (3.57) and eq. (3.63) are computed for the case when the number of subcarriers per optical carrier is 20, i.e., $M = 20$. The subcarrier frequencies are integer multiples of the electric bandpass filter bandwidth. From these numbers, the initial frequency offset is $f_0 = 0$. The choices above represent a typical situation. In the zero laser linewidth case, they also simplify the condition in eq. (3.55) such that only terms in eq. (3.56) and eq. (3.57) for which

$$r = \left[\frac{ni-k}{l}\right]_{r \text{ is integer}} \tag{3.64}$$

are computed.

Figure 3.2 shows a plot of the carrier-to-interference ratio in channel number 10 as a function of the intensity modulation index in the zero laser linewidth case. The curve for eq. (3.57) is denoted 'the large-signal approximation'. Shown also on the same graph is the small-signal approximation to CIR as obtained in [50]. The same curve could also be obtained by keeping only one term instead of three in eq. (3.22), and using the small-signal approximation to the frequency modulation index in eq. (3.25). From Figure 3.2 two observations are obvious. First, CIR is higher for larger intensity modulation indices.

Second, there is about 4.5 dB difference between the small- and the large-signal models in the calculated CIR value at larger modulation indices close to unity.

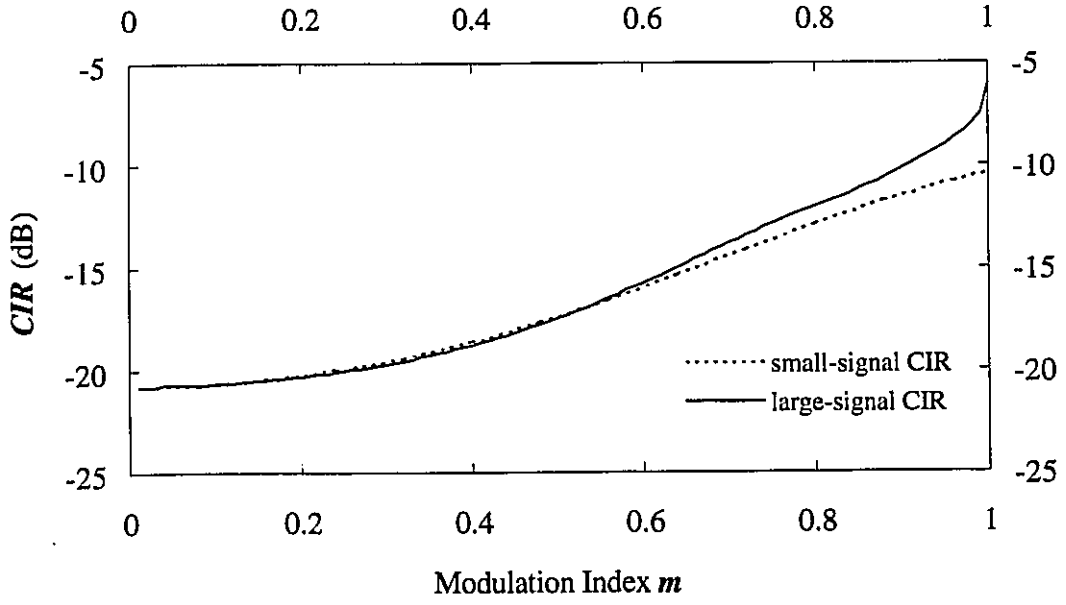

Figure 3.2: Small- and large-signal approximations to *CIR*

The first observation stems from the fact that a higher intensity modulation index implies a wider spread of the modulated laser field spectrum. When two laser fields are mixed at the photodetector, the resulting field bandwidth is roughly the sum of the bands of the two fields. When the individual fields' spectra are wider, the fraction of interference terms that falls within the passband of the electric bandpass filter is naturally less. Hence, an improvement in the CIR is expected.

The second observation can be explained as follows. Small signal model neglects many terms in the modulated laser field phase. These terms amount to a further field

spread, reducing the OBI and improving CIR. The discrepancy between the two models is noticeable at modulation indices approaching unity (about 4.5 dB). This difference is significant and can result in misleading conclusions about the severity of OBI.

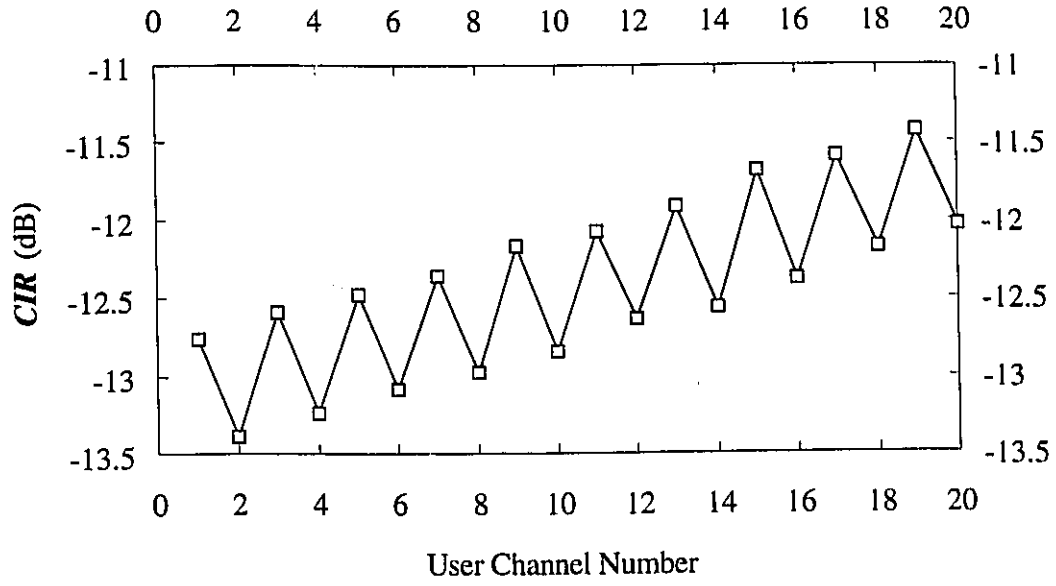

Figure 3.3: *CIR* for user channels when m=0.75

Figure 3.3 and Figure 3.4 illustrate the effect of OBI on different subcarrier channels for modulation indices of 0.75 and 1.0, respectively. In these figures, points were connected to clarify the curve shapes. Laser linewidths were set to zero.

The main observation in these figures is that the CIR has local maxima for odd-numbered channels. This is to be expected because, according to the subcarrier frequency assignment we are adopting, the subcarrier frequencies are integer multiples of one quantity. For odd-numbered channels, it is less frequent than it is for other channels to find

terms in eq. (3.57) that satisfy eq. (3.64). This motivates a suggestion for assigning subcarrier frequency values that are prime to each other. In fact, from Figure 3.4, this can lead to an improvement of several dB's in the CIR. This can be achieved, for example, by choosing 3, 5, 7, 11, ... times B as the subcarrier frequencies. In general, the subcarrier frequencies can be chosen to be prime multiples of the electric bandpass filter bandwidth B.

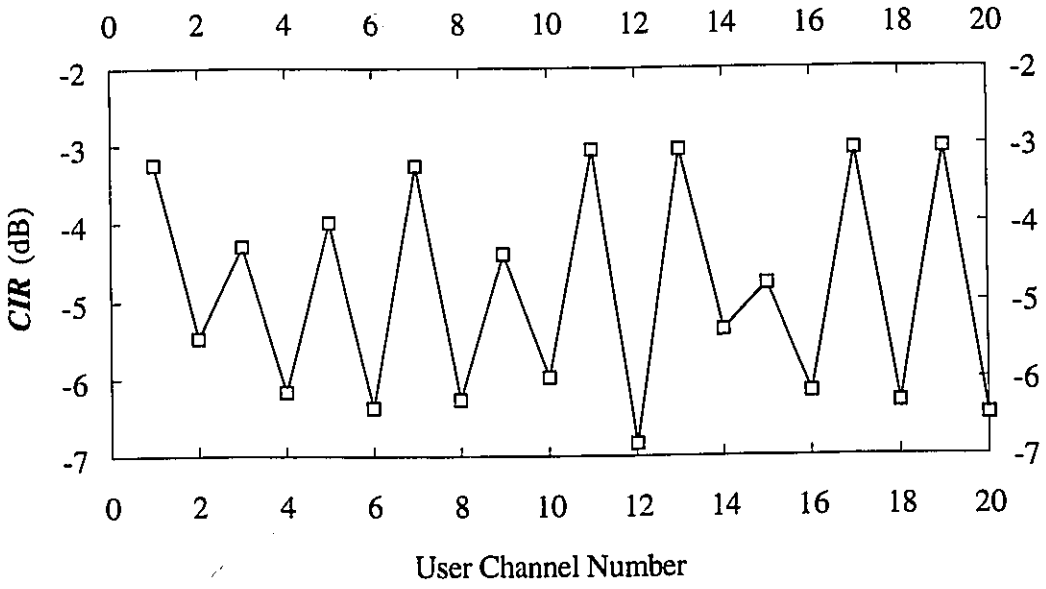

Figure 3.4: *CIR* for user channels when m=1.0

Figure 3.5 shows the effect of nonzero laser linewidth on the CIR as a function of the modulation index. As the figure demonstrates, there is very little effect of the laser linewidth on the CIR at high modulation indices. This is because, at such indices, optical

fields are already spread over wide bands due to deep modulation. Laser linewidths add only a little more broadening to the field spectra.

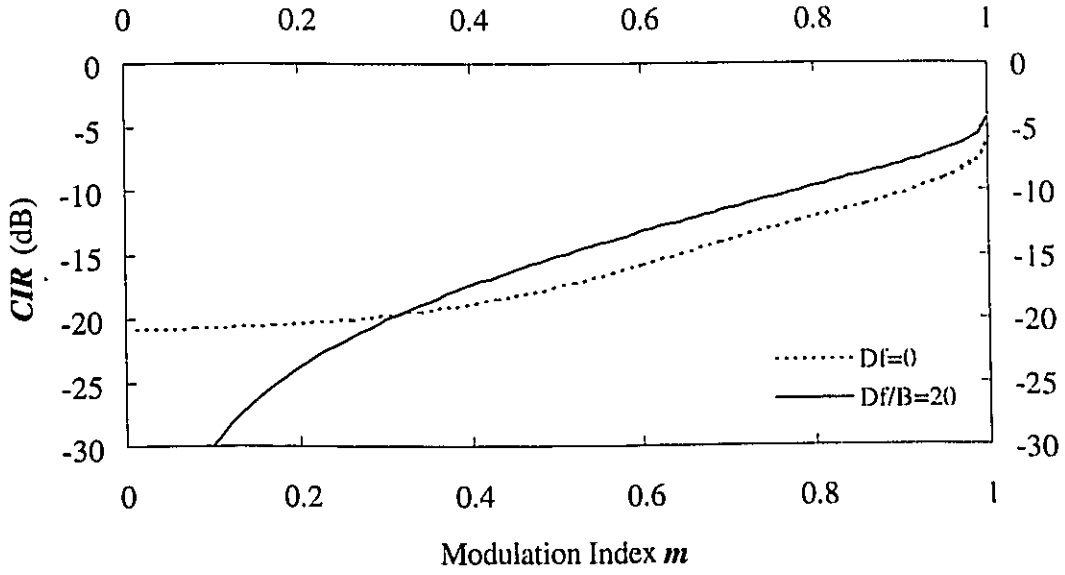

Figure 3.5: Effect of laser linewidth on OBI

Chapter Four

4. Polarization Scrambling and OBI

In this chapter, the use of independent PN signals to vary the polarizations of the subcarrier modulated laser fields in an optical channel is shown to dramatically reduce OBI. When asynchronous PN signals and/or random optical carrier frequencies are employed, further reductions in OBI can be achieved. Since the spatial phase of a field with one polarization component appears indistinguishable from a temporal phase component, the terms polarization and phase will be used interchangeably.

The discussions in this chapter are presented in terms of polarization scrambling, rather than phase modulation. This is because field polarization has two components in general. Both of these components could be phase scrambled. Besides, when fields have two (x and y) polarization components, their spatial variations can be represented by vectors in the xy plane. The angle between these two vectors can be PN modulated (scrambled). In summary, polarization scrambling is a general technique of which phase modulation is a special case.

The presentation in this chapter starts with the calculation of the OBI spectrum under PN polarization scrambling, which is used in calculating the OBI power at the output of the reference user electric BPF. The chapter also includes simulation results that

demonstrate the advantages of this scheme. The performance of a simple two user per optical channel system is studied using simulation.

4.1 The Spread OBI Spectrum

Let us assume, as in eqs. (2.1) and (2.3), that each field has one polarization component which could be along any one of the two directions normal to the wave propagation direction. A more general polarization description may be used, but all it does is to complicate the analyses without adding real information about the system behavior. However, the individual field spatial phases $\varphi_{pi}(t)$ will be assumed to be uniformly distributed and statistically independent.

The phase modulators in user channels are driven by a group of independent pseudorandom (PN) modulating signals. The clock rates of these PN signals are assumed to be all equal and much higher than the subcarrier bandwidths. Assuming each PN signal changes its level in τ_0 seconds, and neglecting the chirp effect, the phase modulated field amplitude corresponding to the i-th user can be represented by:

$$e_i(t) = \mathbf{Re}\left\{\left[S_i(t)\right]^{1/2} e^{j2\pi F_i t} e^{j\varphi_{ni}(t)} \sum_{k=-\infty}^{\infty} g(t-k\tau_0) e^{j\varphi_{pi,k}}\right\} \qquad (4.1)$$

where $g(t)$ is a unit amplitude pulse starting at time $t = 0$ and having a width τ_0. The modulation phase $\varphi_{pi,k}$ is assumed to take one of the two possible values $\pm\varphi_p$ with equal probabilities, depending on the PN modulating signal. Substituting eq. (4.1) into eq. (2.6), we get the signal and the cross-term currents at the output of the photodetector as follows:

$$I_s(t) = \frac{1}{2}\sum_{i=1}^{M} S_i(t) \tag{4.2}$$

and

$$I_c(t) = \sum_{i=1}^{M-1}\sum_{l=i+1}^{M} I_{c_{il}}(t) \tag{4.3}$$

where

$$I_{c_{il}}(t) = \left[S_{il}(t)\right]^{1/2}\sum_{k=-\infty}^{\infty} g\left(t - k\tau_0\right)\cos\left[2\pi F_{il}t + \varphi_{nil}(t) + \varphi_{pil,k}\right] \tag{4.4}$$

In the last equation, the following shorthand notation has been used

$$S_{il}(t) = S_i(t)S_l(t) \tag{4.5}$$

$$F_{il} = F_i - F_l \tag{4.6}$$

$$\varphi_{nil}(t) = \varphi_{ni}(t) - \varphi_{nl}(t) \tag{4.7}$$

and

$$\varphi_{pil,k} = \varphi_{pi,k} - \varphi_{pl,k} \tag{4.8}$$

To evaluate the effect of polarization scrambling on the system performance, we need to calculate the signal-to-noise ratio at the output of a typical user bandpass filter. To do that, we first find the signal and the cross-term power spectral densities. The signal current PSD was evaluated before, and is given by eq. (3.46). The filtered signal power is given by eq. (3.47). When the PN clock rate is sufficiently high (much higher than the subcarrier bandwidth), contributions of phase noise and signal intensities to the cross-term PSDs can be neglected. Hence, in a typical cross-term, $\varphi_{nil}(t)$ will be omitted, and $S_{il}(t)$ will be approximated by a constant S_0^2. On the basis of these approximations, the cross-

term currents $I_{c_{il}}(t)$ become statistically identical, in addition to being statistically independent. As a result, the power spectral density of the total cross-term current $I_c(t)$ can be approximated by the sum of the PSDs of the individual cross-term currents.

The formulas above can be used to find the ***il***-th cross-term power spectral density as follows [56]:

$$S_{I_{c_{il}}}(f) = \frac{S_0^2 \tau_0}{4}\left[\mathbf{sinc}^2\left(\pi(f - F_{il})\tau_0\right) + \mathbf{sinc}^2\left(\pi(f + F_{il})\tau_0\right)\right] \qquad \textbf{(4.9)}$$

4.2 The Polarization Scrambling Advantage

To appreciate the polarization scrambling advantage in reducing the OBI, there are a few note-worthy points at the beginning. First, the optical center frequencies were assumed fixed. This does not need to be the case in practice. However, it can be easily visualized that fluctuations in the optical center frequencies add further expansion to the OBI spectrum. This in turn results in a lower OBI PSD, and hence, less interference power into the reference user BPF. The effects of optical frequency fluctuation are discussed in section 4.4. Second, the individual users PN signals used in polarization scrambling are generally asynchronous to one another. This is yet another source of the OBI spectrum expansion. This results from the fact that the phase difference $\varphi_{pi,k}$ stays only a fraction of τ_0 in one of its possible states. It will be shown later in this section that the required PN rate can be reduced by a factor of two by using asynchronous PN sequences. Additionally, fields have two polarization components in general. Taking into account the

polarization angle fluctuation will be shown later in this section to reduce the required PN rate by another factor of two.

Based on these facts, the assumptions of fixed optical center frequencies and synchronous PN modulating signal are worst case assumptions, since they give the least attainable OBI spectrum expansion. Carrying on with these assumptions, we add the simplifying assumption of equal optical center frequencies of all M fields coming into a photodetector. There is no important loss of generality in introducing this assumption.

It can be seen from eq. (4.4) that under equal optical center frequencies the OBI spectral density becomes:

$$S_{I_{cil}}(f) = S_0^2 \tau_0 \mathrm{sinc}^2(\pi f \tau_0) \tag{4.10}$$

This results in equal PSDs for all OBI terms. Hence, to find the total OBI PSD, we simply multiply eq. (4.10) by $M(M-1)/2$, the number of distinct OBI terms. Assuming ideal bandpass characteristics of the reference (k-th) user BPF, the output OBI power can be calculated as:

$$P_{obi} = M(M-1)S_0^2\tau_0 \int_{f_k - B/2}^{f_k + B/2} \mathrm{sinc}^2(\pi f \tau_0) df \tag{4.11}$$

where B is the electronic BPF bandwidth. Using an infinite series expansion of the integrand in eq. (4.11), we get

$$P_{obi} = \frac{M(M-1)S_0^2}{\pi} \sum_{l=1}^{\infty} \frac{(-1)^{l+1} 2^{2l-1}}{(2l)!(2l-1)} \times \left[\left[\pi\tau_0 (f_k - B/2) \right]^{2l-1} - \left[\pi\tau_0 (f_k + B/2) \right]^{2l-1} \right] \tag{4.12}$$

To get enough OBI spectrum expansion, the quantity $\tau_0 B$ must be as small as possible. For a high data rate transmission, f_k is a few multiples of B. Hence, for an effective OBI spectrum expansion, the terms $\pi\tau_0(f_k \pm B/2)$ have to be very small. For example, if

$$\tau_0 \frac{B}{2} = 0.001$$
$$\tau_0 f_k = 0.005$$

the second term in the summation eq. (4.12) is three orders of magnitude less than the first term. Hence, eq. (4.12) will be approximated by keeping only the first term as follows:

$$P_{obi} \approx M(M-1)S_0^2\tau_0 B \tag{4.13}$$

Dividing the filtered signal power in eq. (3.46) by the filtered OBI power in eq. (4.13) yields the following expression for the carrier-to-interference ratio:

$$CIR \approx \frac{m^2}{8M(M-1)\tau_0 B} \tag{4.14}$$

To evaluate the system performance in terms of the probability of error, we neglect all other kinds of interference and noise, and assume that the spectrum-expanded OBI can be modeled as an AWGN. The last assumption can be justified by noting that the objective is to increase the number of users M per optical channel by as much as possible, in which case the central limit theorem can be used. We also assume binary antipodal signaling, i.e., the subcarrier signal in eq. (2.2) is modified to look like:

$$S_i(t) = S_0\left\{1 \pm m\cos(2\pi f_i t)\right\} \tag{4.15}$$

It is known that for binary antipodal signaling in additive white Gaussian noise, the probability of error is [10]:

$$P(e) = \frac{1}{2}\mathbf{erfc}\left[\sqrt{\gamma}\right] \tag{4.16}$$

where the signal-to-noise ratio γ is approximately equal to $\boldsymbol{CIR}$ in our case. To satisfy the 10^{-9} required probability of error, we solve eq. (4.16) numerically in order to obtain:

$$\gamma \geq 18 \tag{4.17}$$

Substituting this result in eq. (4.14) we get

$$\frac{1}{\tau_0 \boldsymbol{B}} \geq \frac{144\boldsymbol{M}(\boldsymbol{M}-1)}{\boldsymbol{m}^2} \tag{4.18}$$

If we let, for example

$$\boldsymbol{m}^2 = 0.5$$
$$\boldsymbol{M} = 2$$

the required PN signal should satisfy

$$\frac{1}{\tau_0 \boldsymbol{B}} \geq 576$$

To have a feeling about these numbers, assume a 200 MHz BPF bandwidth, which allows data to be transmitted at up to 100 Mb/s. This choice results in a required PN rate of more than 100 GHz. Unfortunately, it is very difficult to generate PN signals at such a rate. Besides, due to device capacitance; an electro-optic phase modulator usually has a much smaller bandwidth (about 20 GHz). However, much lower PN rates are required in practice, as will be shown in the following three paragraphs.

It should be emphasized that independently-generated PN signals are not synchronous in general. For example, if the two PN sequences are $\tau_0/2$ seconds out of synchronism, then τ_0 in eqs. (4.1), (4.4), and (4.9)-(4.14) is replaced by $\tau_0' = \tau_0/2$. This means that rate of the needed PN sequences can be reduced by a factor of two.

Another factor of two reduction in the PN rate can be obtained by assuming that each field has two polarization components (along the x and y directions). This can be seen as follows: Eq. (4.1) will have to be replaced by a vector equation that includes the polarization direction. The resulting field vector can be represented in the form:

$$\vec{e}_i = \hat{u}_i e_i(t) \tag{4.19}$$

where $\hat{u}_i$ is a unit vector in the polarization direction. Similar to eq. 1.3, the two field vectors can be assumed to have an angle ψ between them. This angle is usually random, and it can be assumed to uniformly distributed in the interval $[0,2\pi]$. As a result, he cross-term current given by eqs. (4.3) and (4.4) has to multiplied by $\cos\psi$ (similar to eq. 1.4). Finally, the calculation of the OBI PSD in eqs. (4.9) and (4.10) will have to include the additional step of averaging over ψ. The resulting OBI PSD will thus be half the one given by eqs. (4.9) and (4.10), the OBI power will be half the one given by eqs. (4.11) and (4.12), and the required PN rate will be half the one obtained through eq. (4.18).

More reduction in the required PN rate can be achieved by taking into account optical carrier frequency fluctuation. This will be demonstrated in section 4.4 below. Furthermore, methods for optically achieving very high rates of PN modulation using all-optical processing are listed as future research issues in Chapter 6.

In summary, there are several ways to achieve much more reduction in the OBI power spectral density. Namely, we could:

- modulate the two laser outputs with asynchronous PN signals.
- allow optical fields to have two polarization components instead of one, and randomize the angle between field polarizations.

- randomize the optical center frequencies.

A combination of any two or all three of these methods is expected to produce even further reductions in the OBI PSD. The effects of random optical carrier on the CIR and other performance measures is discussed in section 4.4.

4.3 Simulation Results for CIR with Polarization Scrambling

A two-user system is simulated using MATLAB. The two subcarriers have frequencies of 4 and 5 GHz, respectively. Each subcarrier is PSK-modulated by a 200 Mb/s digital binary source producing two equally likely symbols. The subcarriers then intensity modulate two laser fields with an equal modulation index of $\sqrt{0.5}$.

In all simulations, laser phase noise is neglected because the objective is to evaluate the spectrum expansion achievable by phase modulating the lasers with PN signals. The sampling frequencies used in simulations are equal to four times the rate of the respective PN signals. The signal and OBI spectra are estimated using a 1024-point FFT. In each of the figures about to be presented, the average power spectral density is computed using 100 runs of the respective simulation program. Parseval's theorem is applied to the estimated spectra; such that they ideally have to be equal to theoretical values.

Figure 4.1 shows the subcarrier and the OBI spectra without polarization scrambling. To help identify each of these spectra, the two laser center frequencies were separated by 8 GHz.

Figure 4.2 and Figure 4.3 show the OBI spectra for $\tau_0 B = 0.1$ and $\tau_0 B = 0.01$, respectively. Figure 4.4 and Figure 4.5 show the subcarrier and OBI spectra around the subcarrier frequency range. The PN advantage in reducing the OBI PSD by increasing the PN polarization scrambling rate is obvious in these figures.

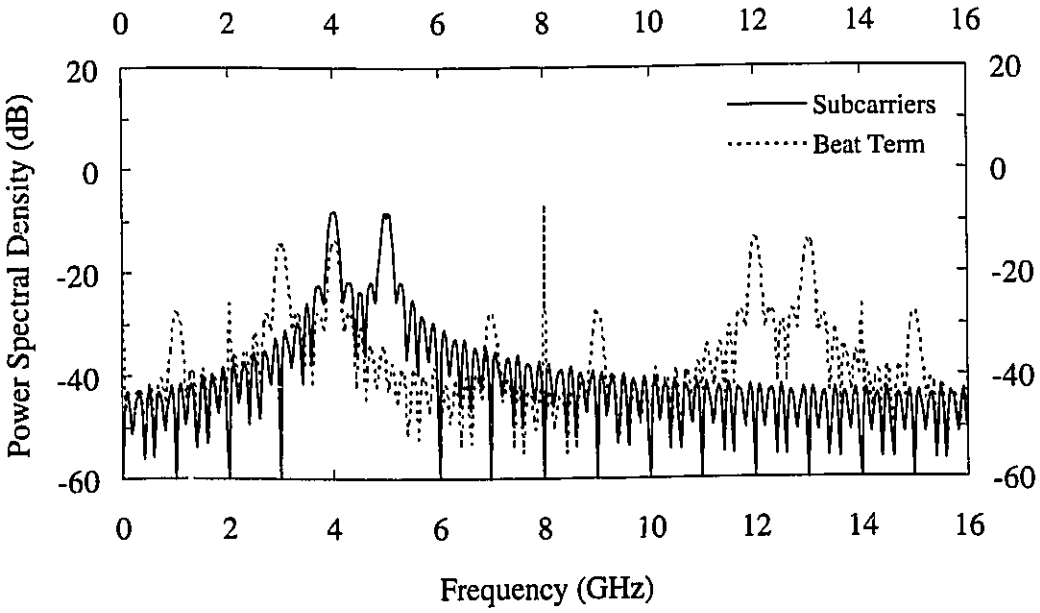

Figure 4.1: Subcarrier and OBI spectra under no polarization scrambling

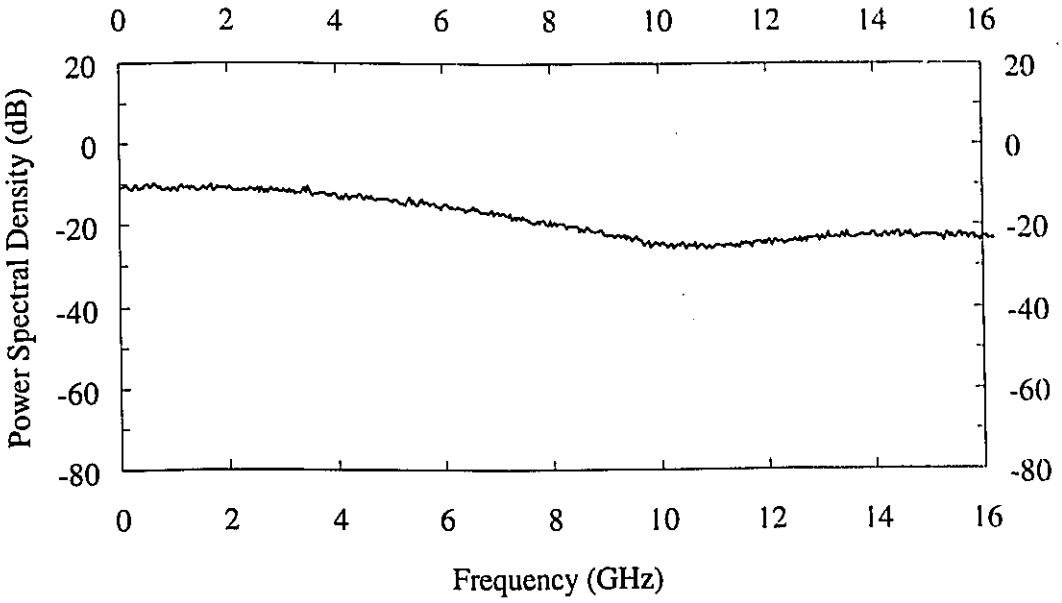

Figure 4.2: OBI spectrum for $\tau_0 B = 0.1$

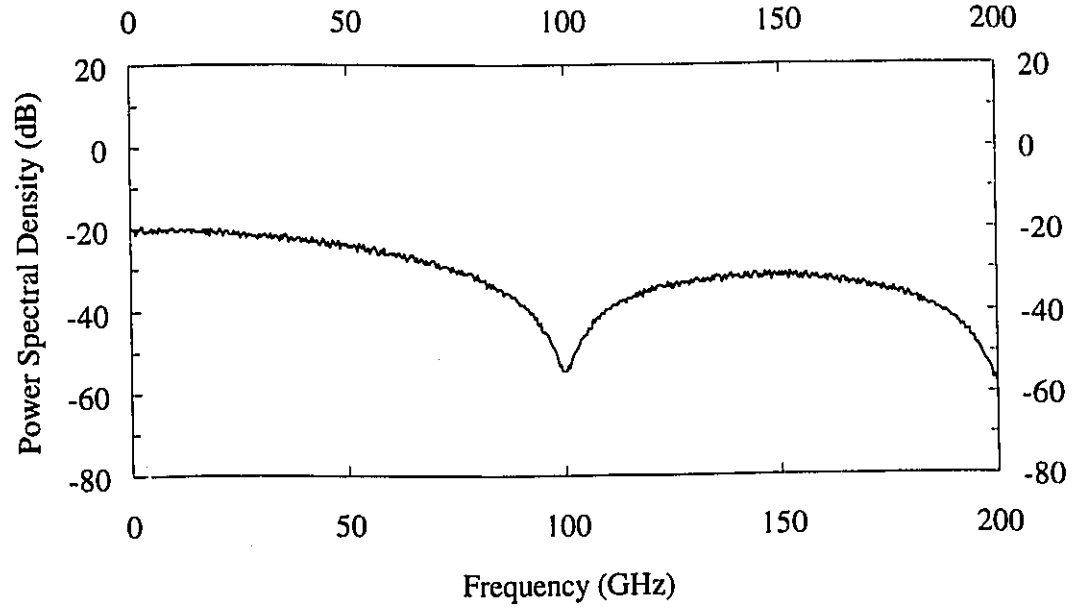

Figure 4.3: OBI spectrum for $\tau_0 B = 0.01$

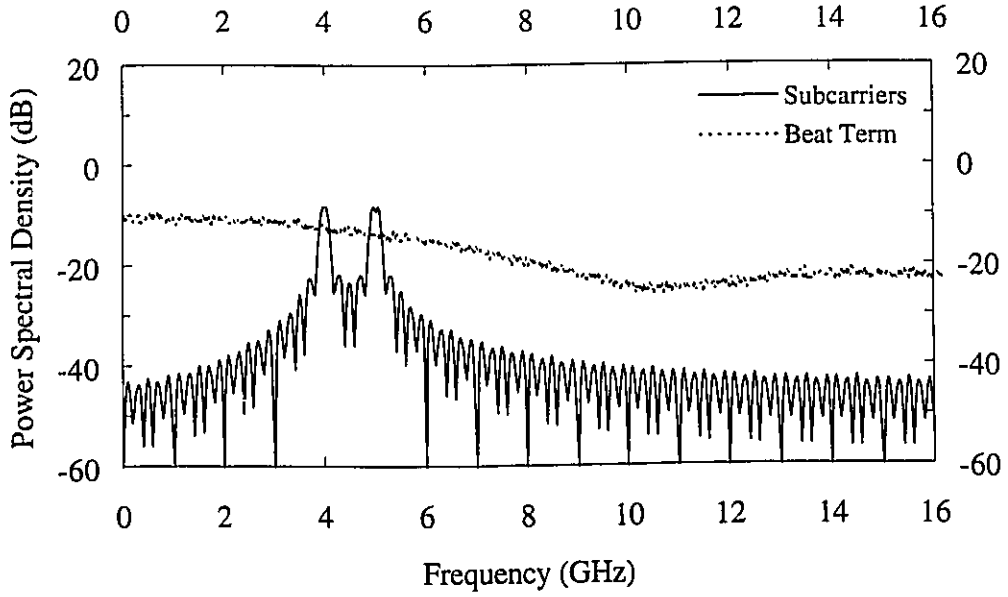

Figure 4.4: Subcarrier and OBI spectra for $\tau_0 B = 0.1$

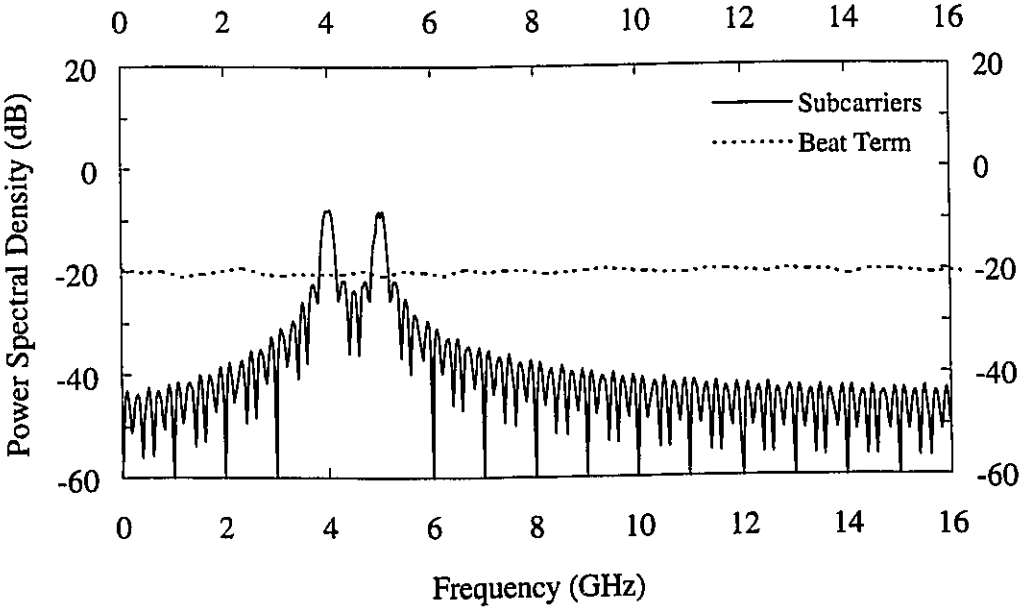

Figure 4.5: Subcarrier and OBI spectra for $\tau_0 B = 0.01$

4.4 Performance of SCM/WDMA with Polarization Scrambling

In the previous section, we presented analytical and simulation results for the OBI PSD in a worst case situation. In this section, we assume a simple two-user per carrier network. Laser frequencies are assumed to wander, rather than being equal and fixed as in section 4.3.

To study the effect of polarization scrambling on the network performance, a two-user system is simulated using MATLAB [52] with the subcarrier center frequencies f_1 and f_2 equal to 4 GHz and 5 GHz, respectively. The electronic BPF bandwidth B is equal to twice the subcarrier bit rate. The subcarrier bit rate assumes values of 200 and 500 Mb/s. Laser frequencies are assumed to fluctuate uniformly in a range R of 50 GHz. Both users have an equal modulation index value of $\sqrt{0.5}$. With this setup, we evaluate the average CIR, average bit probability of error, and outage probability for the first user.

4.4.1 Carrier-to-Interference Ratio

Average CIR is evaluated in the same way it was in subsection 2.3.1. Figure 4.6 shows the result. Significant improvements in the CIR are achieved at high PN rates. Shown also in the same graph is the threshold CIR value needed in the case of Gaussian OBI to obtain a 10^{-9} error probability.

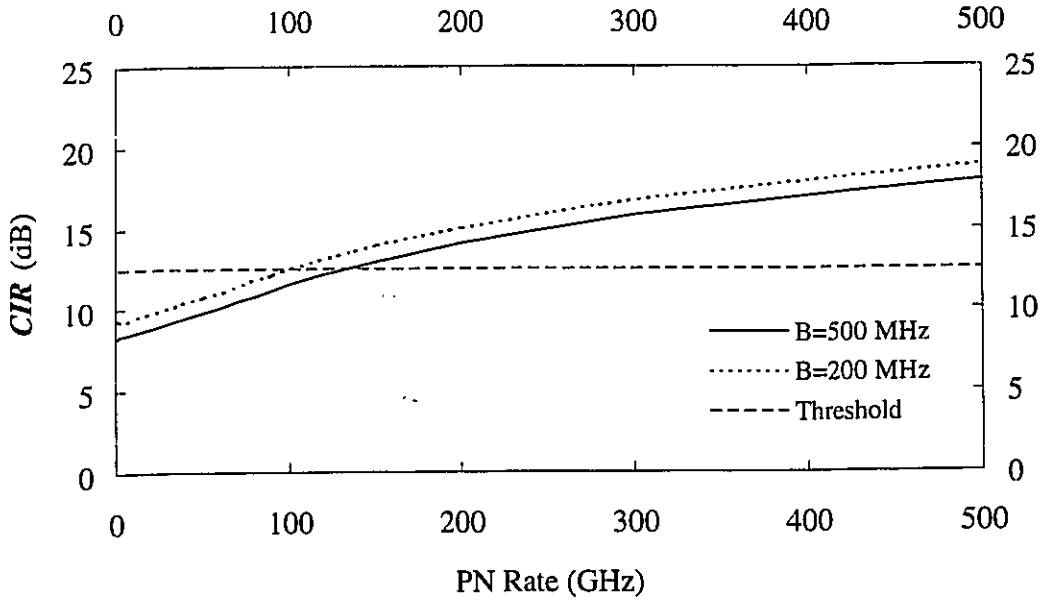

Figure 4.6: ***CIR*** for a two-subcarrier/channel SCM/WDMA network with polarization scrambling

As Figure 4.6 shows, both CIR curves cross the Gaussian threshold line at about 100 GHz PN rate. The same result will be confirmed through error probability estimation in subsection 4.4.2 below. It will also be shown in subsection 4.4.2 that the OBI does become Gaussian for PN rates required to achieve these threshold CIR values.

4.4.2 Probability of Error

In this subsection, we find the probability of error in the first user receiver. The demodulator has the structure shown in Figure 2.4. Field amplitudes are still given by eq. (2.1). Substituting $M = 2$ in eq. (2.4) gives the field amplitude sum as in eq. (2.8).The PN rate is assumed to be related to the subcarrier bit rate through the integer K by:

$$\tau_0 = \frac{T_b}{K}, \qquad K \geq 1 \tag{4.20}$$

where τ_0 is the PN sequence chip duration. With this assumption, and noting that the polarization component of the phase $\varphi_{pi}(t)$ in eq. (2.3) is not neglected, the decision variable in eq. (2.30) can be rewritten in the form:

$$\begin{aligned} Z &= \frac{m_1 T_b}{4} + \sum_{k=1}^{K} b_k G_k(F_x, m_2) \\ &= Z_s + Z_c \end{aligned} \tag{4.21}$$

where b_k is a random variable uniformly taking the values ± 1, that results from the phase difference between the two fields. $G_k(F_x, m_2)$ is given by:

$$\begin{aligned} G_k(F_x, m_2) = \int_{(k-1)\tau_0}^{k\tau_0} & \sqrt{1 + m_1 \cos 2\pi f_1 t}\sqrt{1 + m_2 \cos 2\pi f_2 t} \\ & \times \cos 2\pi f_1 t \cos 2\pi F_x t \, dt \end{aligned} \tag{4.22}$$

This function can be rewritten in the following form using trigonometric Fourier series expansion:

$$G_k(F_x, m_2) = \sum_{n=0}^{\infty} \frac{a_n}{2} \int_{(k-1)\tau_0}^{k\tau_0} \left[\cos 2\pi(F_x + \nu_n)t + \cos 2\pi(F_x - \nu_n)t\right] dt \tag{4.23}$$

Frequencies $\{\nu_n\}$ and Fourier coefficients $\{a_n\}$ were computed numerically. Upon integration of eq. (4.23) we get:

$$G_k(F_x, m_2) = \sum_{n=0}^{\infty} \frac{\tau_0 a_n}{2} \left[Q_{n,k}(F_x, m_2) - Q_{n,k-1}(F_x, m_2)\right] \tag{4.24}$$

where

$$Q_{n,k}(F_x, m_2) = k\left[\operatorname{sinc} 2\pi(F_x + \nu_n)k\tau_0 + \operatorname{sinc} 2\pi(F_x - \nu_n)k\tau_0\right] \tag{4.25}$$

The decision variable in eq. (4.21) consists of a signal term Z_s and an interference cross-term Z_c. These terms are given by:

$$Z_s = \frac{m_1 T_b}{4} \tag{4.26}$$

$$Z_c = \sum_{k=1}^{K} b_k G_k(F_x, m_2) \tag{4.27}$$

To calculate $P(e)$, we need to find the pdf for Z_c. This is done through finding the characteristics function $C_{Z_c}(j2\pi\lambda)$ as follows:

$$C_{Z_c}(j2\pi\lambda) = \left\langle \prod_{k=1}^{K} e^{j2\pi\lambda b_k G_k(F_x, m_2)} \right\rangle_{F_x, m_2, \{b_k\}} \tag{4.28}$$

The operator $\langle\rangle$ denotes ensemble averaging, and the subscripted variables are those to be averaged over. The variables $\{b_k\}$ are statistically independent, hence resulting in the form in eq. (4.28). Carrying out the averaging over $\{b_k\}$, we get:

$$C_{Z_c}(j2\pi\lambda) = \left\langle \prod_{k=1}^{K} \cos\left[2\pi\lambda G_k(F_x, m_2)\right] \right\rangle_{F_x, m_2} \tag{4.29}$$

The averaging over m_2 is done by simply including two terms: $G_{k+}(F_x)$ when m_2 equals $+\sqrt{2}$, and $G_{k-}(F_x)$ when m_2 equals $-\sqrt{2}$. The pdf of F_x was given in eq. (2.29). The result for averaging over m_2 and F_x is:

$$C_{Z_c}(j2\pi\lambda) = \frac{1}{2}\int_0^R \left[\cos 2\pi\lambda G_{k+}(F) + \cos 2\pi\lambda G_{k-}(F)\right] P_{F_x}(F)\, dF \tag{4.30}$$

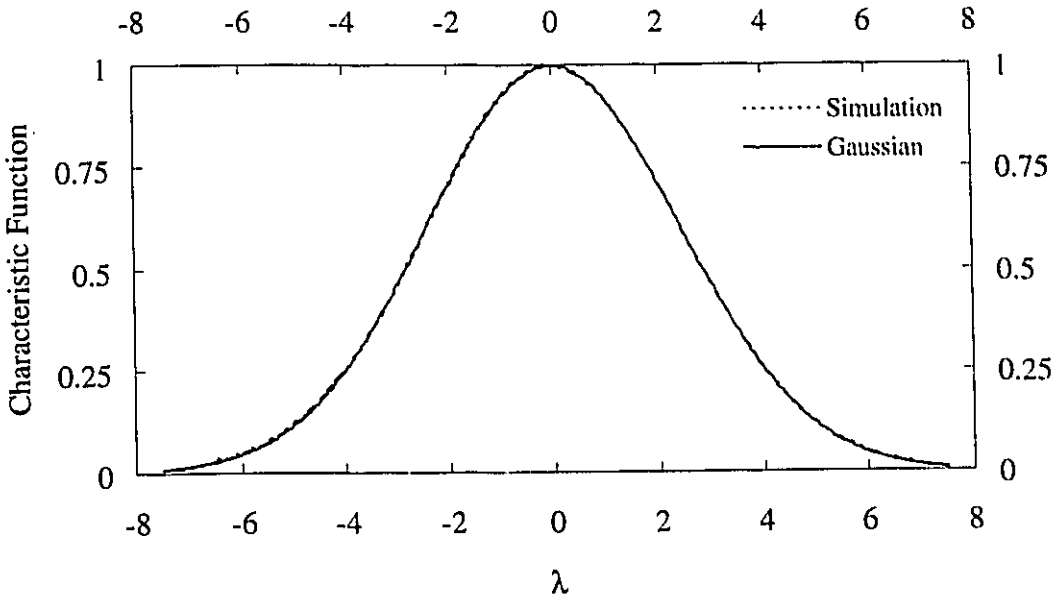

Figure 4.7: Characteristic functions of OBI at a PN rate of 100 GHz and a Gaussian random variable with the same variance

This function was computed numerically for different PN rates and compared to the characteristic function of a Gaussian random variable with the same variance. Excellent agreement was found at PN rates higher than 60 GHz. An example showing this agreement is shown in Figure 4.7 for a subcarrier bit rate of 500 Mb/s and a PN rate of 100 GHz. As can be seen from the figure, it is very difficult to distinguish the two curves.

$P(e)$ is shown in Figure 4.8 in the case of a 500 Mb/s subcarrier bit rate. For PN rates less than 60 GHz, the OBI is not Gaussian and the probability of error was found by numerically computing Z in eq. (4.21), comparing it to zero, and finding the proportion of times in which Z is negative.

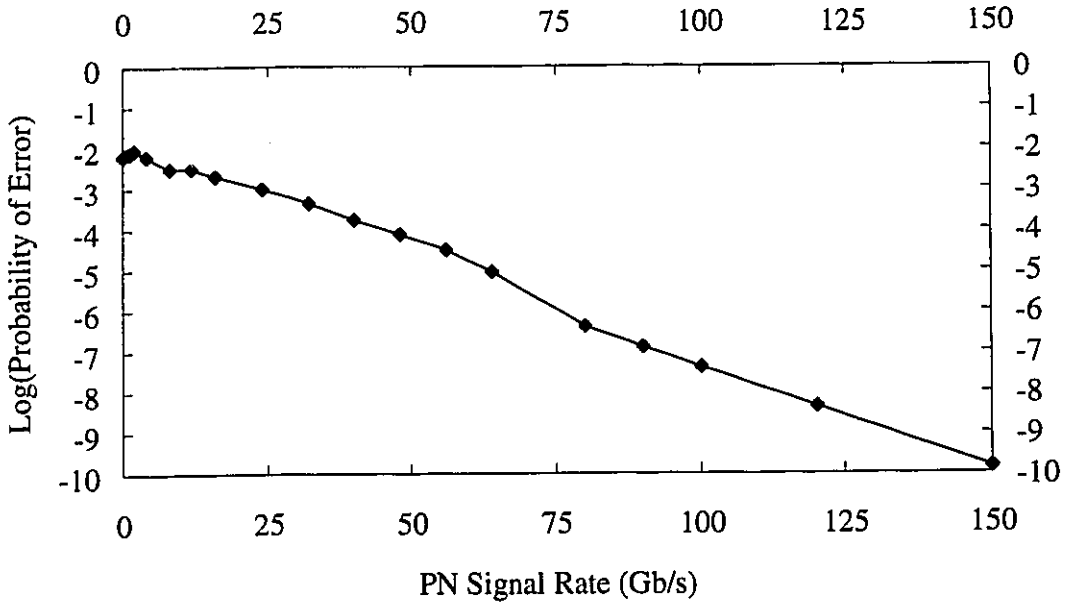

Figure 4.8: Probability of error in a two-subcarrier/channel SCM/WDMA network with polarization scrambling

When the PN rate exceeds 60 GHz, the OBI becomes Gaussian, and we can integrate over its pdf to find $P(e)$. The OBI pdf is totally determined by its variance estimated by the variance of the equivalent Gaussian random variable. The OBI mean value is zero because the characteristic function has no imaginary part as seen in eq. (4.29) and eq. (4.30). A numerical search algorithm using least squares minimization was used to determine the variance value that best fits the simulated values of the OBI characteristic function. With this in mind, $P(e)$ can be calculated from:

$$P(e) = \frac{1}{\sqrt{2\pi\sigma_{obi}^2}} \int_{-\infty}^{-m_1 T_b/4} e^{-x^2/2\sigma_{obi}^2}\, dx \qquad \textbf{(4.31)}$$

This result can be written in terms of the complementary error function in the form:

$$P(e) = \frac{1}{2}\mathrm{erfc}\left[\frac{m_1 T_b}{4\sigma_{obi}\sqrt{2}}\right] \tag{4.32}$$

As can be seen from Figure 4.8, the probability of error decreases almost linearly with the increase in the PN polarization scrambling rate.

It is possible at PN rates around 140 GHz to achieve a 10^{-9} error probability with two subcarriers per channel each transmitting at 500 Mb/s. This makes the throughput of each optical channel equal to 1 Gb/s. With a laser frequency uncertainty range of 50 GHz and a polarization scrambling rate of 140 GHz, optical channels can be allocated at about 200 GHz spacing. Assuming a total fiber bandwidth of about 30 THz, 150 optical channels can be supported. This results in a total network throughput of 150 Gb/s.

As discussed earlier, a much lower PN rate is actually to achieve the same throughput if the PN sequences are asynchronous. The PN rate can also be reduced by taking into account that the fields have a random polarization angle difference between them.

4.4.3 Outage Probability

Outage probability is estimated the same way it was in subsection 2.3.3. An indicator function is computed and averaged using the pdf for the optical frequency separation.

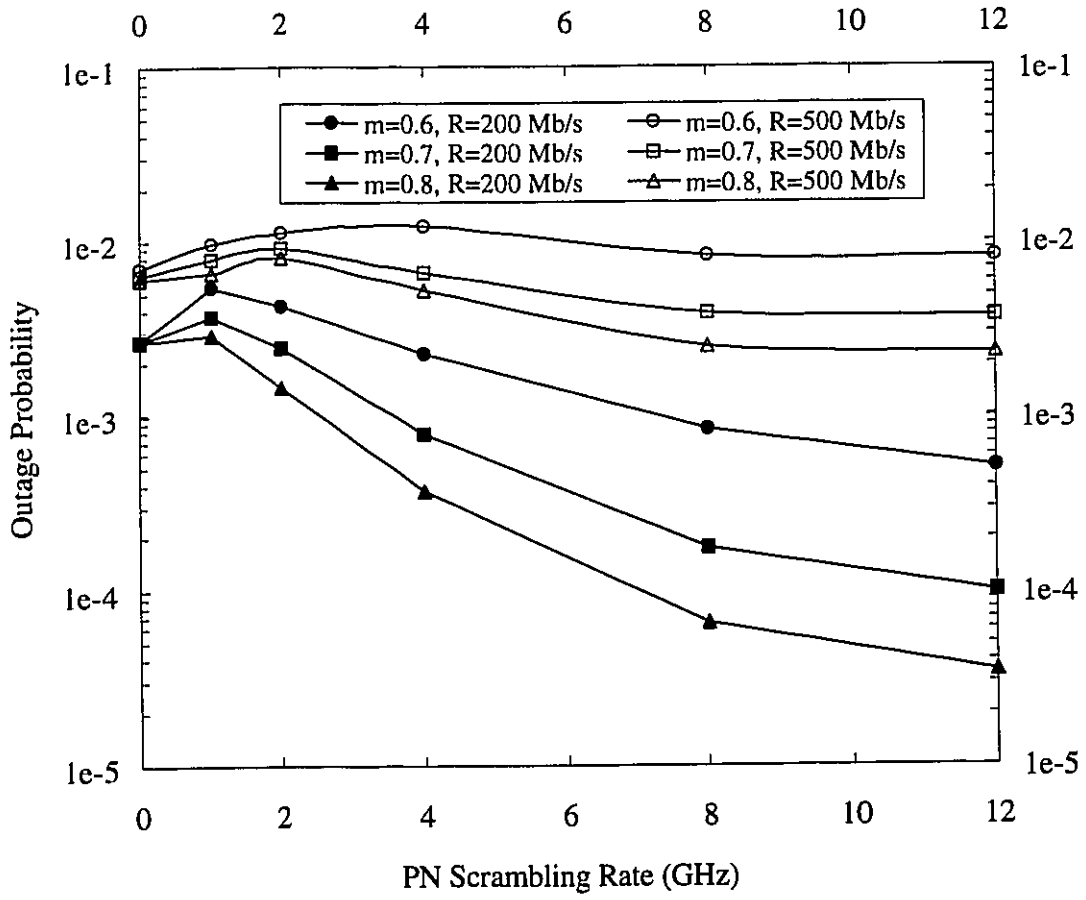

Figure 4.9: Outage probability in a two-subcarrier/channel SCM/WDMA network

Figure 4.9 shows the resulting outage probability. The main observation in this graph is that the outage probability decreases as the PN polarization scrambling rate is increased. The curves for higher modulation indices show lower outage probabilities. When the subcarrier PSK modulation rate is 200 Mb/s, the decrease in the outage probability with the increase in the polarization scrambling rate is significantly sharper than it is for the 500 Mb/s PSK modulation case. Outage probability has a peak at small PN

scrambling rates (compared to the PSK modulation rate). When polarization scrambling is applied, the OBI spectrum is spread over a wider frequency range, and the OBI PSD becomes smaller. When the polarization scrambling rate is small, the drop in the OBI PSD is not sufficient to reduce the error rate below 10^{-9}. Meanwhile, the OBI spectrum widening makes the error rate exceed 10^{-9} for a larger number of F_x values.

4.5 The Phase Modulator

Different kinds of devices can be used to achieve polarization agility. The so-called electro-optic phase modulators [60], [61] are known to be the best to do the job. This is because, unlike other phase modulators, electro-optic modulators do not use mechanical effects to adjust polarization. Electro-optic phase modulators are compact in size, need low drive power, and are easy to integrate [60]. They also offer full-range polarization variation [62]. Finally, they offer a wide bandwidth in excess of 20 GHz [63]. For the purposes of this work, it is believed that much higher modulation rates can be afforded. The modulator output will be attenuated by a few dB at higher modulation rates, but since the same attenuation applies to both signal and OBI terms, it can be tolerated.

Electro-optic phase modulators come in two main structures, longitudinal and transverse [64]. Figure 4.10 depicts the longitudinal phase modulator based on $LiNbO_3$ [64]. The applied field is parallel to the input beam field, hence the name longitudinal. The polarizer's function is to limit the input beam polarization to either x or y polarization. Although in longitudinal modulators this polarizer is not essential, it is very important in transverse modulators. For longitudinal phase modulators, V_π is given by [65].

$$V_\pi = \frac{\lambda}{n^3 r} \tag{4.33}$$

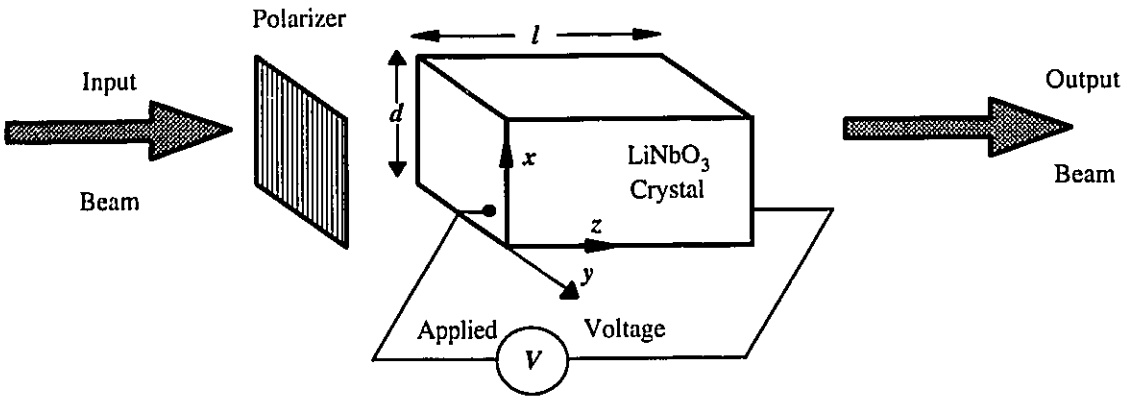

Figure 4.10: Longitudinal electro-optic phase modulator

To find V_π, let's assume that the polarizer transforms the input light into x-polarized light. In such a case, the variables in eq. (4.33) have the following values [65]

$$\begin{aligned} n &= n_x \\ &= 2.286 \\ r &= r_{13} \\ &= 8.6 \times 10^{-12} \text{ m / V} \end{aligned}$$

where r_{13} is the first row-second column element in the electro-optic tensor of $LiNbO_3$ and n_x is its refractive index in the x direction. For an input light of wavelength λ = 1.55 μm we find that

$$V_\pi \approx 15 \text{ KV}$$

If the polarizer transforms the input light into y polarization, the resulting V_π is approximately

$$V_\pi \approx 4.7 \text{ KV}$$

These are very high bias voltages that are quite undesirable in practical applications. Other disadvantages of the longitudinal phase modulators include [66]:

1. Electrodes (to which bias voltage is applied) can interfere with the input optical beam.

2. There is no effect of the crystal length on the induced phase shift.

3. They have a poor response at high modulation frequencies.

An alternative structure that avoids these drawbacks is called the transverse electro-optic phase modulator and is shown schematically in Figure 4.11 [64].

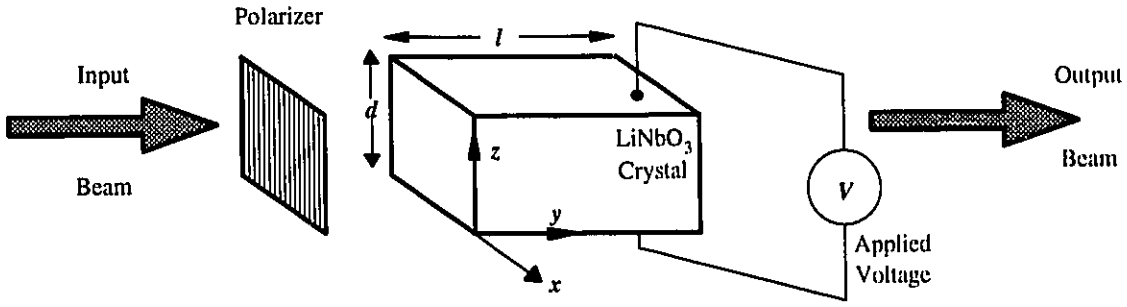

Figure 4.11: Transverse electro-optic phase modulator

In this case, the modulation field is normal to the input field. For this kind of modulator V_π is given by [65]

$$V_\pi = \begin{cases} \dfrac{\lambda d}{n_x^3 r_{13} l}; & \text{input beam } x-\text{polarized} \\ \dfrac{\lambda d}{n_z^3 r_{33} l}; & \text{input beam } z-\text{polarized} \end{cases} \tag{4.34}$$

Since for $LiNbO_3$, $r_{33} = 30.8 \times 10^{-12}$ m / V $> r_{13}$, the polarizer is set to transform input light into z polarization. In this case, assuming

$$d / l = 10^{-3}$$

and substituting in the second equality in eq. (4.34), we get:

$$V_{\pi} \approx 4.7 \text{ V}$$

which is a reasonable value for all practical applications.

Chapter Five

5. Mode Scrambling Using Multimode Fiber

In this chapter, we investigate the effect of mode scrambling on OBI. We use multimode fiber to transform each laser field into a multitude of modes with random distributions. When the sum of such fields is detected by a photodetector, it is anticipated that the OBI power will be distributed over many modes. We report on an experiment performed to test the ability of mode scrambling to remove or reduce OBI.

5.1 Mathematical Formulation

If a linearly-polarized light is injected into a multimode fiber, it will excite a number of propagating modes within the fiber. For the sake of simplicity we assume unmodulated light only. The propagating field (in the z direction) can be written in the form [67]:

$$\vec{e}_i(t) = e^{j2\pi F_i t} \sum_{l=1}^{L} \left\{ e_{i,l}^{(x)}(z)\hat{u}_x + e_{i,l}^{(y)}(z)\hat{u}_y \right\} \tag{5.1}$$

where $e_{i,l}^{(x)}(z)$ and $e_{i,l}^{(y)}(z)$ are the l -th mode's complex spatial amplitudes of the x and y polarization components, respectively, and $\hat{u}_x$ and $\hat{u}_y$ are the corresponding unit vectors.

A typical OBI term at the PD output can be calculated from the dot product of two fields similar to the one in eq. (5.1). Such an OBI term can be written as:

$$I_{c_{ir}}(t) \propto \cos\left[2\pi(F_i - F_r)t\right] \sum_{k=1}^{L} \sum_{l=1}^{L} \left\{ \left\langle e_{i,k}^{(x)}(z) e_{r,l}^{(x)*}(z) \right\rangle + \left\langle e_{i,k}^{(y)}(z) e_{r,l}^{(y)*}(z) \right\rangle \right\} \qquad (5.2)$$

where the asterisk in the superscript denotes complex conjugation.

Note that, $e_{i,k}^{(x)}(z)$ and $e_{r,l}^{(x)}(z)$ are statistically independent; because they are assumed to be generated by independent sources. Similar arguments can be applied for $e_{i,k}^{(y)}(z)$ and $e_{r,l}^{(y)}(z)$. In addition, when the number of propagating modes is large enough, the central limit theorem applies and the electric field becomes a Gaussian distributed stochastic process [67]. In such a case, the complex spatial amplitude of each mode (e.g., $e_{i,k}^{(x)}(z)$) includes a uniformly distributed random phase [67]. Applying the expectation rule for statistically independent random variables, and taking into account the uniformly distributed phases, we find that:

$$I_{c_{ir}}(t) = 0 \qquad (5.3)$$

On the other hand, signal terms are calculated using the dot product of each field with itself. This can be done for the i -th field in the following way:

$$I_s(t) \propto \sum_{k=1}^{L} \sum_{l=1}^{L} \left\{ \left\langle e_{i,k}^{(x)}(z) e_{i,l}^{(x)*}(z) \right\rangle + \left\langle e_{i,k}^{(y)}(z) e_{i,l}^{(y)*}(z) \right\rangle \right\} \qquad (5.4)$$

In the case of a large number of modes, $e_{i,k}^{(x)}(z)$ and $e_{i,l}^{(x)}(z)$ are statistically independent when $k \neq l$ [67]. The same argument applies to $e_{i,k}^{(y)}(z)$ and $e_{i,l}^{(y)}(z)$. With uniform phases taken into account, eq. (5.4) simplifies to:

$$I_s(t) \propto \sum_{l=1}^{L} \left\{ \left\langle \left| e_{i,l}^{(x)}(z) \right|^2 \right\rangle + \left\langle \left| e_{i,l}^{(y)}(z) \right|^2 \right\rangle \right\} \tag{5.5}$$

The quantity on the right hand side of eq. (5.5) is proportional to the desired field power. This means that, while the OBI terms can be averaged out through the multimode fiber, signal terms remain intact. This can represent a remarkable solution to the OBI problem in SCM/WDMA networks. Actually, this is a very simple solution; since all is needed is a piece of multimode fiber before the photodetector.

In the following section we present the results of an experiment performed to verify the above theoretical results.

5.2 Experimental Results

The experimental setup is shown in Figure 5.1 below. Both solid-state Nd:YAG lasers were operating at about 1.3 μm. Each laser has a linewidth on the order of a few KHz. The first laser was intensity modulated using a Mach-Zehnder modulator with a 400 MHz sinewave. The received field was coupled into the photodetector through a piece of multimode fiber. Two variations of this setup where used as explained in the following two subsections.

5.2.1 Single-Mode Directional Coupler

In this case, the two fields were added using a single-mode directional coupler. This represents the situation of most practical interest. That's because it allows for fields

to be transmitted through single-mode fibers. This facilitates transmission over long distances without suffering significant dispersion.

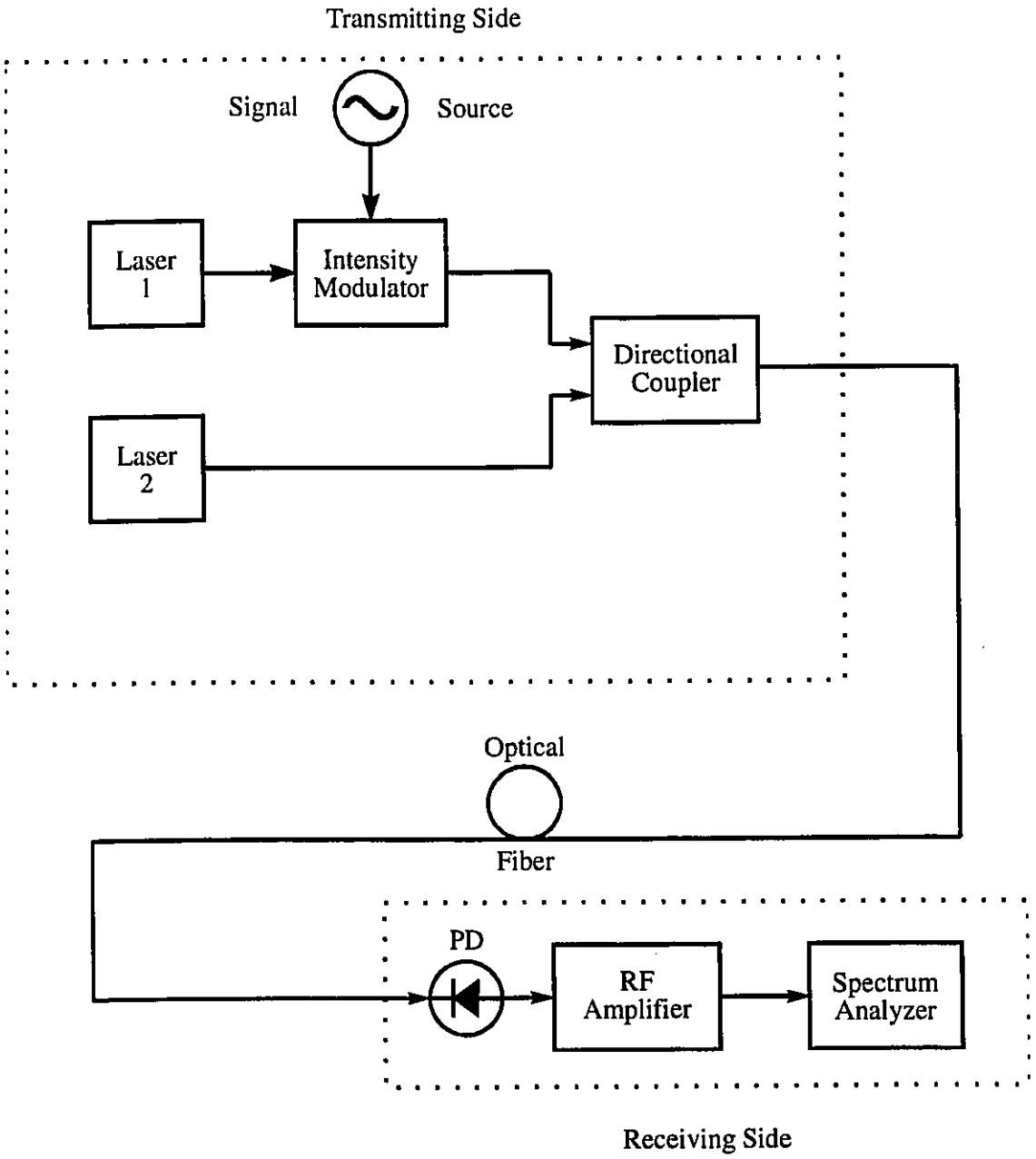

Figure 5.1: Experimental setup

The spectrum of the PD output both with and without the short piece of multimode fiber before the PD is as shown in Figure 5.2.

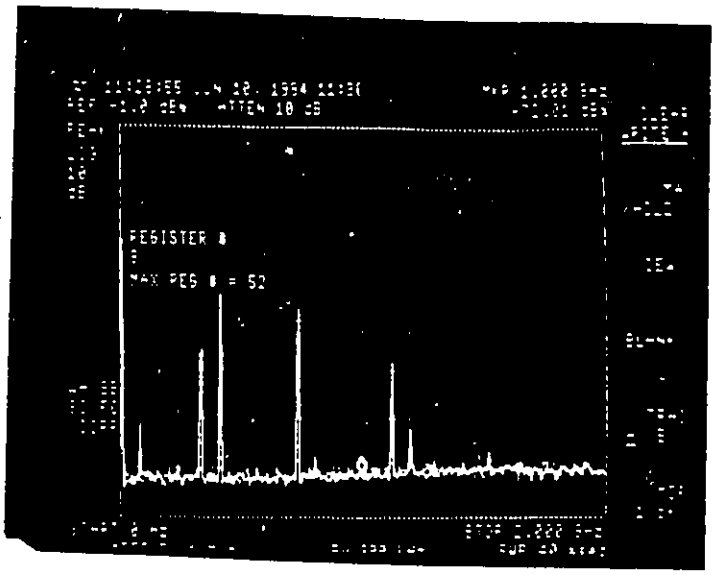

Figure 5.2: PD output spectrum using a single-mode directional coupler

Horizontal scale: 200 MHz/div.

Vertical Scale: 10 dB/div.

The signal component is the one at $f_1 = 400$ MHz. The component at about 720 MHz (note the 200 MHz/division horizontal scale) corresponds to the beating of the two optical carriers. Let's denote the frequency of this OBI component by F_x. As can be seen from Figure 5.2, there are OBI components at $|F_x - f_1| = 320$ MHz, $|F_x + f_1| = 1120$ MHz, and so on.

The result in Figure 5.2 shows that OBI was not removed or reduced using the short piece of multimode fiber. Possible reasons for this behavior are:

1. Number of supported modes in the multimode fiber is not large enough. Actually the number of propagated modes is expected to be very low, because the lasers have very narrow linewidths.
2. Modes generated by the two injected fields are not independent. This is a more likely reason than the first one; because the fields have close optical frequencies, and they propagate in the same fibers. That's why it's likely that both fields will excite the same modes when injected into the piece of multimode fiber placed before the photodetector. When both fields excite the same modes, OBI power will be distributed over the same modes as the signal power, and hence, OBI cannot be removed.

5.2.2 Multimode Directional Coupler

The directional coupler in this case is multimode. This implies that fields have to be transmitted all the way through multimode fiber. This makes it less likely that the two fields will excite the same modes in the multimode fiber piece placed before the PD. It also allows for the addition of modal noise to the fields. It however, and because of multimode fiber dispersion, puts significant constraints on the amount of information that can be transmitted and the distance that can be covered.

The PD output spectrum when using multimode fiber all over the connection is as shown in Figure 5.3. Note the absence of the main OBI component at 720 MHz. Other insignificant OBI components are still present but they are more than 25 dB below the signal level (at 400 MHz).

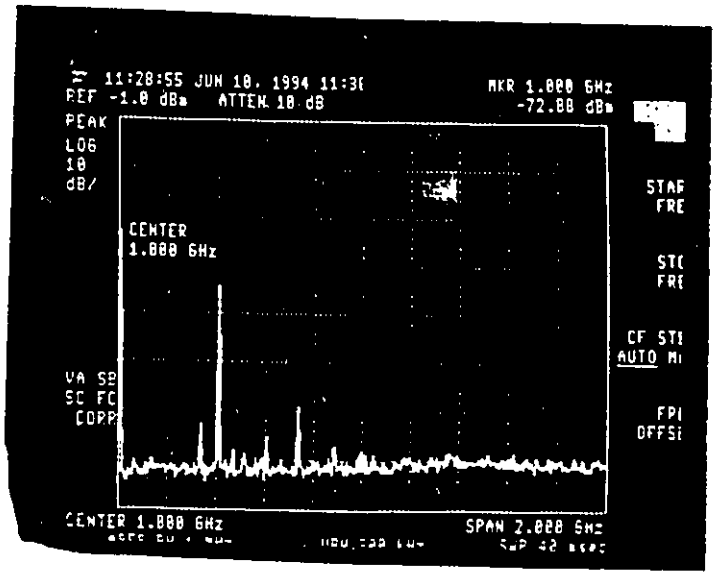

Figure 5.3: PD output using a multimode fiber connection

Horizontal scale: 200 MHz/div.

Vertical Scale: 10 dB/div.

Considering the experimental results of this chapter, we feel that more work needs to be done on mode scrambling as an OBI countermeasure. We believe this will be helpful in developing a better understanding of the effectiveness of this technique. Hence, mode scrambling could be an area of further research on OBI countermeasures.

Chapter Six

6. Optical Frequency Hopping and OBI

6.1 Introduction

Four techniques to reduce OBI have been discussed so far. In the balanced detection scheme, laser frequency stabilization is required. In the case of increasing the intensity modulation index, we have the physical limit of unity modulation index. In the case of PN polarization variation it was found that relatively high-rate PN signals are needed. Finally, using mode scrambling was successful in substantially reducing OBI only when field were propagated in multimode fiber all over the transmission path.

In this chapter, we present a technique that is very effective in reducing OBI, while it can be implemented with today's technology [68]. Optical frequency hopping (OFH) uses the already available tunable laser technology to achieve OBI bandwidth broadening.

A laser consisting of a long gain section followed by a conventional DBR section was shown in [12] to be tunable over 24 frequencies spaced by 40 GHz. This amounts to about 1 THz of tuning range. The lasing frequency could be randomly switched among

these frequencies in less than 8 ns. This kind of laser can be used in SCM/WDMA networks to provide the optical carriers.

The modulated fields are still given by the same formulas as before. The only change is the following: Each one of the M optical frequencies in an optical channel is now uniformly distributed over a certain range. This range has to be slightly less than the separation between the optical channels. This ensures that whatever the instantaneous frequency of a given field is (within its specified range), it can pass its intended optical filters.

6.2 Analysis of Simulation Results

6.2.1 Signal and OBI Power Spectral Densities

Figure 6.1 and Figure 6.2 show the OBI spectra for 100 and 1000 GHz laser tuning ranges, respectively. Figure 6.3 and Figure 6.4 show subcarrier and OBI spectra for laser tuning ranges of 100 and 1000 GHz, respectively. In both cases, two subcarriers at 4 and 5 GHz RF center frequencies were PSK modulated by 200 Mb/s data signals. The laser intensity modulation indices were both 0.707. In the following analyses we try to estimate the best tuning range such that the maximum network throughput can be achieved.

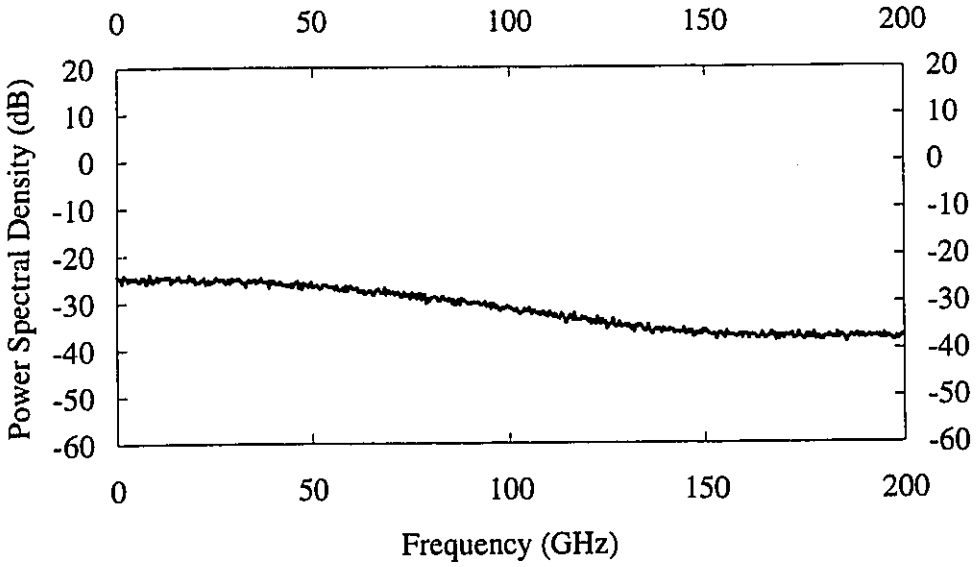

Figure 6.1: OBI spectrum under a 100 GHz frequency tuning range

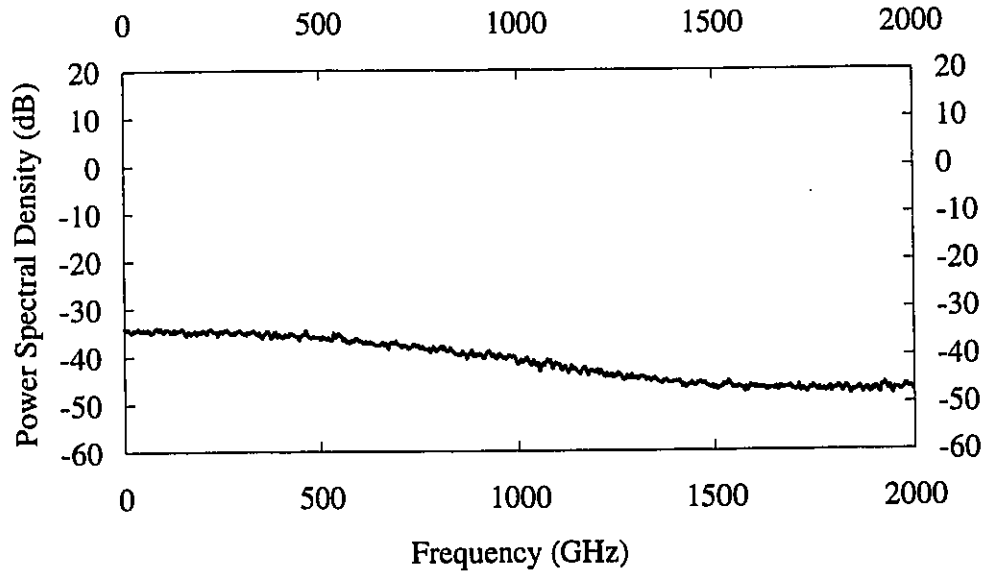

Figure 6.2: OBI spectrum under a 1000 GHz frequency tuning range

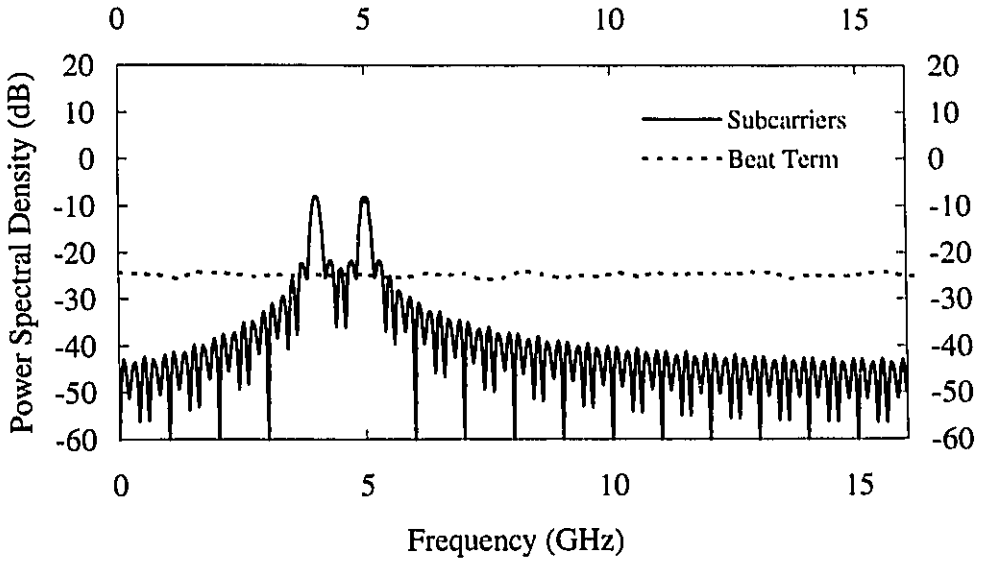

Figure 6.3: Subcarrier and OBI spectra under a 100 GHz frequency tuning range

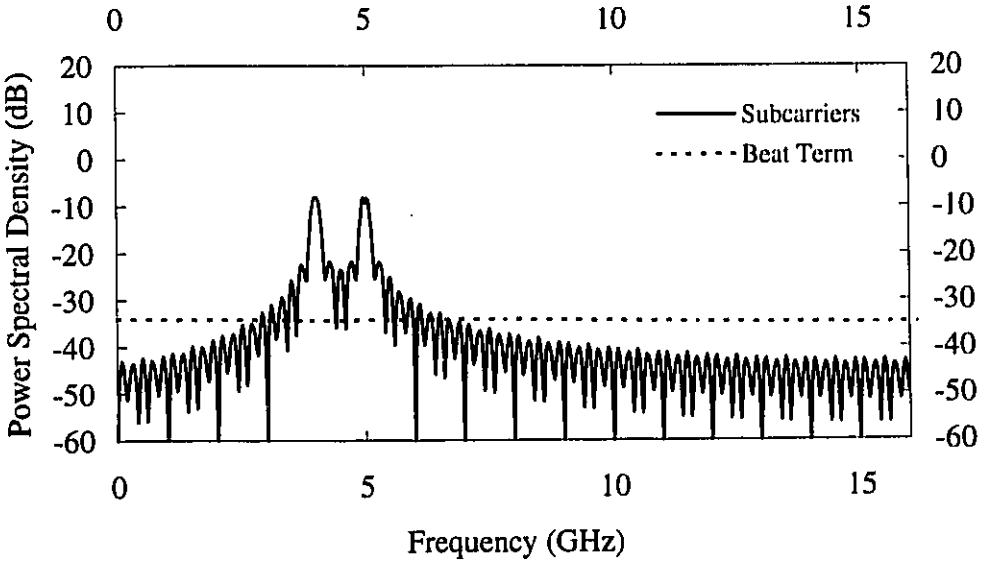

Figure 6.4: Subcarrier and OBI spectra under a 1000 GHz frequency tuning range

The objective is still to achieve a probability of error less than or equal to 10^{-9}. It was shown in chapter 4 that this can be satisfied when the carrier-to-interference ratio is at least 18. Substituting these numbers in eq. (3.47), the signal power at the output of the electric BPF is equal to:

$$P_s = 0.0625\ \text{W}$$

Note that, S_0 appears in both the signal and interference powers, so it was set to unity. Now, from Figure 6.3, and assuming the OBI PSD is flat in the frequency range of interest (in fact, it is almost constant in that range), the two-sided OBI power spectral density is:

$$S_{obi,100} \approx 0.0037\ \text{W/GHz}$$

Multiplying this density by a BPF bandwidth of 0.4 GHz (on both sides of the frequency spectrum) yields:

$$P_{obi,100} = 0.00296\ \text{W}$$

Applying the same procedure to Figure 6.4 gives:

$$P_{obi,1000} = 0.000296\ \text{W}$$

For a laser tuning range equal to R, the maximum number of subcarriers per optical channel that allows a probability of error less than or equal to 10^{-9} is denoted by M_R. Hence, the total OBI power is $M_R(M_R-1)/2$ times the numbers above. As a result, we must have:

$$\frac{P_s}{P_{obi,R} \cdot M_R(M_R-1)/2} \geq 18 \qquad \textbf{(6.1)}$$

where $P_{obi,R}$ denotes either $P_{obi,100}$ or $P_{obi,1000}$ above. Rearranging eq. (6.1), we get:

$$M_R(M_R - 1) \leq \frac{P_s}{9P_{obi,R}} \tag{6.2}$$

Substituting the signal and interference power values in eq. (6.2), we get:

$$M_{100} \leq 2$$
$$M_{1000} \leq 5$$

Obviously, there is no point in using OFH to support just two users per optical channel. On the other hand, increasing the tuning range above 1 THz results in a small number of allowable WDMA channels. Assuming a total optical bandwidth of about 30 THz, the total network throughput in the case of 1 THz tuning range is:

$$C_{tot} = 30 \cdot 5 \cdot 0.2 = 30 \text{ Gb/s}$$

Increasing the subcarrier data rate to 400 Mb/s allows 4 subcarrier per optical channel, which results in a total network throughput of:

$$C_{tot} = 30 \cdot 4 \cdot 0.4 = 48 \text{ Gb/s}$$

It should be emphasized that this throughput is achieved without the need to dehop the optical carriers at the receiver; because of using direct detection, for which it does not matter what the exact value of the optical frequency or phase is. However, each of the cross-terms will have its frequency hopping in a pattern given by the hopping patterns of the two optical frequencies involved in the cross-term. This is the source of processing gain for OFH.

It is also worth noting that the frequency tunability of the lasers does not need to be perfect; because all we care about is to get the laser operating frequency randomly varying within the tuning range. Because the laser tuning range is very high, laser

linewidth does not significantly affect the ability of this method in reducing OBI. Actually, broader-linewidth lasers can be more helpful in achieving OBI reduction.

6.2.2 Outage Probability

Once again, the outage probability was estimated as in subsection 2.3.3. Outage is computed for 200 Mb/s and 500 Mb/s PSK subcarrier modulation bit rates. As can be seen from Figure 6.5, the outage probability can be reduced significantly by increasing the OFH laser tuning range.

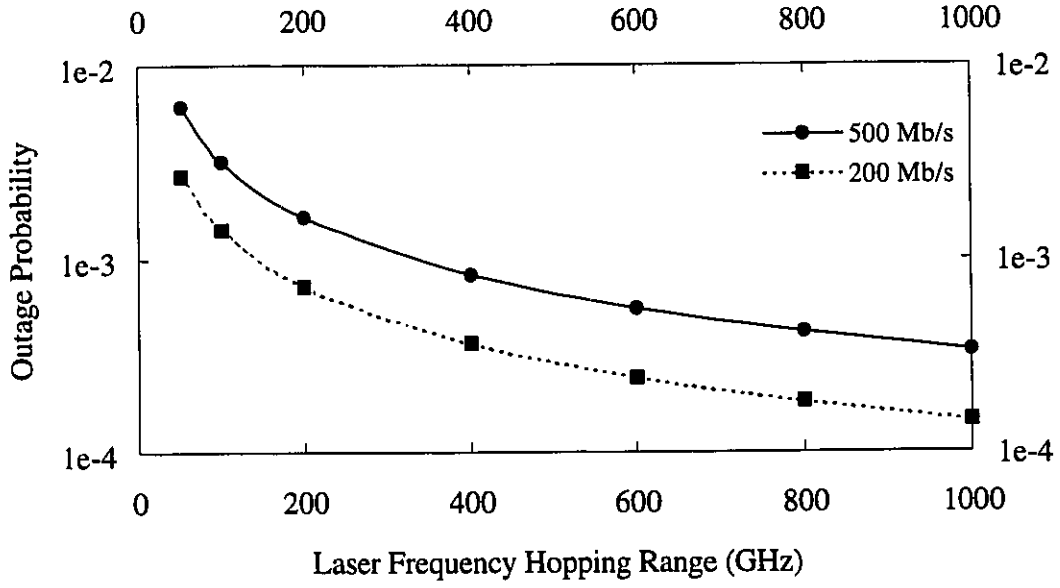

Figure 6.5: Outage probability in a two-subcarrier/channel SCM/WDMA network using OFH

Chapter Seven

7. Conclusions and Future Research

7.1 Conclusions

The results of this thesis have been presented. These results demonstrate the effectiveness of the proposed solutions. For those solutions that require technology that is not available today, it is expected that they will be implementable in the near future. The following is a list of the achieved objectives along with the relevant conclusions:

1. SCM/WDMA was presented as a simple multiple access scheme that has the ability to support very high network throughput values.
2. Sources of OBI have been identified in Chapter 2. The effects of this problem on achievable network throughput were seen throughout this work.
3. Balanced detection was presented in Chapter 2 as a solution to the OBI problem. It is expected that the requirements imposed by this solution on laser frequency stability will be met in the near future.
4. In Chapter 3, an analytical model has been developed for the analysis of large-signal laser modulation. This model has been used to evaluate the large-signal laser field spectrum. Furthermore, it has been used to analyze the effects of increasing

the intensity modulation index on optical beat interference performance of SCM/WDMA networks. It has been confirmed through analysis and graphs that increasing the modulation index helps to reduce the SCM/WDMA network performance degradation due to OBI. Graphs of the CIR vs. the modulation index demonstrated the importance of introducing the large signal analysis model. A difference as high as 4.5 dB in the CIR has been observed between the small- and the large-signal models. Plotting the CIR vs. the user channel number revealed the fact that significant improvements in the CIR could be attained by careful assignment of the subcarrier frequencies such that they are prime to each other.

5 . It has been shown in Chapter 4 through mathematical analyses and simulations that randomly varying field polarizations can be very useful in reducing OBI. High-rate independent PN signals can be used to achieve the goal of reducing OBI. Although presented results indicate very high-rate PN signals may be needed for this method to work, it should be remembered that these are only worst-case results. The reasons why this is true are:

a) The OBI power in eq. (4.13) is more than the actual value because of keeping only one term in eq. (4.12). It can be seen from eq. (4.12) that additional terms tend to reduce the OBI power.

b) Perfectly synchronous PN signals were assumed. Asynchronous PN signals produce more OBI broadening. Effects of asynchronous PN sequences were explained in Chapter 4.

c) If instead of using one polarization component for each laser field, two orthogonal components were used, less OBI power would be produced,

and hence, lower PN rates would be needed. Effects of assuming that fields have two polarization components were shown in Chapter 4.

d) Most importantly, optical carriers were assumed equal and fixed. It can be easily seen that the OBI PSD can be much lower when the optical carriers are not equal. The OBI PSD will much lower when the optical carrier vary randomly with time. This was demonstrated in section 4.4 to reduce the required PN rate by at least ten times. Increasing the range of optical carrier frequency fluctuation leads to the need of lower-rate PN sequences.

6 . The effects of using multimode fiber on OBI in SCM/WDMA networks were presented in Chapter 5. Theoretical analysis indicates that OBI can be removed using a piece of multimode fiber placed before the photodetector. However, experimental results confirmed this only when multimode fiber was used all over the connection. From the experimental results of this chapter, we feel that more research needs to be conducted on mode scrambling as an OBI countermeasure. We believe this will be helpful in developing a better understanding of the effectiveness of this method. Hence, mode scrambling could be an area of further research on OBI countermeasures.

7 . Optical frequency hopping was presented in Chapter 6. A total network throughput as high as 48 Gb/s was shown to be achievable using a laser tunable over a 1000 GHz range. OFH appears to be the best OBI countermeasure studied in this thesis. OFH makes use of available tunable laser diodes, does not need high-rate PN signals, and does not need frequency dehopping at the receiver. The last advantage includes the other very important advantage of not requiring

synchronization between two PN hopping patterns at the transmitter and the receiver. There is no strict constraints on laser tunability. Lasers are only required to provide randomly varying operating frequencies within the tuning range. Laser linewidth is not a major concern to the efficiency of this method, actually larger laser linewidths may be helpful in achieving more OBI spreading, and hence, better performance.

7.2 Future Work

The idea behind most of the OBI solutions presented in this thesis has been spectrum expansion. This can be extended to spread spectrum solutions that make use of high-speed optical processing components and coherent ultrashort laser pulses. The following techniques can be investigated:

1. Optical bipolar PN modulation using a programmable optical switch [69], [70].
2. Femtosecond laser pulse encoding [71]-[74].
3. Direct multiplication of the optical with a bipolar optical PN signal generated by an optical PN code generator [11].
4. Multiplying individual fields in an optical channel by coherent short pulse trains having different repetition frequencies [75].

Although it is expected that some of these methods may turn out to be somehow sophisticated, it is believed that with some refinement all of them will be implementable. Successful realization of these methods is expected to reduce OBI to negligible amounts and increase network throughput value significantly. These methods can be very useful in

broadcast type networks were many receivers can share the same transmitted signal, which may justify some of the foreseen complexities in these schemes.

OBI spectrum expansion can also be done by applying electronic spread spectrum on the subcarriers before they modulate the lasers. This will allow several users to use one laser, and consequently, significantly increase the network throughput.

More work can be done on most of the solutions presented in this thesis. For example, more experimental research can be performed on the mode scrambling method. Another possibility is allowing more than one subcarrier to modulate the same laser, while using several lasers per optical channel.

Other possible extensions to the research in this thesis is to study OBI produced by other nonlinear phenomena along the signal transmission path. The following is a partial list of examples:

1. Laser nonlinearities.
2. Fiber nonlinearities.
3. Optical amplifier nonlinearities.

References

[1] A. H. Cherin, *An Introduction to Optical Fibers*, McGraw-Hill, 1983.

[2] E. A. Lee and D. G. Messerschmitt, *Digital Communications*, Kluwer Academic Publishers, 1988.

[3] T. Okoshi and K. Kikuchi, *Coherent Optical Fiber Communications*, Kluwer Academic Publishers, 1988.

[4] P. E. Green, Jr., *Fiber Optic Networks*, Prentice Hall, 1993.

[5] R. D. Rosner, *Packet Switching*, Lifetime Learning Publications, 1982.

[6] F. A. Tobagi, "Fast packet switch architectures for broadband integrated services digital networks,", *IEEE Proc.*, Vol. 78, No. 1, pp. 133-167, Jan. 1990.

[7] P. R. Prucnal, M. A. Santoro and S. K. Sehgal, "Ultrafast all-optical synchronous multiple access fiber networks,", *IEEE J-SAC*, Vol. 4, No. 9, pp. 1484-1493, Dec. 1986.

[8] R. S. Tucker, G. Eisenstein and S. K. Korotky, "Optical time-division multiplexing for very high bit-rate transmission,", *J. Light. Tech.*, Vol. 6, No. 11, pp. 1737-1749, Nov. 1988.

[9] R. L. Pickholtz, D. L. Schilling and L. B. Milstein, "Theory of spread spectrum communications - a tutorial,", *IEEE Trans. Comm.*, Vol. 30, No. 5, pp. 855-884, May 1982.

[10] J. G. Proakis, *Digital Communications*, McGraw-Hill, 1989.

[11] P. R. Prucnal, M. A. Santoro and T. R. Fan, "Spread spectrum fiber-optic local area network using optical processing,", *J. Light. Tech.*, Vol. 4, No. 5, pp. 547-554, May 1986.

[12] B. S. Glance, J. M. Wiesenfield, U. Koren and R. W. Wilson, "New advances on optical components needed for FDM optical networks,", *J. Light. Tech.*, Vol. 11, No. 5/6, pp. 882-890, May/Jun. 1993.

[13] K. Kiasaleh, "Fiber optic frequency hopping multiple access communication system,", *IEEE Phot. Tech. Lett.*, Vol. 3, No. 2, pp. 173-175, Feb. 1991.

[14] F. R. K. Chung, J. A. Salehi and V. K. Wei, "Optical orthogonal codes: design, analysis, and applications,", *IEEE Trans. Info. Theory*, Vol. 35, No. 3, pp. 595-604, May 1989.

[15] J. A. Salehi, "Code division multiple-access techniques in optical fiber networks - part I: fundamental principles,", *IEEE Trans. Comm.*, Vol. 37, No. 8, pp. 824-833, Aug. 1989.

[16] J. A. Salehi and C. A. Brackett, "Code division multiple-access techniques in optical fiber networks - part II: systems performance analysis,", *IEEE Trans. Comm.*, Vol. 37, No. 8, pp. 834-842, Aug. 1989.

[17] D. Brady and S. Verdú, "A semiclassical analysis of optical code division multiple access,", *IEEE Trans. Comm.*, Vol. 39, No. 1, pp. 85-93, Jan. 1991.

[18] M. Azizoğlu, J. A. Salehi and Y. Li, "Optical CDMA via temporal codes,", *IEEE Trans. Comm.*, Vol. 40, No. 7, pp. 1162-1170, Jul. 1992.

[19] S. V. Maric, Z. I. Kostic and E. L. Titlebaum, "A new family of optical code sequences for use in spread-spectrum fiber-optic local area networks,", *IEEE Trans. Comm.*, Vol. 41, No. 8, pp. 1217-1221, Aug. 1993.

[20] G. J. Foschini and G. Vannucci, "Using spread-spectrum in a high-capacity fiber-optic local network,", *J. Light. Tech.*, Vol. 6, No. 3, pp. 370-379, Mar. 1988.

[21] A. S. Holmes and R. R. A. Syms, "All-optical CDMA using quasi-prime codes,", *J. Light. Tech.*, Vol. 10, No. 2, pp. 279-286, Feb. 1992.

[22] R. M. Gagliardi, A. J. Mendez, M. R. Dale and E. Park, "Fiber-optic digital video multiplexing using optical CDMA,", *J. Light. Tech.*, Vol. 11, No. 1, pp. 20-26, Jan. 1993.

[23] G. Vannucci and S. Yang, "Experimental spreading and despreading of the optical spectrum,", *IEEE Trans. Comm.*, Vol. 37, No. 7, pp. 777-780, Jul. 1989.

[24] P. C. Neusy and M. Kavehrad, "Proposal for an all-optical code-division multiple access for local area networks,", *Elec. Lett.*, Vol. 26, No. 18, pp. 1471-1473, 30th Aug. 1990.

[25] Y. L. Chang and M. E. Marhic, "Fiber-optic ladder networks for inverse decoding coherent CDMA,", *J. Light. Tech.*, Vol. 10, No. 12, pp. 1952-1962, Dec. 1992.

[26] M. E. Marhic, "Coherent optical CDMA networks,", *J. Light. Tech.*, Vol. 11, No. 5/6, pp. 854-864, May/Jun. 1993.

[27] S. T. Wagner and H. Kobrinski, "WDM applications in broadband telecommunication networks,", *IEEE Comm. Mag.*, Vol. 29, No. 3, pp. 22-30, March 1989.

[28] C. A. Brackett, "Dense wavelength division multiplexing networks: principles and applications,", *IEEE J-SAC*, Vol. 8, No. 6, pp. 948-964, Aug. 1990.

[29] N. Shibata, K. Nosu, K. Iwashita and Y. Azuma, "Transmission limitations due to fiber nonlinearities in optical FDM systems,", *IEEE J-SAC*, Vol. 8, No. 6, pp. 1068-1077, Aug. 1990.

[30] R. G. Waarts, A. A. Friesem, E. Lichtman, H. H. Yaffe and R. P. Braun, "Nonlinear effects in coherent multichannel transmission through optical fibers,", *IEEE Proc.*, Vol. 78, No. 8, pp. 1344-1368, Aug. 1990.

[31] G. J. Foschini and L. J. Greenstein, "Spectral efficiency of optical FDM systems impaired by phase noise,", *IEEE Trans. Comm.*, Vol. 41, No. 1, pp. 125-131, Jan. 1993.

[32] C. S. Li, F. F. K. Tong, K. Liu and D. G. Messerschmitt, "Channel capacity optimization of chirp-limited dense WDM/WDMA systems using OOK/FSK modulation and optical filters,", *J. Light. Tech.*, Vol. 10, No. 8, pp. 1148-1161, Aug. 1992.

[33] L. J. Cimini and G. J. Foschini, "Can multilevel signaling improve the spectral efficiency of ASK optical FDM systems?", *IEEE Trans. Comm.*, Vol. 41, No. 7, pp. 1084-1090, Jul. 1993.

[34] A. S. Acampora, M. J. Karol and M. G. Hluchyj, "Terabit lightwave networks: the multihop approach,", *AT&T Tech. Jour.*, Vol. 66, No. 6, pp. 21-34, Nov./Dec. 1987.

[35] M. I. Irshid and M. Kavehrad, "A WDM cross-connected star topology for multihop lightwave networks,", *J. Light. Tech.*, Vol. 10, No. 6, pp. 828-835, Jun. 1992.

[36] M. Tabiani, M. Kavehrad and M. I. Irshid, "A novel integrated-optic WDM cross-connect for wide area all optical networks,", *J. Light. Tech.*, Vol. 11, No. 3, pp. 512-522, Mar. 1993.

[37] T. E. Darcie, "Subcarrier multiplexing for multiple-access lightwave networks,", *J. Light. Tech.*, Vol. 5, No. 8, pp. 1103-1110, Aug. 1987.

[38] M. Kavehrad and E. Savov, "Fiber-optic transmission of microwave 64-QAM signals,", *IEEE J-SAC*, Vol. 8, No. 7, pp. 1320-1326, Sep. 1990.

[39] C. Desem, "Optical interference in subcarrier multiplexed systems with multiple optical carriers,", *IEEE J-SAC*, Vol. 8, No. 7, pp. 1290-1295, Sep. 1990.

[40] R. Gross, R. Olshansky and P. Hill, "Five-channel coherent heterodyne subcarrier multiplexed system,", *IEEE Phot. Tech. Lett.*, Vol. 1, No. 7, pp. 179-181, Jul. 1989.

[41] R. Gross, R. Olshansky and P. Hill, "20 channel coherent FSK system using subcarrier multiplexing,", *IEEE Phot. Tech. Lett.*, Vol. 1, No. 8, pp. 224-226, Aug. 1989.

[42] W. I. Way, "Subcarrier multiplexed lightwave system design considerations for subscriber loop applications,", *J. Light. Tech.*, Vol. 7, No. 11, pp. 1806-1818, Nov. 1989.

[43] R. Gross and R. Olshansky, "Multichannel coherent FSK experiments using subcarrier multiplexing techniques,", *J. Light. Tech.*, Vol. 8, No. 3, pp. 406-415, Mar. 1990.

[44] C. Desem, "Optical interference in lightwave subcarrier multiplexing systems employing multiple optical carriers,", *Elec. Lett.*, Vol. 24, No. 1, pp. 50-52, 7th Jan. 1988.

[45] R. Olshansky, V. A. Lanzisera and P. M. Hill, "Subcarrier multiplexed lightwave systems for broad-band distribution,", *J. Light. Tech.*, Vol. 7, No. 9, pp. 1329-1342, Sep. 1989.

[46] C. Desem, "Measurement of optical interference due to multiple optical in subcarrier multiplexing,", *IEEE Phot. Tech. Lett.*, Vol. 3, No. 4, pp. 387-389, Apr. 1991.

[47] N. K. Shankaranarayanan, S. D. Elby, and K. Y. Lau, "WDMA/subcarrier-FDMA lightwave networks: limitations due to optical beat interference,", *J. Light. Tech.*, Vol. 9, No. 7, pp. 931-943, Jul. 1991.

[48] T. H. Wood and N. K. Shankaranarayanan, "Measurements of the effect of optical beat interference (OBI) on the bit-error-rate of a subcarrier-based passive optical network (PON),", *OFC'93*, pp. 231-233.

[49] C. H. Chang, "Interference of multiple optical carriers in subcarrier-multiplexed systems,", *IEEE Phot. Tech. Lett.*, Vol. 5, No. 7, pp. 848-850, Jul. 1993.

[50] T. H. Wood and N. K. Shankaranarayanan, "Operation of a passive optical network with subcarrier multiplexing in the presence of optical beat interference,", *J. Light. Tech.*, Vol. 11, No. 10, pp. 1632-1640, Oct. 1993.

[51] T. Durhuus, B. Mikkelsen and K. E. Stubkjaer, "Detailed dynamic model for semiconductor optical amplifiers and their crosstalk and intermodulation distortion,", *J. Light. Tech.*, Vol. 10, No. 8, pp. 1056-1065, Aug. 1992.

[52] M. M. Banat and M. Kavehrad, "Bit-error-rate of an SCM/WDMA optical network employing polarization scrambling under optical beat interference,", *International Conference on Applications of Photonics Technology*, Toronto, Ont., Canada, Jun. 21-23, 1994.

[53] M. M. Banat and M. Kavehrad, "Effects of laser direct intensity modulation index on optical beat interference in subcarrier multiplexed wavelength division multiple access networks,", *IEEE Trans. Comm.*, Accepted for publication.

[54] L. G. Kazovsky, "Multichannel coherent optical communications system,", *J. Light. Tech.*, Vol. 5, No. 8, pp. 1095-1102, Aug. 1987.

[55] G. P. Agrawal, "Power spectrum of directly modulated single-mode semiconductor lasers: chirp-induced fine structure,", *J. Quant. Elec.*, Vol. 21, No. 6, pp. 680-686, Jun. 1985.

[56] M. M. Banat and M. Kavehrad, "Reduction of optical beat interference (OBI) in SCM/WDMA networks using pseudorandom phase modulation,", *J. Light. Tech.*, Vol. 12, No. 10, pp. 1863-1868, Oct. 1994.

[57] K. Petermann, *Laser Diode Modulation and Noise*, Kluwer Academic Publishers, 1988.

[58] D. P. Agrawal and N. K. Dutta, *Long-Wavelength Semiconductor Lasers*, Van Nostrand Reinhold Company, New York, 1986.

[59] M. Nazarathy, W. V. Sorin, D. M. Baney and S. A. Newton, "Spectral analysis of optical mixing measurements,", *J. Light. Tech.*, Vol. 7, No. 7, pp. 1083-1096, Jul. 1989.

[60] R. C. Alferness, "Waveguide electrooptic modulators,", *IEEE Trans. MTT*, Vol. 30, No. 8, pp. 1121-1137, Aug. 1982.

[61] E. Voges and A. Neyer, "Integrated-optic devices on $LiNbO_3$ for optical communication,", *J. Light. Tech.*, Vol. 5, No. 9, pp. 1229-1238, Sep. 1987.

[62] N. G. Walker and G. R. Walker, "Polarization control for coherent communications,", *J. Light. Tech.*, Vol. 8, No. 3, pp. 438-458, Mar. 1990.

[63] S. Y. Wang and S. H. Lin, "High speed III-V electrooptic waveguide modulators,", *J. Light. Tech.*, Vol. 6, No. 6, pp. 758-771, Jun. 1988.

[64] P. Das, *Lasers and Optical Engineering*, Springer-Verlag, 1991.

[65] R. Syms and J. Cozens, *Optical Guided Waves and Devices*, McGraw-Hill, 1992.

[66] A. Yariv, *Optical Electronics*, 4th ed., Saunders College Publishing, 1991.

[67] L. Yu and B. S. Rawat, "Mode-coupling analysis of depolarization effects in a multimode optical fiber,", *J. Light. Tech.*, Vol. 10, No. 5, pp. 556-561, May 1992.

[68] M. M. Banat and M. Kavehrad, "OBI Reduction in SCM/WDMA Networks Using Pseudorandom Optical Frequency Hopping,", *17th Biennial Symp. Comm.*, Kingston, Ont., Canada, pp. 3-6, May 29-Jun. 1, 1994.

[69] P. W. Smith, "On the physical limits of digital optical switching and logic elements,", *Bell Sys. Tech. J.*, Vol. 61, No. 8, pp. 1975-1993, Oct. 1982.

[70] S. R. Friberg, A. M. Weiner, Y. Silberberg, B. G. Sfez and P. S. Smith, "Femtosecond switching in a dual-core-fiber nonlinear coupler,", *Opt. Lett.*, Vol. 13, No. 10, pp. 904-906, Oct. 1988.

[71] A. M. Weiner, J. P. Heritage and J. A. Salehi, "Encoding and decoding of femtosecond pulses,", *Opt. Lett.*, Vol. 13, No. 4, pp. 300-302, Apr. 1988.

[72] A. M. Weiner, J. A. Salehi, J. P. Heritage and M. Stern, "Encoding and Decoding of Femtosecond Pulses for code-division multiple access,", *Proc. of OSA Topical Meeting on Photonic Switching*, pp. 263-269, Salt Lake City, Utah, March 1-3, 1989.

[73] J. A. Salehi, A. M. Weiner and J. P. Heritage, "Coherent ultrashort light Pulse code-division multiple access communication systems,", *J. Light. Tech.*, Vol. 8, No. 3, pp. 478-491, Mar. 1990.

[74] D. J. Hajela and J. A. Salehi, "Limits on encoding and bounds on the performance of coherent ultrashort light pulse code-division multiple-access systems,", *IEEE Trans. Comm.*, Vol. 40, No. 2, pp. 325-336, Feb. 1992.

[75] A. Frenkel, "Pulse frequency division multiplexing is new way to increase the capacity of a local fiber-optic communications network,", *J. Light. Tech.*, Vol. 10, No. 11, pp. 1674-1679, Nov. 1992.